ECOLE
POLYTECHNIQUE
DE BRUXELLES

ULB

Study of autonomous
quantum thermodynamical machines

Mémoire présenté en vue de l'obtention du diplôme
d'Ingénieur Civil Physicien à finalité Photonique et Applications Quantiques

Emmanouil Grigoriou

Promoteur
Professeur Nicolas J. Cerf

Co-Promoteur
Dr. Carlos Navarrete-Benlloch

Résumé / Summary in French

La théorie des systèmes ouverts offre de nombreux outils de modélisation mathématique de systèmes quantiques en interaction avec un environnement. Ce mémoire donne un aperçu de la manière dont une classe de ces outils peut être utilisée pour la modélisation de machines thermodynamiques quantiques. Il porte sur des systèmes simples, comportant deux cavités unimodes non corrélées, chacune en interaction avec un environnement. Le système contient une composante mécanique soumise aux pressions de radiation des modes des cavités. Par ailleurs, contrairement aux machines conventionnelles qui comportent en général un ou plusieurs rotors, ne sont considérés ici que des degrés de liberté mécaniques linéaires, par exemple un piston quantique ou une membrane opto-mécanique. Ceci rend les systèmes plus aptes à une modélisation mathématique complète. L'effet d'un couplage entre les deux cavités via un beam-splitter est aussi analysé. A notre connaissance, les contributions d'une telle interaction n'ont jamais été étudiées dans le contexte des machines quantiques auparavant. Si le couplage entre chaque cavité et son environnement est adéquat, l'intervention d'un operateur(humain) externe n'est alors pas nécessaire et ces machines sont dites autonomes. Ceci les rend particulièrement intéressantes et elles font l'objet de nombreuses recherches. La méthodologie proposée ici consiste, dans un premier temps, à dériver l'équation maîtresse décrivant l'évolution temporelle de l'opérateur densité du système réduit. La procédure d'application de la trace partielle sur les environnements sous certaines hypothèses est état de l'art. Il est alors possible d'en déduire des équations d'évolution portant sur des distributions quantiques de quasi-probabilité dans l'espace des phases. En particulier, une généralisation de la distribution de Glauber-Sudarshan appelée '*positive P distribution*' peut être définie dans un espace des phases étendu. Son équation d'évolution est alors équivalente à un système différentiel stochastique décrivant l'évolution temporelle quantique des variables définissant l'espace des phase. Il est aussi possible de faire la même chose dans le cas de la distribution de Wigner, à condition de tronquer les dérivées d'ordre trois ou plus dans son équation d'évolution. Le système d'équations différentielles ainsi obtenu correspond alors à la limite quasi-classique du système précédent. Ces systèmes d'équations sont résolus numériquement à l'aide de XMDS2 pour différentes conditions initiales, notamment le cas de cavités intriquées. L'exactitude des simulations peut être évaluée à l'aide de solutions exactes, obtenues grâce aux équations d'Heisenberg, pour le cas le plus simple. Le dernier chapitre présente les différents résultats des simulations dans le cas sans environnement. Finalement, une conclusion et des perspectives sur de futurs travaux possibles, permettant de compléter l'analyse et généraliser les modèles, sont données à la fin.

Abstract

This master thesis investigates the mathematical modeling of quantum thermodynamical systems using the tools of open systems dynamics. As a test case, we study two double-cavity models of unconventional linear thermodynamical machines, differing in their mechanical component: a quantum piston and a membrane. Unlike conventional thermodynamical machines based on circular motion (rotors), these machines exploit a linear mechanical degree of freedom, making them very convenient for a precise mathematical modeling. In addition, as with most current studies of quantum thermodynamics, they are autonomous, that is, they are not operated by any external agent. For each machine, we derive a master equation describing the time evolution of its density operator using state-of-the-art assumptions. Then, we derive two equivalent phase-space evolution equations, one for the Wigner distribution and one for the positive P-distribution. From these evolution equations in phase space, we finally obtain two systems of stochastic differential equations describing the time evolution. The one based on the positive P is equivalent to a fully quantum description, while the other one corresponds to a sort of classical limit. We also analyze the effect of adding a strong coupling between the two cavities through a beam-splitter interaction, showing that this can have a big impact on the master equation. We perform numerical simulations of the stochastic equations for different initial conditions, and benchmark them against exact solutions available in certain limits. The tools developed in this thesis will be determinant to understand the role of quantum coherence and entanglement when extending our models to more complicated autonomous machines based on linear mechanical degrees of freedom, which is our goal in the long term.

Keywords: quantum thermodynamics, optomechanics, open quantum systems, phase-space techniques, Wigner distribution, positive P distribution, master equations, stochastic simulations.

Acknowledgements

I would like to thank Carlos Navarrete-Benlloch for all the hours spent guiding, correcting, and explaining me the topics related to this thesis. Without him this work wouldn't even be.

I would like to thank Nicolas J. Cerf, for the opportunity to work on this subject, for providing me with a nice workplace, and for putting me in contact with Carlos.

I would also like to thank all the members of QuIC for their warm welcome.

I would like to thank my parents and my sisters for their constant support, always being there for me.

I would like to dedicate this to my grandpa, Claude Herlant, who I love very much, to my grandma, Liliane Herlant, who is no longer with us but still lives in my heart, and to all the people I didn't spent enough time with, these last 5 years of studies.

Finally, I would like to thank all the readers for their time and interest.

Contents

1 Context and motivation

1.1 Introduction: thermodynamics in the era of quantum mechanics

Converting heat into useful mechanical work or using mechanical work in order to heat or cool, that is the purpose of thermodynamical machines. Such machines rule our everyday routine and are at the heart of the technological advent of modern society. Thermodynamics has formalized in one single theory the results of most of the experiments and experiences acquired through trial and error since the early years of human evolution. Nowadays, the analysis of different ways in which different forms of energy can be transformed into each other efficiently, or physical/mathematical concepts such as entropy, do not seem so mysterious anymore.

Since the last two centuries though, new physical theories have come into play. The biggest paradigm shift was quantum physics, which was born from the observation of unseen, until then, phenomena, specially when microscopic systems were involved. Coherence and entanglement are major discoveries of modern physics, which have yet to unravel their full potential, but are already creating an impact in modern quantum technologies. To complete our understanding of how to use these phenomena for concrete applications, thermodynamics has to be extended with these quantum mechanical phenomena. Quantum information theory already allowed to quickly lay solid foundations for this new field of study, coined quantum thermodynamics. There is a lot of extremely flourishing work being carried out nowadays [1]. One of the major goals of current research is to reassess the theoretical limitations of efficiency displayed by classical machines. Thus, there is a particularly significant effort of the scientific community directed towards possible contributions of quantum effects such as coherence, entanglement, or squeezing in that prospect.

But this time things are being done the other way around. The research is first being conducted on the theoretical aspects and limitations of quantum machines, hoping that technological applications will be able to follow soon after. For example, one proposal suggests that cooling can be seen as a form of error correction, which shows how ideas from quantum thermal machines can be incorporated directly in quantum technologies as a way to fight decoherence. It is thus possible that in the near future thermodynamical machines may become important from the perspective of nanotechnology and the implementation of quantum information processing devices [1].

Of course, on the way to that promising future, one may wonder what exactly could be called a quantum thermodynamical machine today. On a broad scale, one can define it as a quantum system in contact with several thermal baths (environments). For example, a maser can be interpreted as a heat engine [1]. Currently, thermal machines comprised of a single qutrit or a few qubits have been constructed [1], and moreover, it was shown that they can approach Carnot efficiency. Further than that, however, there are not many practical examples yet.

Although the study of quantum thermodynamical machines is a relatively new field, it is rapidly evolving into a broad and vast discipline. Though a bit more concrete, the title of this thesis is still similarly broad and ambitious. However, rather than focusing on studying the various thermodynamical machines that fall into the category of autonomous, and proposing new ones, we have focused as a first step on the modeling of the basic ingredients that such devices contain, and the development of tools capable of analyzing efficiently the corresponding models. In the remaining of this introductory chapter we elaborate on these points.

1.2 Warm up models for quantum thermodynamical machines

The initial motivation for this thesis stems from [2], where the authors analyze the thermodynamical cycle of an autonomous quantum rotor heat engine inspired in classical piston engines. The engine is sketched in Fig. 1. A rotor, characterized by an angular variable, is connected to a piston that also acts as a mirror of a cavity. The cavity field exerts a radiation pressure force onto the piston, and this way gets effectively coupled to the rotor's motion. On the other hand, the cavity is connected to two separate heat baths at different temperatures. Crucially, the coupling to each bath depends on the angular position of the rotor: the coupling to the hot (cold) bath is larger when the clamping point of the rotor is on the left (right) side. Hence, starting from the position shown in the figure and no coupling to the cold bath, radiation pressure pushes the piston down, which makes the rotor rotate clockwise. Once the bottom turning point is reached, the coupling to the cold bath starts opening (and the one to the hot bath starts closing), such that the photon number decreases in the cavity, and the rotor has enough inertia to overcome the radiation pressure force and reach the upper turning point. At that point the coupling strengths start to invert again, and this way unidirectional continuous rotation is achieved. This system acts then as an autonomous quantum thermodynamical machine, which allows to convert heat into work through the rotor.

The authors analyze the model both in the classical limit and in a fully quantum mechanical fashion. The main result turns out to be rather unsatisfying, though, since it states that the quantum analysis exhibits consistently lower efficiency than the corresponding classical one due to quantum noise. Specifically, in the conclusions the authors state: "*We have also explored the role of quantum effects, and our results show, in the case of our engine, they meanly give rise to additional noise in the motion of the rotor. It is a relevant question whether other quantum effects such as entanglement and coherence can lead to a better performance compared to a fully classical version of the engine*".

While this model is very interesting for its direct connection with practical classical engines, the use of a quantum rotor makes the theoretical analysis of the system very challenging. Indeed, in the paper the authors are limited to the analysis of the extremely low-temperature regime, in which the cold bath is assumed at zero temperature and the hot bath at an average of a single quantum. This is due to the fact that for systems containing a rotor, the only general techniques available for their analysis are based on brute-force simulations of the dynamical equations for the state represented in the Hilbert space [3].
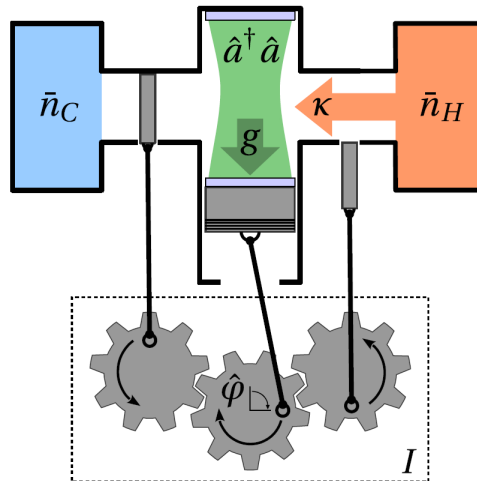

Figure 1: Sketch of the autonomous rotor heat engine considered in [2] (taken from it).

Now, even for the low temperatures considered in the paper, the Hilbert-space dimension required to capture the physics accurately is at the edge of what we can simulate with current computers. Moreover, it is a known fact that the Hilbert-space dimension increases exponentially with the number of elements considered in the system. Hence, it seems that the analysis of quantum effects such as entanglement will be extremely challenging in this system or generalizations of it.

On the long term, the project presented in this thesis aims at providing models that are still equally rich physics wise, but are based on mechanical elements that allow for a wider range of mathematical tools for their analysis. Among these, mechanical systems based on linear continuous degrees of freedom such as position or momentum would be the most desirable ones. In regimes where the evolution equations are quadratic in these degrees of freedom, a vast toolbox based on symplectic analysis and Gaussian states has been developed since a few decades ago [4, 5]. But even when the dynamics are beyond quadratic in positions and momenta, one can go around Hilbert-space simulations by using phase-space representations and related stochatic tools [6, 7]. We will elaborate on this in the next section, and in far greater depth along the next chapters, since these techniques are the main focus of this thesis.

While our long term ambition is providing an autonomous heat engine based solely on bosonic or linear degrees of freedom, where the role of quantum effects can be analyzed in a more transparent way, the specific aim of this thesis is a bit more humble. We aim at developing the tools that will be used to analyze theoretically such ambitious machines, specifically, phase-space stochastic techniques. For this, we introduce two models that, although cannot be considered heat engines, are autonomous thermodynamical machines that contain what we believe will be the main ingredients expected to appear in engine models: mechanical and optical elements interacting via radiation pressure, and heat baths.

We present the models in Figure 2. Both models have two cavities separated by a perfectly reflecting mechanical element, which can be a piston (left) or a membrane (right). In both cases, each cavity is coupled to their own heat bath. Presumably, the autonomous rotor heat engine of [2] could be generalized to linear degrees of freedom by allowing the coupling to the heat baths to depend on the position of the mechanical element, although we still don't explore this possibility in this thesis.

Let us comment on why we consider two different mechanical elements. Note that a piston is modeled as a rigid solid characterized by a single degree of freedom, the position of its center of mass, which is assumed to move as a free particle. Obviously, this is a not very realistic situation for experiments, where friction is unavoidable for such bulky elements. Moreover, because the displacement of the piston is not bounded by any potential, the usual assumption of a radiation pressure force independent of the displacement cannot realistically model the optomechanical interaction, since it assumes small displacements [8].
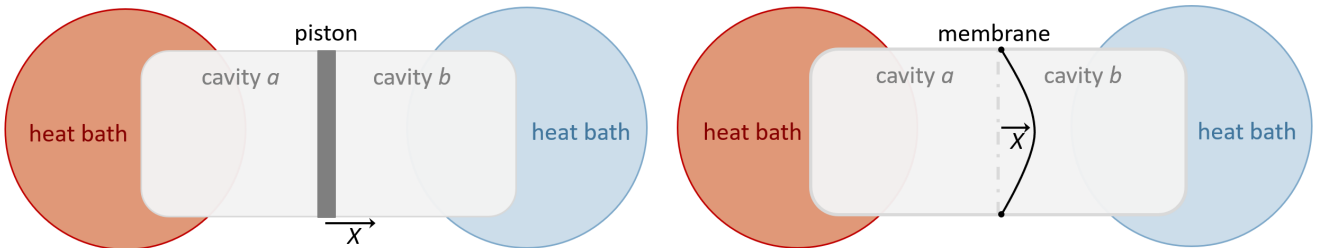

Figure 2: Sketch of the toy models considered in this thesis. In both cases a perfectly reflecting mechanical element separates the field of two cavities, each in turn connected to a heat bath. The mechanical element feels a radiation pressure force exerted by the cavity fields, and can be either a piston (left) or a membrane (right).

All these reasons motivate the introduction of a more realistic mechanical element, a membrane, or in general a mechanical element harmonically bound to a certain position. Since a little over a decade ago [8], we indeed have such mechanical harmonic oscillators operating deep at the quantum regime in various labs all over the world. In addition, a membrane has an intrinsic cycle linked to its periodic motion, so it might be more suited for the definition of thermodynamical cycles.

1.3   Open systems and phase-space techniques

At the most basic level, the description of the dynamics of the state of a thermal machine is based on open systems theory [1, 9]. This is the theory that aims at describing the dynamics of a system when it is in contact with a large environment [10], as it is the case of the cavities of the previous section in contact with a heat bath. Since the system exchanges energy with the environment, phenomena such as dissipation appears, which forces us to abandon pure states in favor of mixed states. Under certain typical conditions (known as Born-Markov, which we will introduce in detail later) one can find a simple linear differential equation for the dynamics of the density operator, the so-called master equation. This contains terms that cannot be written as a commutator with the state, meaning that the system dynamics are no longer described by just a Hamiltonian.

The master equation is usually found by formally integrating out the environment, starting from a Hamiltonian model for its interaction with the system. Once we have it, ideally it can be solved by representing the state in a basis of the Hilbert space (density matrix), and solving the system of coupled linear equations for its components. Unfortunately, this is only possible when the system doesn't explore too many basis states of its Hilbert space, as otherwise the dimension of the linear problem becomes too large for state-of-the-art computers.

One can alternatively opt for a Heisenberg picture description, which leads to the so called quantum Langevin equations [11]. These are stochastic nonlinear dynamical equations for the system operators, which are in general very hard to treat analytically, or even numerically, requiring again a representation in a basis of the Hilbert space.

These high cost of the numerical simulations in the Hilbert space motivates us to seek for alternative descriptions. For bosonic systems, one can describe the state of the system through a phase-space quasiprobability distribution [6], that is, a function dependent on the phase-space variables, which satisfies many properties of usual probability distributions, except for crucial ones such as positivity or absence of strong divergences. One can turn the master equation into an evolution equation for these quasiprobability density functions. While the remaining equation is a partial differential equation as difficult to solve as the original master equation in general, one can devise approximations that allow to treat it at least numerically.

One usual numerical route consists in finding approximate limits where the evolution equation of the quasiprobability distribution can be mapped to a set of stochastic equations for the phase-space variables, so that the evolution of the quantum state can be sampled stochastically with a computer. We will see that the so-called truncated Wigner representation allows precisely for this. However, the approximation required is in general too strong, and leads to a model in which quantum noise is mimicked with additive classical noise, what is acceptable only in the high-temperature limit and when quantum coherence is not very relevant.

One can wonder whether there exists a way of sampling quantum dynamics with classical stochastic variables without approximations. Remarkably, the answer is yes, but with a catch: it requires defining a distribution, the positive P representation, that lives in an extended phase space with twice the number of variables [7, 12]. While for numerical purposes this is not a huge overhead, conceptually it is a very daring idea: a bosonic mode is no longer described only by position and momentum, but also by two more variables with no intuitive interpretation in general. Nevertheless, from a purely practical point of view, this is a very useful technique, that

allows treating the full quantum mechanical evolution via a set of classical stochastic equations, whose complexity does not scale with the Hilbert space dimension required to describe the states explored by the system.

The biggest part of this thesis is devoted to develop these stochastic techniques for the models presented in the previous section, setting the stage for the analysis of the more complicated autonomous heat engines that we plan on developing in the future.

1.4   Structure of the thesis and original contributions

Let us conclude this introductory chapter by offering a guide through the structure of the thesis and what we consider are its main original contributions.

We have divided the thesis in three main chapters. In Chapter 2 we review the basics of open systems theory, using our models of Figure 2 as the guiding examples. In particular we derive the master equation that governs the evolution of the state of the cavity modes and the mechanical element.

As a first original contribution, in Section 2.2.5 we derive the master equation when a beam-splitter interaction between the cavities is included. To the best of our knowledge, this case hasn't been treated in the literature, and we show that it is a neat example of how the energy spectrum of the system has a strong influence on the final form of the master equation. In particular, we show that deriving first the master equation in the absence of interaction, to add the interaction later as an extra Hamiltonian is only correct when the beam-splitter coupling is much weaker than the coupling to the environments. In the opposite case, we actually show that the cavities see identical effective environments, at a temperature which is the average of the temperatures of the heat baths. Our general master equation allows to interpolate between these two regimes.

In Chapter 3 we introduce rigorously phase-space quasiprobability distributions. Using the master equations derived in the previous chapter as the guiding example, we explain in detail how to find evolution equations for these distributions, and analyze whether these can be mapped to dynamical stochastic equations for the phase space variables. These examples will allow us to show that only one specific distribution, the Wigner distribution, allows for such map and only after a specific approximation (truncation of third order phase-space derivatives) is performed. We show that, as is well known [13], such an approximation leads to a set of equations in which quantum noise is simulated as additive classical noise that provides half a quantum of noise even at zero temperature, which is known as stochastic electrodynamics. For high temperatures, this model converges then to the expected classical one, and therefore it is not expected to capture the effects of quantum coherent effects. This motivates us to resort to the positive P representation in a doubled phase space, and show that it allows for the stochastic map without any approximations.

As small original contribution in this part, we adapt the use of phase-space methods to the piston (or, in general, to any mechanical element which is not harmonically bound). Conceptually, this is not a completely trivial procedure, since phase-space representations are naturally defined only for harmonic oscillators (except the Wigner representation). We show that the way to generalize phase-space techniques to such cases is by choosing a reference harmonic oscillator, and use its corresponding distribution to represent the state of the mechanical element. The situation is equivalent to analyzing the dynamics of a particle in a general potential in the basis of eigenfunctions of a reference harmonic oscillator. Of course, this might be very complicated in general (think of describing the evolution of the initial wave packet of a free particle in the Hermite-Gauss basis of a harmonic oscillator). Hence an interesting and nontrivial part of this thesis is showing that phase-space representations can indeed capture the quantum dynamics of the piston. To our knowledge, this is a subtle point that no one has explicitly mentioned before.

Chapter 4 contains our main original results: we show that the stochastic equations we develop are indeed capable of sampling the dynamics of our models. Specifically, in order to benchmark the

simulations, we consider an analytical limit: absence of coupling to the environment. We show that in this limit the dynamics are analytically solvable in the Heisenberg picture, if we further neglect the beam splitter interaction between the cavities. We use this analytical solution to benchmark our stochastic simulations, showing that they agree very well. Since in this limit the dynamics are very sensitive to the initial conditions, we consider two initial conditions that showcase how entanglement can make a big difference when optomechanical interactions are considered. In particular, we show that starting with the cavities in a two-mode squeezed state, the mechanical element becomes completely insensitive to the cavities. Finally, we move away from the analytical case by considering the effect of the beam splitter. We show that the simulations provide results consistent with what we can expect from physical arguments, and show that the optomechanical interaction if effectively suppressed for large beam-splitter couplings, what we also manage to explain analytically.

We use the final chapter to offer some conclusions and comment on the future steps that we will take.

2 Open quantum systems

Open quantum systems theory is one of the distinctive features of quantum optics. It was introduced in order to deal with the fact that real physical systems cannot be described as completely isolated from their environment. Implementations in real systems always include some interaction with the external world. This interaction is typically a source of energy dissipation, although it can also involve energy provision, both processes usually characterized by the impossibility of creating quantum coherence through them (incoherent energy exchange). The question is how to describe such processes. The state of the external world is in general too complex to be monitored by experimentalists, and hence it is useful to find effective descriptions involving only the experimentally accessible system. A very powerful way is through so-called 'master equations', which is what we concentrate on in this chapter.

By definition, an open quantum system is a system S coupled to another quantum system called the environment [9] (S is sometimes also denoted by the 'reduced system'). In most cases, it is assumed that the combined system S plus environment is closed, hence evolving according to some Hamiltonian $H = H_S \otimes I_B + I_S \otimes H_B + H_{int}$, where H_j and I_j are the Hamiltonian and identity operator in the corresponding subspace in the absence of interaction, the latter being fully encoded in H_{int}. Then, the evolution of the combined system is described by a unitary $U(t) = \exp(Ht/i\hbar)$. From a general point of view, the reduced density operator $\rho_S(t)$ at time t is obtained from the density operator $\rho(t)$ of the total system using

$$\rho_S(t) = \text{tr}_B \left\{ U(t)\rho(t_0)U^\dagger(t) \right\}, \tag{1}$$

As we will see in section 2.1, under certain conditions, we can neglect the effects of the system dynamics on the environment, and completely integrate the environmental degrees of freedom out.

The interaction of the system with its environment leads to correlations between them. Thus, even if the total system starts in a separable state, the state of the reduced system will become mixed over time. To generalize the description of the time evolution to an open quantum system, some superoperators[1] called dynamical maps are used. Let's say that at time $t = 0$ the state of the total system S plus its environment is in an uncorrelated product state $\rho_0 = \rho_S(0) \otimes \rho_B$ where $\rho_S(0)$. The transformation describing the change of the reduced system from its initial time $t = 0$ to some time $t > 0$ is described by the dynamical map $V(t)$ defined by

$$\rho_S(t) = V(t)\rho_S(0) \equiv \text{tr}_B \left\{ U(t) \left[\rho_S(0) \otimes \rho_B \right] U^\dagger(t) \right\}. \tag{2}$$

It's possible to show that, as long as the system and environment are initially uncorrelated, a dynamical map represents a convex-linear, completely positive and trace-preserving quantum operation [9]. It is also interesting to note that $\{V(t)|t \geq 0\}$ is a continuous one-parameter family of dynamical maps where V(0) is the identity map. Such a family describes the whole future time evolution of the open system. If furthermore, $V(t)$ satisfies the following property called the semigroup property

$$V(t_1)V(t_2) = V(t_1 + t_2), \quad t_1, t_2 \geq 0, \tag{3}$$

then $\{V(t)|t \geq 0\}$ is called a quantum dynamical semigroup [9]. As we shall see, this naturally occurs in quantum optics under suitabble approximations (Born-Markov).

The ultimate goal of this formalism is to derive an equation describing the dynamics of the open system. The study of open quantum systems is a very broad field though, and many approaches are possible, the choice usually depending on the system that one wants to analyze. For example, the effective integration of the environmental degrees of freedom can be done either in the Schrödinger

---

[1]We denote them by superoperators because they are a map between operators, not between Hilbert space vectors.

picture or in the Heisenberg picture. The obtained equations that describe the dynamics of the system are called master equation or quantum Langevin equations, respectively. The tools and methods used to describe the open quantum optical system described above are presented in the following sections, where we focus on the Schrödinger picture approach.

2.1 Interaction with a reservoir, heat bath and Gibbs states

Reservoir and heat bath are terms used to describe some type of environments. The term reservoir refers to an environment with an infinite number of degrees of freedom. It may consist of particles with 3 degrees of freedom each, for example. In our case we focus on a reservoir consisting on the electromagnetic field in free space. The electromagnetic field can be described as a collection of harmonic oscillators (modes) which represent the degrees of freedom of the electromagnetic field [10, 14]. In 3D, these generally labeled by 4 indices (e.g., wave vector and polarization). However, when we only care about the modes outside a cavity, it is enough to consider the external modes matching the cavity mode we work with in transverse profile and polarization, so that they form a quasi-1D reservoir of harmonic oscillators completely characterized by a single label: their frequency ω [10]. When treated as a reservoir, the frequencies form a continuum (in fact, it can be shown that a rapid decay of the reservoir correlations needed for the Markov approximation, requires such a continuum of frequencies [9]). On the other hand, the term bath or heat bath is used for a reservoir which is in a thermal equilibrium state.

In what follows, we consider the open system coupled to a heat bath of harmonic oscillators representing a radiation field. The bath is supposed to be much larger than the system. This means that, in the weak-coupling limit (assumed in what follows), the environment isn't really affected by the system. In contrast, the reduced system is strongly influenced by its coupling to the bath.

In quantum optical scenarios, the following assumptions are almost always universally made:

- The system-bath interactions are linear in the bath annihilation and creation operators.

- The effects of any frequency dependence in the coupling constant are neglected. This, as will be clear later, is usually allowed because of energy conservation (only reservoir frequencies close to the system's transitions contribute). Moreover, in certain common experimental situations the coupling can be designed to be frequency-independent. Let us point out that such a frequency-independent coupling constant is a stronger condition than Markovianity.

- In the final master equation, there may be some rapidly oscillating terms. It's possible to show that these terms do not contribute to the dynamics of ρ_S, and thus they are usually neglected. This is the so-called rotating-wave approximation [10].

Now, let's clarify these assumptions with the example of an open optical single mode cavity, with annihilation operator a. We denote by $b(\omega)$ the annihilation bosonic operators for each mode of the bath, which satisfy the continuous canonical commutation relations $[b(\omega), b^\dagger(\omega)] = \delta(\omega - \omega')$. The Hamiltonian of the system and the reservoir in the absence of interaction is then

$$H_S = \hbar\omega_c a^\dagger a, \tag{4a}$$

$$H_B = \int_0^\infty d\omega \hbar\omega b^\dagger(\omega)b(\omega), \tag{4b}$$

where ω_c is the cavity frequency.

It is common to model the interaction between the cavity and the external modes by a beam-splitter interaction, that is, a coherent process that transfers photons from the cavity to the external field and vice versa. Indeed, this is an exact model in the case of a partially transmitting

8

mirror. As there is a continuous set of frequencies, the sum of all possible processes must be considered. The interaction Hamiltonian is then

$$H_{int} = i\hbar \int_0^\infty d\omega \kappa(\omega)[b^\dagger(\omega)a - a^\dagger b(\omega)], \tag{5}$$

where $\kappa(\omega)$ is the coupling function between the environment and the cavity. It depends on the transmissivity of the mirror at frequency ω and is in full generality frequency dependent. We will however assume, as is usually the case, that it is small (large mirror reflectivity) and can be consider approximately frequency independent over a large frequency domain, see below.

On the other hand, note that in the weak coupling case that we are dealing with, the energy of the full system is still mainly defined by the free Hamiltonians (4). Hence, energy conservation implies that only reservoir frequencies close to the cavity frequency will contribute to the interaction, which is thus called a resonant interaction. Specifically, rewriting the coupling as $\kappa(\omega) = \sqrt{\gamma/\pi}$, weak coupling (or large mirror reflectivity) means that we assume $\gamma \ll \omega_c$. Therefore, only reservoir frequencies around the interval $[\omega_c - \gamma, \omega_c + \gamma]$ will contribute, around which we can assume the mirror reflectivity to be frequency-independent. Indeed, the transmissivity of typical mirror can be made pretty flat as a function of the frequency, so this will be correct as long as the allowed interval is small enough [10]. In addition, we can extend the integration limits to $]-\infty, \infty[$ which will simplify the upcoming integrals. The unphysical negative frequency modes will not contribute, as they are very off-resonant. After these considerations, the Hamiltonian of the system reads then

$$H = H_{sys} + H_B + H_{int}, \tag{6a}$$

$$H_B = \int_{-\infty}^\infty d\omega \hbar\omega b^\dagger(\omega)b(\omega), \tag{6b}$$

$$H_{int} = i\hbar\sqrt{\frac{\gamma}{\pi}} \int_{-\infty}^\infty d\omega[b^\dagger(\omega)a - a^\dagger b(\omega)]. \tag{6c}$$

We will consider a bath that is initially in a thermal state, such that ρ_B is the Gibbs state defined as the equilibrium distribution of the canonical ensemble

$$\rho_B = \frac{e^{-H_B/k_BT}}{\text{tr}\left\{e^{-H_B/k_BT}\right\}} = \underset{\forall\omega}{\otimes}\rho_{th}[\bar{n}(\omega)], \tag{7}$$

where $\otimes_{\forall\omega}$ denotes a continuous tensor product over all frequencies, and

$$\rho_{th}(\bar{n}) = \frac{e^{-(\hbar\omega/k_BT)b^\dagger b}}{\text{tr}\left\{e^{-(\hbar\omega/k_BT)b^\dagger b}\right\}}, \tag{8}$$

is the thermal state for a single harmonic oscillator with annihilation operator b, parametrized by its average photon number $\bar{n}(\omega) = \text{tr}\{b^\dagger b\rho_{th}\} = [\exp(\hbar\omega/k_BT) - 1]^{-1}$ which follows the Bose-Einstein distribution as a function of the frequency.

Note that for such a thermal state the first and second moments of the multimode reservoir read

$$\langle b(\omega)\rangle = \text{tr}\left\{b(\omega)\right\}\rho_B = 0, \tag{9a}$$

$$\langle b(\omega)b(\omega')\rangle = \text{tr}\left\{b(\omega)b(\omega')\rho_B\right\} = 0, \tag{9b}$$

$$\langle b^\dagger(\omega)b(\omega')\rangle = \text{tr}\left\{b^\dagger(\omega)b(\omega')\rho_B\right\} = \bar{n}(\omega)\delta(\omega - \omega'), \tag{9c}$$

$$\langle b(\omega)b^\dagger(\omega')\rangle = \text{tr}\left\{b(\omega)b^\dagger(\omega')\rho_B\right\} = [\bar{n}(\omega) + 1]\delta(\omega - \omega'). \tag{9d}$$

These relations are easy to prove by taking into account that different reservoir modes are uncorrelated, and thermal states are phase invariant.

Finally, let us point out that we will work at temperatures where the Bose-Einstein distribution is approximately flat in the relevant interval $\omega \in [\omega_c - \gamma, \omega_c + \gamma]$, so that we can make a frequency-independent approximation $\bar{n}(\omega) = \bar{n}(\omega_c) \equiv \bar{n}$ in the equations above.

2.2 Master equations and Lindblad form

The aim of this section is to derive an equation describing the dynamics of the open system. Since we do it in the Schrodinger picture, the resulting equation is called a master equation. These differential equations are very similar to their counterparts in classical physics. All the quantumness is contained in the variables, which in the quantum formalism correspond to the entire density matrix, including off-diagonal elements. Otherwise, a density matrix with only diagonal elements can be modeled as a classical random process, and there is nothing quantum in the equation. This section shows how the master equation is derived, first considering one single-mode cavity in contact with a piston or a membrane, and then adding a second cavity as in Figure 2.

2.2.1 The piston-cavity Hamiltonian

As a first step let's derive the Hamiltonian of the system. It is the sum of the piston Hamiltonian (which we model as that of a free particle, it's center of mass, given by $P^2/2m$) and the cavity Hamiltonian, given by $\hbar\omega(X)a^\dagger a$. Here X and P are the position and momentum of the piston, respectively, which satisfy the commutation relation $[X, P] = i\hbar$. The frequency $\omega(X)$ of the cavity is inversely proportional to its length $l = l_c + X$, where l_c is the length of the cavity at time zero. Using the expansion $(1 + X/l_c)^{-1} \approx 1 - X/l_c$, valid for small piston displacements, $X \ll l_c$, and denoting by ω_c the cavity frequency at time zero, we then obtain the system Hamiltonian

$$H_{sys} = \frac{P^2}{2m} + \hbar\omega_c a^\dagger a - \hbar G X a^\dagger a, \tag{10}$$

where we have defined the optomechanical coupling $G = \omega_c/l_c$.

This system Hamiltonian replaces in (6) the simple single-mode cavity Hamiltonian of the previous section. Note, however, that we will assume that $GX_0 \ll \gamma$ (where X_0 is some measure of the mechanical displacement, for example its average position plus uncertainty, $|\langle X \rangle| + \sqrt{\langle X^2 \rangle - \langle X \rangle^2}$), such that the piston does not change the cavity appreciably from the point of view of the environment, as otherwise the elimination of the latter becomes more complicated (we will see this clearly when considering a similar situation in Section 2.2.5, specifically an interaction between cavities that changes the Hamiltonian's spectrum considerably).

2.2.2 Elimination of the bath

We can proceed now to eliminate the environmental degrees of freedom. Our starting point is the von Neumann equation for the full system

$$i\hbar\frac{d\rho}{dt} = [H_{sys} + H_B + H_{int}, \rho] \equiv [H_0 + H_{int}, \rho]. \tag{11}$$

Since we are going to use a perturbative approach valid under weak-coupling conditions, let us move to a picture where we remove the free dynamics induced by H_0. With full generality, given a density operator ρ evolving according to $d\rho/dt = [H/i\hbar, \rho]$ and a unitary transformation of the form $U = \exp(H_U t/i\hbar)$, the transformed density operator $\tilde{\rho}(t) = U^\dagger(t)\rho(t)U(t)$ is easily shown to obey the evolution equation

$$d\tilde{\rho}/dt = [H_I(t)/i\hbar, \tilde{\rho}], \qquad \text{with } H_I(t) = U^\dagger(t)HU(t) - H_U \tag{12}$$

Considering (11) and choosing the change of picture defined by $H_U = H_0$, the interaction Hamiltonian becomes

$$H_I(t) = e^{-H_0 t/i\hbar}(H_0 + H_{int})e^{H_0 t/i\hbar} - H_0 = e^{-H_0 t/i\hbar}H_{int}e^{H_0 t/i\hbar}$$

$$= i\hbar\sqrt{\frac{\gamma}{\pi}}\int d\omega\, e^{-(H_{sys}+H_B)t/i\hbar}[b^\dagger(\omega)a - a^\dagger b(\omega)]e^{(H_{sys}+H_B)t/i\hbar}. \tag{13}$$

Since $[H_{sys}, H_B] = 0$, we have

$$H_I(t) = i\hbar\sqrt{\frac{\gamma}{\pi}} \int d\omega \left(e^{\frac{i}{\hbar}H_B t}\hat{b}^\dagger(\omega)e^{-\frac{i}{\hbar}H_B t}e^{\frac{i}{\hbar}H_{sys}t}\hat{a}e^{-\frac{i}{\hbar}H_{sys}t} - e^{\frac{i}{\hbar}H_{sys}t}\hat{a}^\dagger e^{-\frac{i}{\hbar}H_{sys}t}e^{\frac{i}{\hbar}H_B t}b(\omega)e^{-\frac{i}{\hbar}H_B t} \right). \tag{14}$$

We can calculate each term independently:

$$e^{\frac{i}{\hbar}H_B t}\hat{b}^\dagger(\omega)e^{-\frac{i}{\hbar}H_B t} = \hat{b}^\dagger(\omega) + \frac{it}{\hbar}[H_B, \hat{b}^\dagger(\omega)] + \frac{(it)^2}{2\hbar^2}\left[H_B, [H_B, \hat{b}^\dagger(\omega)]\right] + \dots \tag{15}$$

$$= \hat{b}^\dagger(\omega) + \frac{it}{\hbar}\int_0^\infty d\omega' \hbar\omega' \hat{b}^\dagger(\omega')\delta(\omega - \omega') + \dots = \hat{b}^\dagger(\omega)\sum_{n=0}^\infty \frac{(i\omega t)^n}{n!} = \hat{b}^\dagger(\omega)e^{i\omega t}. \tag{16}$$

Similarly,

$$e^{\frac{i}{\hbar}H_B t}\hat{b}(\omega)e^{-\frac{i}{\hbar}H_B t} = \hat{b}(\omega)e^{-i\omega t}.$$

If we further define the interaction picture cavity annihilation operator $\tilde{a}(t) \equiv e^{-H_{sys}t/i\hbar}\hat{a}e^{H_{sys}t/i\hbar}$, we obtain

$$H_I(t) = i\hbar\sqrt{\frac{\gamma}{\pi}} \int_{-\infty}^\infty d\omega \left[\tilde{a}(t)b^\dagger(\omega)e^{i\omega t} - \tilde{a}^\dagger(t)b(\omega)e^{-i\omega t} \right] \tag{17}$$

The master equation follows directly from the von Neumann equation by solving formally, replacing the solution into the equation, and tracing out the environment. Let us show this next. Formal integration of equation (12) gives us

$$\tilde{\rho}(t) = \tilde{\rho}(0) + \frac{1}{i\hbar}\int_0^t dt' \left[H_I(t'), \tilde{\rho}(t')\right], \tag{18}$$

which reintroduced in (12) leads to

$$\frac{d\tilde{\rho}_S}{dt} = \frac{1}{i\hbar}\operatorname{tr}_B\left\{[H_I(t), \tilde{\rho}(0)]\right\} - \frac{1}{\hbar^2}\int_0^t dt' \operatorname{tr}_B\left\{[H_I(t), [H_I(t'), \tilde{\rho}(t')]]\right\}$$

$$= -\frac{1}{\hbar^2}\int_0^t d\tau \operatorname{tr}_B\left\{[H_I(t), [H_I(t-\tau), \tilde{\rho}(t-\tau)]]\right\}, \tag{19}$$

where the term depending on the initial condition disappears because $\operatorname{tr}_B\left\{[H_I(t), \tilde{\rho}(0)]\right\} \propto \langle b(\omega)\rangle = 0$ according to (9). Up to here all the derivations are exact. To go further, two more approximations are made.

The first one is the Born approximation [10], which consists in considering only terms up to second order in the interaction, and is equivalent to setting $\tilde{\rho}(t-\tau) = \tilde{\rho}_S(t-\tau) \otimes \rho_B$ in equation (19), as we argue next. Initially the environment and the system are in a separable state. As time goes by the interaction induces correlations between them, but these are therefore at least of order one in the interaction. Furthermore, the environment is a huge system barely perturbed by the weak interaction with the system, so we expect deviations with respect to its initial state ρ_B to appear only at a large order in the interaction. These then justifies the use of the $\tilde{\rho}(t-\tau) = \tilde{\rho}_S(t-\tau) \otimes \rho_B$ ansatz.

The second approximation is the Markov approximation [6, 10]: we assume that the evolution equation of the state at a given time, depends only on the state at that same time (memoryless evolution). This is justified when the two-time reservoir correlation functions decay much faster than the characteristic rate at which the system evolves. However, in our case it naturally appears as a direct consequence of the frequency-independent approximation for γ, which is therefore an

even stronger condition than Markovianity. We therefore proceed without explicitly applying the Markov approximation, which will come naturally at a later stage.

Applying the Born approximation, equation (19) becomes

$$\frac{d\tilde{\rho}_S}{dt} = \frac{1}{\hbar^2} \int_0^t d\tau \, \mathrm{tr}_B \left\{ [H_I(t), [H_I(t-\tau), \tilde{\rho}_S(t-\tau) \otimes \rho_B]] \right\}. \tag{20}$$

In order to perform the time integral (20), let's now write down all the terms contained in the kernel. Since the Hamiltonian has 2 terms and there are two nested commutators, we will have $(2 \cdot 1 + 2 \cdot 1) \cdot 2 + 2 \cdot 1 + (2 \cdot 1) \cdot 2 = 16$ terms in total. Putting the frequency integrals, the partial trace over the environment, and the constant γ/π aside, the integral's kernel is the sum of the following terms:

$$Q_1 = e^{i\omega'(t-\tau)+i\omega t}\tilde{a}(t)\tilde{a}(t-\tau)\tilde{\rho}_S(t-\tau) \otimes b^\dagger(\omega)b^\dagger(\omega')\tilde{\rho}_B, \tag{21a}$$

$$Q_2 = -e^{i\omega t}e^{-i\omega'(t-\tau)}\tilde{a}(t)\tilde{a}^\dagger(t-\tau)\tilde{\rho}_S(t-\tau) \otimes b^\dagger(\omega)b(\omega')\tilde{\rho}_B, \tag{21b}$$

$$Q_3 = -e^{i\omega t}e^{i\omega'(t-\tau)}\tilde{a}(t)\tilde{\rho}_S(t-\tau)\tilde{a}(t-\tau) \otimes b^\dagger(\omega)\tilde{\rho}_B b^\dagger(\omega'), \tag{21c}$$

$$Q_4 = e^{i\omega t}e^{-i\omega'(t-\tau)}\tilde{a}(t)\tilde{\rho}_S(t-\tau)\tilde{a}^\dagger(t-\tau) \otimes b^\dagger(\omega)\tilde{\rho}_B b(\omega'), \tag{21d}$$

$$Q_5 = -e^{-i\omega t}e^{i\omega'(t-\tau)}\tilde{a}^\dagger(t)\tilde{a}(t-\tau)\tilde{\rho}_S(t-\tau) \otimes b(\omega)b^\dagger(\omega')\tilde{\rho}_B, \tag{21e}$$

$$Q_6 = e^{-i\omega t}e^{-i\omega'(t-\tau)}\tilde{a}^\dagger(t)\tilde{a}^\dagger(t-\tau)\tilde{\rho}_S(t-\tau) \otimes b(\omega)b(\omega')\tilde{\rho}_B, \tag{21f}$$

$$Q_7 = e^{-i\omega t}e^{i\omega'(t-\tau)}\tilde{a}^\dagger(t)\tilde{\rho}_S(t-\tau)\tilde{a}(t-\tau) \otimes b(\omega)\tilde{\rho}_B b^\dagger(\omega'), \tag{21g}$$

$$Q_8 = -e^{-i\omega t}e^{-i\omega'(t-\tau)}\tilde{a}^\dagger(t)\tilde{\rho}_S(t-\tau)\tilde{a}^\dagger(t-\tau) \otimes b(\omega)\tilde{\rho}_B b(\omega'), \tag{21h}$$

$$Q_9 = -e^{i\omega'(t-\tau)}e^{i\omega t}\tilde{a}(t-\tau)\tilde{\rho}_S(t-\tau)\tilde{a}(t) \otimes b^\dagger(\omega')\tilde{\rho}_B b^\dagger(\omega), \tag{21i}$$

$$Q_{10} = e^{i\omega'(t-\tau)}e^{-i\omega t}\tilde{a}(t-\tau)\tilde{\rho}_S(t-\tau)\tilde{a}^\dagger(t) \otimes b^\dagger(\omega')\tilde{\rho}_B b(\omega), \tag{21j}$$

$$Q_{11} = e^{-i\omega'(t-\tau)}e^{i\omega t}\tilde{a}^\dagger(t-\tau)b(\omega')\tilde{\rho}_S(t-\tau)\tilde{a}(t) \otimes \tilde{\rho}_B b^\dagger(\omega), \tag{21k}$$

$$Q_{12} = -e^{-i\omega'(t-\tau)}e^{-i\omega t}\tilde{a}^\dagger(t-\tau)\tilde{\rho}_S(t-\tau)\tilde{a}^\dagger(t) \otimes b(\omega')\tilde{\rho}_B b(\omega), \tag{21l}$$

$$Q_{13} = e^{i\omega'(t-\tau)}e^{i\omega t}\tilde{\rho}_S(t-\tau)\tilde{a}(t-\tau)\tilde{a}(t) \otimes \tilde{\rho}_B b^\dagger(\omega')b^\dagger(\omega), \tag{21m}$$

$$Q_{14} = -e^{i\omega'(t-\tau)}e^{-i\omega t}\tilde{\rho}_S(t-\tau)\tilde{a}(t-\tau)\tilde{a}^\dagger(t) \otimes \tilde{\rho}_B b^\dagger(\omega')b(\omega), \tag{21n}$$

$$Q_{15} = e^{-i\omega'(t-\tau)}e^{i\omega t}\tilde{\rho}_S(t-\tau)\tilde{a}^\dagger(t-\tau)\tilde{a}(t) \otimes \tilde{\rho}_B b(\omega')b^\dagger(\omega), \tag{21o}$$

$$Q_{16} = e^{-i\omega'(t-\tau)}e^{-i\omega t}\tilde{\rho}_S(t-\tau)\tilde{a}^\dagger(t-\tau)\tilde{a}^\dagger(t) \otimes \tilde{\rho}_B b(\omega')b(\omega). \tag{21p}$$

The trace over the environment is now easily performed with the help of (9). We see that $Q_1, Q_3, Q_6, Q_8, Q_9, Q_{12}, Q_{13}, Q_{16}$ all vanish. The remaining terms are found as

$$\frac{\gamma}{\pi} \int_0^t d\tau \int_{-\infty}^{\infty} d\omega \int_{-\infty}^{\infty} d\omega' \, \mathrm{tr}_B \{Q_4\} \tag{22}$$

$$= \frac{\gamma}{\pi} \int_0^t d\tau \int_{-\infty}^{\infty} d\omega \int_{-\infty}^{\infty} d\omega' e^{i\omega t - i\omega'(t-\tau)}\tilde{a}(t)\tilde{\rho}_S(t-\tau)\tilde{a}^\dagger(t-\tau)\underbrace{\mathrm{tr}_B \left\{ b^\dagger(\omega)\rho_B b(\omega') \right\}}_{\mathrm{tr}_B\left\{ b(\omega')b^\dagger(\omega)\rho_B \right\}}$$

$$= \frac{\gamma(\bar{n}+1)}{\pi} \int_0^t d\tau \underbrace{\int_{-\infty}^{\infty} d\omega e^{i\omega\tau}}_{2\pi\delta(\tau)}\tilde{a}(t)\tilde{\rho}_S(t-\tau)\tilde{a}^\dagger(t-\tau)$$

$$= 2\gamma(\bar{n}+1) \int_0^t d\tau \delta(\tau)\tilde{a}(t)\tilde{\rho}_S(t-\tau)\tilde{a}^\dagger(t-\tau)$$

$$= \gamma(\bar{n}+1)\tilde{a}(t)\tilde{\rho}_S(t)\tilde{a}^\dagger(t),$$

where we have used the property $\int_0^t d\tau \delta(\tau) f(\tau) = f(0)/2$. Proceeding in a similar way, we can evaluate the rest of the terms, obtaining

$$\frac{\gamma}{\pi} \int_0^t d\tau \int_{-\infty}^{\infty} d\omega \int_{-\infty}^{\infty} d\omega' \, \mathrm{tr}_B \{Q_5\} = -\gamma(\bar{n}+1)\tilde{a}^\dagger \tilde{a}\tilde{\rho}_S, \tag{23a}$$

$$\frac{\gamma}{\pi} \int_0^t d\tau \int_{-\infty}^{\infty} d\omega \int_{-\infty}^{\infty} d\omega' \, \mathrm{tr}_B \{Q_7\} = \gamma\bar{n}\tilde{a}^\dagger \tilde{\rho}_S \tilde{a}, \tag{23b}$$

$$\frac{\gamma}{\pi} \int_0^t d\tau \int_{-\infty}^{\infty} d\omega \int_{-\infty}^{\infty} d\omega' \, \mathrm{tr}_B \{Q_{10}\} = \gamma(\bar{n}+1)\tilde{a}\tilde{\rho}_S \tilde{a}^\dagger, \tag{23c}$$

$$\frac{\gamma}{\pi} \int_0^t d\tau \int_{-\infty}^{\infty} d\omega \int_{-\infty}^{\infty} d\omega' \, \mathrm{tr}_B \{Q_{11}\} = \gamma\bar{n}\tilde{a}^\dagger \tilde{\rho}_S \tilde{a}, \tag{23d}$$

$$\frac{\gamma}{\pi} \int_0^t d\tau \int_{-\infty}^{\infty} d\omega \int_{-\infty}^{\infty} d\omega' \, \mathrm{tr}_B \{Q_{14}\} = -\gamma\bar{n}\tilde{\rho}_S \tilde{a}\tilde{a}^\dagger, \tag{23e}$$

$$\frac{\gamma}{\pi} \int_0^t d\tau \int_{-\infty}^{\infty} d\omega \int_{-\infty}^{\infty} d\omega' \, \mathrm{tr}_B \{Q_{15}\} = -\gamma(\bar{n}+1)\tilde{\rho}_S \tilde{a}^\dagger \tilde{a}. \tag{23f}$$

Adding all these terms we get the master equation

$$\frac{d\tilde{\rho}_S}{dt} = \gamma(\bar{n}+1)[2\tilde{a}\tilde{\rho}_S \tilde{a}^\dagger - \tilde{a}^\dagger \tilde{a}\tilde{\rho}_S - \tilde{\rho}_S \tilde{a}^\dagger \tilde{a}] + \gamma\bar{n}[2\tilde{a}^\dagger \tilde{\rho}_S \tilde{a} - \tilde{a}\tilde{a}^\dagger \tilde{\rho}_S - \tilde{\rho}_S \tilde{a}\tilde{a}^\dagger]. \tag{24}$$

This is the master equation for the single open cavity mode in the interaction picture. We can write it in the more compact form

$$\frac{d\tilde{\rho}_S}{dt} = \gamma(\bar{n}+1)D_{\tilde{a}}[\tilde{\rho}_S] + \gamma\bar{n}D_{\tilde{a}^\dagger}[\tilde{\rho}_S], \tag{25}$$

where $D_J[\rho] = 2J\rho J^\dagger - \{J^\dagger J, \rho\}$, and D_J is known as Lindblad superoperator. We then say that the master equation is written in Lindblad form.

Now let's to come back to the initial picture. In order to do this, we simply find the evolution equation of the original state $\rho_S(t) = U_S(t)\tilde{\rho}_S(t)U_S^\dagger(t)$, with $U_S = \exp(H_{sys}t/i\hbar)$, which is easily shown to be

$$\begin{aligned}
\frac{d\rho_S}{dt} &= \frac{H_{sys}}{i\hbar}U_S\tilde{\rho}_{SS}U_S^\dagger - U_S\tilde{\rho}_S U_S^\dagger \frac{H_{sys}}{i\hbar} + U_S\frac{d\tilde{\rho}_S}{dt}U_S^\dagger \\
&= \left[\frac{H_{sys}}{i\hbar}, \rho_S\right] + \gamma(\bar{n}+1)U_S D_{\tilde{a}}[\tilde{\rho}_S]U_S^\dagger + \gamma\bar{n}U_S D_{\tilde{a}^\dagger}[\tilde{\rho}_S]U_S^\dagger \\
&= \left[\frac{H_{sys}}{i\hbar}, \rho_S\right] + \gamma(\bar{n}+1)D_{U_S\tilde{a}U_S^\dagger}[\rho_S] + \gamma\bar{n}D_{U_S\tilde{a}^\dagger U_S^\dagger}[\rho_S] \\
&= \left[\frac{H_{sys}}{i\hbar}, \rho_S\right] + \gamma(\bar{n}+1)D_a[\rho_S] + \gamma\bar{n}D_{a^\dagger}[\rho_S].
\end{aligned} \tag{26}$$

This master equation is similar to the von Neumann equation of the system plus some more terms (the Lindblad terms) which stem from the interaction with the environment. For this reason they are called dissipative terms. Note that in many open system problems the dissipative terms can be written in Lindblad form.

In full generality, a Markov process is usually formulated in terms of the Chapman-kolmogorov equation [2] which has similarities with the semigroup property. In fact, it is possible to show that

---

[2] If $T(x|x')$ is a transition probability from state $x' \equiv x(t')$ to state $x \equiv x(t)$, the Chapman-kolmogorov equation states that $T(x|x') = \int dx'' T(x|x'')T(x''|x)$. For discrete Markov processes, it can be written in matrix form as $T(x(t+t')) = T(x(t))T(x(t'))$.

the semigroup property (3) is the property of any Markov process [9]. Then, if it is justified to neglect memory effects in the reduced system dynamics, the family of dynamical maps describing the evolution of the reduced system forms a quantum dynamical semigroup. Furthermore, if we assume no explicit time dependence in the Hamiltonian of the whole system, it's the possible to show that the generator of this group $\mathcal{L}$, such that $V(t) = e^{\mathcal{L}t} \Leftrightarrow d\rho_S/dt = \mathcal{L}[\rho_S]$, is

$$\mathcal{L}[\rho_S] = -i[H, \rho_S] + \sum_{k=1}^{N^2-1} \frac{\gamma_k}{2} D_{J_k}(\rho_S), \tag{27}$$

where N is the dimension of the system's Hilbert space and J_k are operators that are usually denoted by jump operators.

Furthermore, note that in the absence of optomechanical coupling, the thermal state $\rho_{th}(\bar{n})$ is the stationary state of the problem, $\mathcal{L}[\rho_{th}(\bar{n})] = 0$, as expected: the cavity reaches thermal equilibrium with the environment.

2.2.3 Double cavity model

We are now in conditions to write down the master equation corresponding to the model shown in Figure 2 (left): the piston acts as a moving mirror shared by two cavities (coupled to independent heat baths), which then exert radiation pressure forces onto it in opposite directions. The Hamiltonian of the full system is in this case is

$$H_{sys} = \frac{P^2}{2m} + \hbar\omega_c a^\dagger a - \hbar G X a^\dagger a + \hbar\omega_c b^\dagger b + \hbar G X b^\dagger b, \tag{28a}$$

$$H_B = \int_{-\infty}^{\infty} d\omega \hbar\omega e^\dagger(\omega)e(\omega) + \int_{-\infty}^{\infty} d\omega \hbar\omega d^\dagger(\omega)d(\omega), \tag{28b}$$

$$H_{int} = i\hbar\sqrt{\frac{\gamma}{\pi}} \int_{-\infty}^{\infty} d\omega[e^\dagger(\omega)a - a^\dagger e(\omega)] + i\hbar\sqrt{\frac{\gamma}{\pi}} \int_{-\infty}^{\infty} d\omega[d^\dagger(\omega)b - b^\dagger d(\omega)]. \tag{28c}$$

Where we have denoted the annihilation operators of the left (right) cavity and its bath by a and e (b and d). Note that for simplicity we have assumed that the cavities are identical, including their coupling strengths to the piston and their respective baths.

We can trace out the baths following the same procedure as in the previous section. Since the baths are independent, and the cavities interact only through their common coupling to the piston, which we assumed weak as explained above ($GX_0 \ll \gamma$), the master equation will just trivially combine the terms corresponding to each independent cavity. We get:

$$\frac{d\rho_S}{dt} = \left[\frac{H_{sys}}{i\hbar}, \rho_S\right] + \gamma(\bar{n}_a + 1)D_a[\rho_S] + \gamma\bar{n}_a D_{a^\dagger}[\rho_S] + \gamma(\bar{n}_b + 1)D_b[\rho_S] + \gamma\bar{n}_b D_{b^\dagger}[\rho_S], \tag{29}$$

where we have denoted by $\bar{n}_a$ and $\bar{n}_b$ the thermal photon number of the corresponding cavity.

2.2.4 The membrane model

So far we have considered the mechanical component to be a piston whose center of mass moves freely. Although this is a very interesting model that already contains a lot of the physics we ought to explore, it's not experimentally realizable. From this point of view, a more interesting mechanical element consists of a membrane[3] as shown in Figure 2 (right). The resulting model is still very close to the previous one, except that now the free mechanical Hamiltonian is replaced

---

[3]Technically, the membrane has many mechanical modes, similarly to an optical cavity. Here, as in most optomechanics works, we assume to work only with one specific mode.

with a harmonic oscillator. Such type of models have been experimentally implemented with actual membranes or other types of mechanical oscillators, and are ubiquitous to the young field of quantum cavity optomechanics [8].

The Hamiltonian of the membrane reads

$$H_{mem} = \frac{P^2}{2m} + \frac{m\Omega^2}{2}X^2 = \hbar\omega_m\left(c^\dagger c + \frac{1}{2}\right), \tag{30}$$

where we have defined the annihilation and creation operators ($[c, c^\dagger] = 1$) through $X = x_0(c + c^\dagger)$ and $P = -ip_0(c - c^\dagger)$. $x_0 = \sqrt{\hbar/2m\Omega}$ and $p_0 = \hbar/2x_0 = \sqrt{\hbar m\Omega/2}$ are, respectively, the position and momentum uncertainties of the membrane in its ground state (zero-point fluctuations).

The models, including the optical cavities and their heat baths, take the same form as in (26) and (29), for the single-cavity and double-cavity cases, respectively, with a system Hamiltonian that reads

$$H_{sys} = \hbar\Omega c^\dagger c + \hbar\omega a^\dagger a + \hbar\omega b^\dagger b - \hbar g(c^\dagger + c)\left(a^\dagger a - b^\dagger b\right), \tag{31}$$

where we have defined optomecanical coupling rate $g = Gx_0$, which is assumed small similarly to the piston case, $g \ll \gamma$. Changing the mechanical component between the two cavities does not influence the way they interact with their environment. Thus, the dissipative Lindblad terms remain exactly the same. The master equation is still of the form (29) but the H_{sys} term is now given by (31).

2.2.5 Coupling the optical modes through a beam splitter

The previous examples allowed for the naive procedure of modeling the open system just adding terms of the form (25) for any mode coupled to a bath. This, however, is only allowed when the effect of the coupling between the modes of the reduced system is negligible from the point of view of the reservoirs. In this section we consider a relevant example that shows how this naive approach has to be modified in the presence of strong coupling. In particular, we analyze what happens when we add a beamsplitter interaction between the two cavities.

Since the optomechanical coupling is still treated as a small perturbation that can be added at the end, we don't consider it now, so we focus on the optical modes. The Hamiltonian of the full system is then

$$H_{sys} = \hbar\omega_c a^\dagger a + \hbar\omega_c b^\dagger b + \hbar\lambda(ab^\dagger + a^\dagger b), \tag{32a}$$

$$H_B = \int_0^\infty d\omega\hbar\omega e^\dagger(\omega)e(\omega) + \int_0^\infty d\omega\hbar\omega d^\dagger(\omega)d(\omega), \tag{32b}$$

$$H_{int} = i\hbar\int_0^\infty d\omega\sqrt{\frac{\gamma(\omega)}{\pi}}[e^\dagger(\omega)a - e(\omega)a^\dagger] + i\hbar\int_0^\infty d\omega\sqrt{\frac{\gamma(\omega)}{\pi}}[d^\dagger(\omega)b - d(\omega)b^\dagger], \tag{32c}$$

where $\lambda > 0$ characterizes the strength of the beam splitter. If the condition $\lambda \ll \gamma$ is satisfied, then the model of the previous section (modified just by the addition of the beam splitter Hamiltonian) works. Here, however, we are interested in understanding what happens when $\lambda > \gamma$ (the so-called strong coupling regime), so we derive a new master equation that will work in this regime.

To this aim, let us first write the evolution equations of a and b under the action of H_{sys},

$$\frac{d}{dt}\begin{pmatrix} a \\ b \end{pmatrix} = -i\underbrace{\begin{pmatrix} \omega_c & \lambda \\ \lambda & \omega_c \end{pmatrix}}_{M}\begin{pmatrix} a \\ b \end{pmatrix}. \tag{33}$$

The matrix M is readily diagonalized, yielding the eigenvalues $\Omega_{A,B} = \omega_c \pm \lambda$. Defining the normal modes

$$\begin{pmatrix} A \\ B \end{pmatrix} = \frac{1}{\sqrt{2}} \begin{pmatrix} 1 & 1 \\ -1 & 1 \end{pmatrix} \begin{pmatrix} a \\ b \end{pmatrix}, \tag{34}$$

and similarly for the reservoir modes,

$$\begin{pmatrix} E(\omega) \\ D(\omega) \end{pmatrix} = \frac{1}{\sqrt{2}} \begin{pmatrix} 1 & 1 \\ -1 & 1 \end{pmatrix} \begin{pmatrix} e(\omega) \\ d(\omega) \end{pmatrix}. \tag{35}$$

The Hamiltonian is then rewritten as

$$H_{sys} = \hbar\Omega_A A^\dagger A + \hbar\Omega_B B^\dagger B, \tag{36a}$$

$$H_B = \int_0^\infty d\omega \hbar\omega \left[E^\dagger(\omega)E(\omega) + D^\dagger(\omega)D(\omega) \right], \tag{36b}$$

$$H_{int} = i\hbar \int_0^\infty d\omega \sqrt{\frac{\gamma(\omega)}{\pi}} \left[E^\dagger(\omega)A + D^\dagger(\omega)B - E(\omega)A^\dagger - D(\omega)B^\dagger \right]. \tag{36c}$$

It might look as if by moving to the normal mode basis, we have turned the problem into two modes (A and B) interacting with independent reservoirs (D and E, respectively). However, this is not the case, since the reservoirs are now correlated. Consider, for example, the term

$$\text{tr}\left\{ E(\omega')D^\dagger(\omega)\rho_B \right\} = \frac{1}{2}\text{tr}\left\{ [e(\omega') + d(\omega')] \left[-e^\dagger(\omega) + d^\dagger(\omega) \right] \rho_B \right\}$$

$$= \frac{1}{2}\left[-\underbrace{\text{tr}\left\{ e(\omega')e^\dagger(\omega)\rho_B \right\}}_{(\bar{n}_a+1)\delta(\omega-\omega')} - \underbrace{\text{tr}\left\{ d(\omega')e^\dagger(\omega)\rho_B \right\}}_{0} + \underbrace{\text{tr}\left\{ e(\omega')d^\dagger(\omega)\rho_B \right\}}_{0} + \underbrace{\text{tr}\left\{ d(\omega')d^\dagger(\omega)\rho_B \right\}}_{(\bar{n}_b+1)\delta(\omega-\omega')} \right] \tag{37}$$

$$= \frac{1}{2}(\bar{n}_b - \bar{n}_a)\delta(\omega - \omega'),$$

which is only zero when the heat baths are at the same temperature, while in any other case, shows non-zero correlations between the heat baths. Similarly[4], we can evaluate all the other non-zero reservoir correlation functions, obtaining

$$\text{tr}\left\{ E^\dagger(\omega)E(\omega')\rho_B \right\} = \text{tr}\left\{ D^\dagger(\omega)D(\omega')\rho_B \right\} = \frac{1}{2}(\bar{n}_a + \bar{n}_b)\delta(\omega - \omega'), \tag{38a}$$

$$\text{tr}\left\{ E(\omega)E^\dagger(\omega')\rho_B \right\} = \text{tr}\left\{ D(\omega)D^\dagger(\omega')\rho_B \right\} = \frac{1}{2}(\bar{n}_a + \bar{n}_b + 2)\delta(\omega - \omega'), \tag{38b}$$

$$\text{tr}\left\{ E^\dagger(\omega)D(\omega')\rho_B \right\} = \text{tr}\left\{ D(\omega)E^\dagger(\omega')\rho_B \right\} = \text{tr}\left\{ D^\dagger(\omega)E(\omega')\rho_B \right\} = \frac{1}{2}(\bar{n}_b - \bar{n}_a)\delta(\omega - \omega'). \tag{38c}$$

The rest of the correlation functions, specifically the ones containing two annihilation or two creation operators, are zero.

It is also important to comment on one subtle point: since we have modified the spectrum of the Hamiltonian H_{sys}, the Born-Markov conditions have to be reassessed. For example, the weak coupling approximation means now that $\Omega_B \gg \gamma$. Note that this condition, automatically implies $\lambda \ll \omega_c$, that is, as the beam splitter interaction must stay away from the so-called ultra-strong coupling regime. We assume to work in these limits in the following. These conditions also allow us to extend the frequency integrals to $-\infty$, as well as applying the frequency-independent approximation for $\gamma(\omega)$. However, note that since the resonant frequencies of A and B are different,

---

[4]See Appendix A for more details on the calculations.

when $\lambda \gg \gamma$ we can allow for different reference values for each of the interactions. Specifically, the interaction-picture Hamiltonian, defined by (12) with $H_U = H_{sys} + H_B$, takes the form

$$H_I(t) = i\hbar \int_{-\infty}^{\infty} d\omega \sqrt{\frac{\gamma_A}{\pi}} E^{\dagger}(\omega)\tilde{A}(t)e^{i\omega t} + i\hbar \int_{-\infty}^{\infty} d\omega \sqrt{\frac{\gamma_B}{\pi}} D^{\dagger}(\omega)\tilde{B}(t)e^{i\omega t} + \text{H.c.}, \qquad (39)$$

where $\gamma_j = \gamma(\Omega_j)$. Note that we are allowed to take $\gamma_A \neq \gamma_B$ only when $\lambda \gg \gamma_{A,B}$.

With these considerations at hand, it is now simple (but slightly lengthy) to trace out the reservoirs[5] following the same steps as in Section 2.2.2, starting from expression (20). Let us present and discuss the final form of the master equation in the interaction picture, that is, for the state $\tilde{\rho}_S(t) = U_S^{\dagger}(t)\rho_S(t)U_S(t)$, with $U_S(t) = \exp(H_{sys}t/i\hbar)$. The equation reads

$$\frac{d\tilde{\rho}_S}{dt} = \gamma_A(\bar{n}+1)D_{\tilde{A}}[\tilde{\rho}_S] + \gamma_A\bar{n}D_{\tilde{A}^{\dagger}}[\tilde{\rho}_S] + (\bar{n}+1)\gamma_B D_{\tilde{B}}[\tilde{\rho}_S] + \gamma_B\bar{n}D_{\tilde{B}^{\dagger}}[\tilde{\rho}_S]$$

$$+ \sqrt{\gamma_A\gamma_B}\Delta\bar{n}\left(2\tilde{A}\tilde{\rho}_S\tilde{B}^{\dagger} - \left\{\tilde{\rho}_S, \tilde{B}^{\dagger}\tilde{A}\right\} + 2\tilde{B}^{\dagger}\tilde{\rho}_S\tilde{A} - \left\{\tilde{\rho}_S, \tilde{A}\tilde{B}^{\dagger}\right\} + \text{H.c.}\right), \qquad (40)$$

where we have defined $\bar{n} = (\bar{n}_a + \bar{n}_b)/2$ and $\Delta\bar{n} = (\bar{n}_b - \bar{n}_a)/2$. Note that the interaction-picture operators can be written as $\tilde{A} = U^{\dagger}(t)AU(t) = e^{-i\Omega_A t}A$ and $\tilde{B} = U^{\dagger}(t)BU(t) = e^{-i\Omega_B t}B$, where we remind that A and B are time-independent because we started in the Schrodinger picture. Using this expressions, the previous equation is rewritten as

$$\frac{d\tilde{\rho}_S}{dt} = \gamma_A(\bar{n}+1)D_A[\tilde{\rho}_S] + \gamma_A\bar{n}D_{A^{\dagger}}[\tilde{\rho}_S] + (\bar{n}+1)\gamma_B D_B[\tilde{\rho}_S] + \gamma_B\bar{n}D_{B^{\dagger}}[\tilde{\rho}_S] \qquad (41)$$

$$+ \sqrt{\gamma_A\gamma_B}\Delta\bar{n}\left[e^{-2i\lambda t}\left(2A\tilde{\rho}_S B^{\dagger} - \left\{\tilde{\rho}_S, B^{\dagger}A\right\} + 2B^{\dagger}\tilde{\rho}_S A - \left\{\tilde{\rho}_S, AB^{\dagger}\right\}\right) + \text{H.c.}\right].$$

This form of the master equation allows us to discuss the different regimes of the beam-splitter interaction λ in a very transparent way. In particular, note that while the terms in the first line are time-independent, the terms in the second line oscillate at a frequency proportional to λ. Hence, how much they contribute to the dynamics will depend on how slow is the oscillation. Two limits are particularly interesting:

- First, the limit $\lambda \to 0$, where the oscillations disappear. As expected, replacing A and B by their relations with a and b, we recover the naive terms appearing in (29) corresponding to modes a and b seeing their independent environments. The steady state in this limit is then $\rho_{th}(\bar{n}_a) \otimes \rho_{th}(\bar{n}_b)$, so that each oscillator thermalizes to its respective temperature.

- The second limit is $\lambda \gg \gamma_{A,B}\Delta\bar{n}$, where the second line of (41) can be neglected within the rotating wave approximation. Hence, we are left with the terms of the first line that describe two modes that see two identical heat baths (but might exchange energy with them at different rates $\gamma_{A,B}$), which can be described as the average of the previous two environments (average thermal photon number $\bar{n}$). The steady state in this limit is then $\rho_{th}(\bar{n}) \otimes \rho_{th}(\bar{n})$, so that both oscillators thermalize to the same effective temperature.

We then see that the beam-splitter interaction radically changes the character of the open model.

Let is finally come back to the original Schrödinger picture, where the master equation reads

$$\frac{d\rho_S}{dt} = -i\left[\Omega_A A^{\dagger}A + \Omega_B B^{\dagger}B + \frac{P^2}{2m\hbar} - GX(A^{\dagger}B + AB^{\dagger}), \rho_S\right] \qquad (42)$$

$$+ \gamma_A(\bar{n}+1)D_A[\rho_S] + \gamma_A\bar{n}D_{A^{\dagger}}[\rho_S] + (\bar{n}+1)\gamma_B D_B[\rho_S] + \gamma_B\bar{n}D_{B^{\dagger}}[\rho_S]$$

$$+ \sqrt{\gamma_A\gamma_B}\Delta\bar{n}\left(2A\rho_S B^{\dagger} - \left\{\rho_S, B^{\dagger}A\right\} + 2B^{\dagger}\rho_S A - \left\{\rho_S, AB^{\dagger}\right\} + \text{H.c.}\right),$$

---

[5]See detailed calculations in Appendix A.2.

where we have included the piston motion and the corresponding optomechanical coupling, which we remind we are allowed to do as long as $G \ll \gamma_{A,B}$.

One final remarkable fact is that, if we allow the transmissivity of the cavity mirrors to be completely flat over the whole 2λ interval, so that $\gamma_A = \gamma_B \equiv \gamma$, this master equation takes keeps the naive form (29) when written in the original modes a and b. Specifically, for the piston model we get

$$\frac{d\rho_S}{dt} = -i \left[\omega_c a^\dagger a + \omega_c b^\dagger b + \lambda(ab^\dagger + a^\dagger b) + \frac{P^2}{2m\hbar} - GX(a^\dagger a - b^\dagger b), \rho_S \right] \tag{43}$$
$$+ \gamma(\bar{n}_a + 1)D_a[\rho_S] + \gamma\bar{n}_a D_{a^\dagger}[\rho_S] + \gamma(\bar{n}_b + 1)D_b[\rho_S] + \gamma\bar{n}_b D_{b^\dagger}[\rho_S],$$

while for the membrane we get

$$\frac{d\rho_S}{dt} = -i \left[\omega_c a^\dagger a + \omega_c b^\dagger b + \lambda(ab^\dagger + a^\dagger b) + \Omega c^\dagger c - g(c + c^\dagger)(a^\dagger a - b^\dagger b), \rho_S \right] \tag{44}$$
$$+ \gamma(\bar{n}_a + 1)D_a[\rho_S] + \gamma\bar{n}_a D_{a^\dagger}[\rho_S] + \gamma(\bar{n}_b + 1)D_b[\rho_S] + \gamma\bar{n}_b D_{b^\dagger}[\rho_S].$$

For definiteness, we will consider this limit in the following, so that these are the most general master equations that we will consider in this thesis.

3 Phase space stochastic techniques

In the previous section we derived the master equation of our system. This equation provides the evolution of the density operator. While ideally it is interesting to have the full state of the system, most of the time it is enough to consider simpler quantities or observables with more intuitive interpretation, that can even have a classical interpretation (take the average photon number or the quadrature fluctuations as examples). One of the main uses of phase-space techniques in quantum optics is to derive different types of evolution equations from the master equation. In many situations, these equations are simpler to solve and easier to interpret. They also offer a natural route towards the classical limit.

The goal of this section is to introduce such phase-space techniques. We first introduce the concept of phase-space quasi-probability distributions. Then, we explain how to find evolution equations for them, when given as a starting point the master equation. Later, we make the connection between these phase-space evolution equations and a system of stochastic equations, both in the classical limit and the quantum regime.

3.1 Phase space distributions

Phase space distributions are an alternative way to represent quantum states [6]. There are usually three main distributions that are used. The oldest one is the Wigner distribution. The two others are the Glauber-Sudarshan P distribution and the Husimi Q distribution.

Similarly to what is done in classical mechanics, the Wigner distribution was introduced in order to visualize quantum states in phase space, the space (x, p) spanned by position and momentum (we consider a single degree of freedom for concreteness). In classical physics these two quantities are enough to completely describe the physical state. In quantum physics though, position and momentum do not commute, and therefore obey Heisenberg's uncertainty principle. As it is not possible to have them perfectly defined simultaneously, quantum states will be intrinsically fuzzy in phase space: they cannot be represented by a point. The function representing such fuzzy state is called the Wigner distribution. As a result, quantum noise implies that there are no well defined trajectories in phase space. Moreover, the Wigner distribution can be negative, reason why it cannot be considered as a true probability distribution, which shows that quantum noise cannot be simulated with classical phase-space noise.

Let us now introduce formally the Wigner distribution. If we want the phase-space formalism to be equivalent to quantum mechanics, the Wigner distribution must contain the same information as quantum states. Accordingly, one way of building the Wigner distribution associated to a quantum state ρ is by asking for the function $W(x, p)$ whose marginals coincide with the probability distribution of obtaining an outcome for x or p. It's possible to show [10] that these conditions uniquely define the Wigner distribution

$$W(x, p) = \int_{\mathbb{R}^2} \frac{dx' dp'}{(4\pi)^2} e^{\frac{i}{2}(x'p - p'x)} \operatorname{tr} \{\rho D(x', p')\}, \tag{45}$$

where we use dimensionless versions of position and momentum (quadratures) with commutator $[\hat{x}, \hat{p}] = 2i$ and $D(x', p') = e^{\frac{i}{2}(p\hat{x} - x\hat{p})}$ is the displacement operator. Note that in the following we will include the hats in the operators whenever they can be confused with classical variables. The object $\chi(x', p') = \operatorname{tr} \{\rho D(x', p')\}$ is called the quantum characteristic function, because of its Fourier transform relation with the Wigner distribution. This will allow us to draw conclusions on the relations with the two other distributions.

It is easy to check that these expression has the right marginals, $\int_{\mathbb{R}} dp W(x, p) = \langle x|\rho|x\rangle$ for example, and is therefore normalized. It's also easy to see that it is real and bounded ($W^2 < \infty$), but nothing prevents it from being negative.

Sometimes, it is useful to express the distribution in terms of the complex variable $\alpha = (x + ip)/2$. Performing the change of variables in equation (45), imposing the normalization $\int_{\mathbb{C}} d^2\alpha W(\alpha)$, we get

$$W(\alpha) = \int_{\mathbb{C}} \frac{d^2\beta}{\pi^2} e^{\beta^*\alpha - \beta\alpha^*} \operatorname{tr}\left\{\rho e^{\beta a^\dagger - \beta^* a}\right\}. \tag{46}$$

The characteristic function $\chi_\rho = \langle D(\beta)\rangle_\rho = \operatorname{tr}\left\{\rho e^{\beta a^\dagger - \beta^* a}\right\}$ is the expectation value of the displacement operator $D(\alpha) = e^{\alpha a^\dagger - \alpha^* a}$. The different distributions appear when we generalize it as $D_z(\beta) = D(\beta)e^{z|\beta|^2/2}$, where $z \in [-1, 1]$. For the following values of z we obtain the most common distributions:

- For $z = 0$ we get the Wigner function.

- For $z = -1$ we get the Husimi distribution, $Q(\alpha) = \langle\alpha|\rho|\alpha\rangle$ ($|\alpha\rangle$ is a coherent state), which is always positive and bounded.

- For $z = 1$ we get the Glauber-Sudarshan distribution, defined through $\rho = \int_{\mathbb{C}} d\alpha P(\alpha)|\alpha\rangle\langle\alpha|$. In this case, $P(\alpha)$ can be negative or even have strong divergences. For example, for a coherent state $\rho = |\alpha_0\rangle\langle\alpha_0|$ it is a delta function $P(\alpha) = \delta^{(2)}(\alpha - \alpha_0)$.

Let's call $\chi_z(\beta) \equiv \langle D_z(\beta)\rangle_\rho$ the generalized characteristic function. Its Fourier transform provides then a generalized quasi-probability distribution

$$F_z(\alpha) = \int_{\mathbb{C}} \frac{d^2\beta}{\pi^2} e^{\beta^*\alpha - \beta\alpha^*} \chi_z(\beta) = \int_{\mathbb{C}} \frac{d^2\beta}{\pi^2} e^{\beta^*\alpha - \alpha^*\beta} \operatorname{tr}\{\rho D_z(\beta)\}, \tag{47}$$

where $z = \{1, 0, -1\}$ correspond to the common choices exposed above.

For our purposes, apart from their definition, the most important property of these distributions is their connection to quantum expectation values. It is possible to show [6] from (47) that the choices $z = 0, 1$, and -1 are related, respectively, to symmetrically, normally, and antinormally ordered moments, that is,

$$\int_{\mathbb{C}} d^2\alpha W(\alpha)\alpha^{*m}\alpha^n = \langle(a^{\dagger m}a^n)^{(s)}\rangle, \tag{48a}$$

$$\int_{\mathbb{C}} d^2\alpha P(\alpha)\alpha^{*m}\alpha^n = \langle a^{\dagger m}a^n\rangle, \tag{48b}$$

$$\int_{\mathbb{C}} d^2\alpha Q(\alpha)\alpha^{*m}\alpha^n = \langle a^n a^{\dagger m}\rangle, \tag{48c}$$

where the notation $(a^{\dagger m}a^n)^{(s)}$ means taking the weighted sum of all possible orderings. For example, $(a^\dagger a)^{(s)} = (a^\dagger a + aa^\dagger)/2$.

All the expressions presented in this section can be trivially generalized to multimode situations such as the one we considered in the previous chapter.

3.2 Fokker-Planck equations and stochastic representations

Before proceeding let's introduce the concept of Fokker-Planck equations. A Fokker–Planck equation is a particular type of partial differential equation describing the time evolution of a probability density function. One famous example is the Smoluchowski equation describing the time evolution of the probability density function of the position of particles undergoing Brownian motion in a force field.

More precisely, let's call $P(\mathbf{x}, t)$ the probability density function for $\mathbf{x} \in \mathbb{R}^N$, satisfying the following equation:

$$\partial_t P(\mathbf{x}, t) = \left[-\sum_{i=1}^{N} \partial_j A_j(\mathbf{x}) + \frac{1}{2} \sum_{j,l=1}^{N} \partial_j \partial_l D_{jl}(\mathbf{x}) \right] P(\mathbf{x}, t). \tag{49}$$

When the matrix D is positive semidefinite, then this is called a Fokker-Planck equation. $\mathbf{A}$ is then called the drift vector and D is called the diffusion matrix.

Fokker-Planck equations are equivalent to the following system of equations describing a stochastic process [6]

$$\frac{d\mathbf{x}}{dt} = \mathbf{A}(\mathbf{x}) + B(\mathbf{x})\boldsymbol{\eta}(t), \tag{50}$$

where $D(\mathbf{x}) = B(\mathbf{x})B^T(\mathbf{x})$, and the components of $\boldsymbol{\eta}(t)$ are independent real white Gaussian noises, that is, their multi-time stochastic correlation functions are given by

$$\overline{\eta_j(t)} = 0, \tag{51a}$$

$$\overline{\eta_j(t)\eta_l(t')} = \delta_{jl}\delta(t - t'), \tag{51b}$$

$$\overline{\eta_{j_1}(t_1)\eta_{j_2}(t_2)\eta_{j_3}(t_3)} = 0, \tag{51c}$$

$$\overline{\eta_{j_1}(t_1)\eta_{j_2}(t_2)\eta_{j_3}(t_3)\eta_{j_4}(t_4)} = \overline{\eta_{j_1}(t_1)\eta_{j_2}(t_2)}\ \overline{\eta_{j_3}(t_3)\eta_{j_4}(t_4)} + \overline{\eta_{j_1}(t_1)\eta_{j_3}(t_3)}\ \overline{\eta_{j_2}(t_2)\eta_{j_4}(t_4)}, \tag{51d}$$

$$\vdots \qquad\qquad + \overline{\eta_{j_1}(t_1)\eta_{j_4}(t_4)}\ \overline{\eta_{j_2}(t_2)\eta_{j_3}(t_3)}.$$

Note that we denote stochastic averages with an overbar. B is usually called the noise matrix.

The equivalence between the Fokker-Planck equation (49) and the stochastic Langevin equations (50) can be understood in the statistical sense, that is, given any function $f(\mathbf{x})$, its average at a given time t is given by

$$\overline{f[\mathbf{x}(t)]} = \int_{\mathbb{R}^N} d^N x P(\mathbf{x}, t) f(\mathbf{x}). \tag{52}$$

As shown in the next section, we can turn the master equation into a partial differential equation describing the evolution of the quasi-probability distribution F_z. Was this equation of the form of a Fokker-Planck, we would then be able to obtain a system of stochastic equations to describe the quantum dynamics, which are in general easier to treat than master equations.

3.3 Phase-space dynamical equations from the master equation

Here we derive some equivalence rules allowing us to write the evolution equation of F_z. In order to introduce them, let us consider the single-cavity system (26), governed by the master equation

$$\frac{d\rho}{dt} = \left[-\frac{i}{2m\hbar}P^2 - i\omega_c a^\dagger a + iGXa^\dagger a, \rho_S \right] + \gamma(\bar{n} + 1)D_a[\rho] + \gamma\bar{n}D_{a^\dagger}[\rho]. \tag{53}$$

The addition of the second cavity or the membrane will be trivial, and the rules we will provide can also be easily applied to the model including a beam-splitter interaction between the cavities, as we will show later.

3.3.1 General phase space correspondences

In the following we prove that each of the following fundamental terms in the master equation correspond to very specific differential operators in the evolution equations for the phase-space distribution:

$$a\rho \rightarrow \left(\alpha - \frac{z-1}{2}\partial_{\alpha^*} \right) F_z(\alpha), \tag{54a}$$

$$\rho a \rightarrow \left(\alpha - \frac{z+1}{2}\partial_{\alpha^*} \right) F_z(\alpha), \tag{54b}$$

$$\rho a^\dagger \rightarrow \left(\alpha^* - \frac{z-1}{2}\partial_{\alpha} \right) F_z(\alpha), \tag{54c}$$

$$a^\dagger \rho \rightarrow \left(\alpha^* - \frac{z+1}{2}\partial_{\alpha} \right) F_z(\alpha). \tag{54d}$$

For example, consider the equation $\frac{d\rho}{dt} = a\rho$. Then

$$\partial_t F_z(\alpha) = \int_{\mathbb{C}} \frac{d^2\beta}{\pi^2} e^{\beta^*\alpha - \alpha^*\beta} \,\mathrm{tr}\{\dot{\rho}D_z(\beta)\} = \int_{\mathbb{C}} \frac{d^2\beta}{\pi^2} e^{\beta^*\alpha - \alpha^*\beta} \,\mathrm{tr}\{a\rho D_z(\beta)\} \tag{55}$$

$$= \int_{\mathbb{C}} \frac{d^2\beta}{\pi^2} e^{\beta^*\alpha - \alpha^*\beta} \,\mathrm{tr}\{\rho D_z(\beta)a\}$$

Now, noting that

$$\partial_{\beta^*} D_z(\beta) = \partial_{\beta^*} \left[e^{\beta a^\dagger - \beta^* a} e^{z\frac{\beta\beta^*}{2}} \right] = \partial_{\beta^*} \left[e^{\beta a^\dagger} e^{-\beta^* a} e^{(z-1)\frac{\beta\beta^*}{2}} \right] \tag{56}$$

$$= e^{\beta a^\dagger}(-a)e^{-\beta^* a} e^{(z-1)\frac{\beta\beta^*}{2}} + e^{\beta a^\dagger} e^{-\beta^* a} \frac{z-1}{2}\beta e^{(z-1)\frac{\beta\beta^*}{2}} = D_z(\beta)\left[-a + \frac{z-1}{2}\beta \right]$$

$$\Downarrow$$

$$D_z(\beta)a = \left(-\partial_{\beta^*} + \frac{z-1}{2}\beta \right) D_z(\beta),$$

we obtain

$$\partial_t F_z(\alpha) = \int_{\mathbb{C}} \frac{d^2\beta}{\pi^2} e^{\beta^*\alpha - \alpha^*\beta} \,\mathrm{tr}\left\{ \rho \left(-\partial_{\beta^*} + \frac{z-1}{2}\beta \right) D_z(\beta) \right\} \tag{57}$$

$$= \int_{C} \frac{d^2\beta}{\pi^2} e^{\beta^*\alpha - \alpha^*\beta} \left(-\partial_{\beta^*} + \frac{z-1}{2}\beta \right) \mathrm{tr}\{\rho D_z(\beta)\}$$

$$= \int_{\mathbb{C}} \frac{d^2\beta}{\pi^2} tr\{\rho D_z(\beta)\} \left(\partial_{\beta^*} + \frac{z-1}{2}\beta \right) e^{\beta^*\alpha - \alpha^*\beta} - \int_{C} \partial_{\beta^*} \left[e^{\beta^*\alpha - \alpha^*\beta} tr\{\rho D_z(\beta)\} \right],$$

where in the last step we have integrated by parts. The second term goes to zero if we assume that the characteristic function $\chi_z(\beta) = \mathrm{tr}\{\rho D_z(\beta)\}$ falls sufficiently fast to zero at the boundaries of phase space. Therefore, we finally obtain the desired result by operating on the exponential of the first term:

$$\partial_t F_z(\alpha) = \int_{\mathbb{C}} \frac{d^2\beta}{\pi^2} tr\{\rho D_z(\beta)\} \left(\alpha - \frac{z-1}{2}\partial_{\alpha^*} \right) e^{\beta^*\alpha - \alpha^*\beta} = \left(\alpha - \frac{z-1}{2}\partial_{\alpha^*} \right) F_z(\alpha), \tag{58}$$

which is the result we wanted to prove.

It is interesting to consider the correspondence rules in terms of the quadratures. Let us define them both in operator form, $\hat{x} = a^\dagger + a$ and $\hat{p} = i(a^\dagger - a)$, and stochastic form, $x = \alpha^* + \alpha$ and

$p = i(\alpha^* - \alpha)$. From the later relations, it is easy to find the relations between the derivatives:

$$\begin{cases} \partial_x = \frac{1}{2}(\partial_\alpha + \partial_{\alpha^*}) \\ \partial_p = \frac{i}{2}(\partial_\alpha - \partial_{\alpha^*}) \end{cases} \Leftrightarrow \begin{cases} \partial_\alpha = \partial_x - i\partial_p \\ \partial_{\alpha^*} = \partial_x + i\partial_p \end{cases} \tag{59}$$

leading to the correspondence rules

$$\hat{x}\rho \to (x + i\partial_p - z\partial_x)\, F_z(x, p), \tag{60a}$$
$$\rho\hat{x} \to (x - i\partial_p - z\partial_x)\, F_z(x, p), \tag{60b}$$
$$\rho\hat{p} \to (p + i\partial_x - z\partial_p)\, F_z(x, p), \tag{60c}$$
$$\hat{p}\rho \to (p - i\partial_x - z\partial_p)\, F_z(x, p). \tag{60d}$$

The set of equations (54) and (60) provide the general equivalence rules to go from the master equation to the evolution equation in phase space. Next we apply them to the terms relevant for our master equation.

3.3.2 Harmonic oscillator terms

Let's take as a first example the harmonic oscillator term that appears in (53):

$$\left[-ia^\dagger a, \rho \right] \to \left[\partial_\alpha(i\alpha) + \partial_{\alpha^*}(-i\alpha^*) \right] F_z(\alpha). \tag{61}$$

There is no diffusion at all since there are no second order derivatives.

3.3.3 Lindblad terms

Let us now consider the Lindblad terms of (53), which we consider separately:

$$2a\rho a^\dagger - a^\dagger a\rho - \rho a^\dagger a \to \left[\partial_\alpha\left(\alpha\right) + \partial_{\alpha^*}\left(\alpha^*\right) - (z - 1)\partial_\alpha\partial_{\alpha^*} \right] F_z(\alpha), \tag{62a}$$
$$2a^\dagger \rho a - aa^\dagger \rho - \rho aa^\dagger \to \left[\partial_\alpha\left(-\alpha\right) + \partial_{\alpha^*}\left(-\alpha^*\right) + (z + 1)\partial_\alpha\partial_{\alpha^*} \right] F_z(\alpha). \tag{62b}$$

The two cases have positive semidefinite diffusion. In order to see this we have to move to a real (quadrature) representation. Using the correspondences (59), we obtain

$$\partial_\alpha\partial_{\alpha^*} = \partial_x^2 + \partial_p^2 \Rightarrow D = \mp 2(z \mp 1)\begin{pmatrix} 1 & 0 \\ 0 & 1 \end{pmatrix} \geq 0 \quad \forall z \in [-1, 1], \tag{63}$$

which is indeed positive definite.

Adding up the the Lindblad terms with their corresponding prefactors as they appear in (26), we get the correspondece

$$(\bar{n} + 1)D_a[\rho] + \bar{n}D_{a^\dagger}[\rho] \to \left[\partial_\alpha(\alpha) + \partial_{\alpha^*}(\alpha^*) + \partial_\alpha\partial_{\alpha^*}\left(2\bar{n} + 1 - z\right) \right] F_z(\alpha). \tag{64}$$

3.3.4 Free piston motion

Let's analyse now the term in (26) accounting for the free motion of the piston, which is described in terms of the position $\hat{X}$ and momentum $\hat{P}$ of its center of mass, satisfying $[\hat{X}, \hat{P}] = i\hbar$.

In order to use the equivalence rules as defined before, we have to define annihilation and creation operators for the piston. This means that we have to work in the basis of a harmonic oscillator. Of course, the choice of oscillator is arbitrary. Specifically, the choice is effected by fixing a single parameter such as the width of its ground-state wave function, x_0. Once this choice

is made, the relation between position and momentum of the piston and the annihilation and creation operators of the oscillator (denoted by c and $c^\dagger$, respectively) is fixed to

$$\hat{X} = x_0(\hat{c} + \hat{c}^\dagger), \qquad \hat{P} = -ip_0(\hat{c} - \hat{c}^\dagger), \tag{65}$$

where $p_0 = \hbar/2x_0$. Let us point out that in the case of the membrane, the choice of x_0 is fixed by the frequency of the harmonic potential, unlike for the piston, which is truly arbitrary. We will keep however the same notation for both cases, as it will be convenient later.

We can find the correspondence rules for position X and momentum P from those of the quadratures (60), simply using the replacements $x = X/x_0$ and $p = P/p_0$, leading to

$$\hat{X}\rho \to \left(X + i\frac{\hbar}{2}\partial_P - zx_0^2\partial_X \right) F_z(\mathbf{R}), \tag{66a}$$

$$\rho\hat{X} \to \left(X - i\frac{\hbar}{2}\partial_P - zx_0^2\partial_X \right) F_z(\mathbf{R}), \tag{66b}$$

$$\rho\hat{P} \to \left(P + i\frac{\hbar}{2}\partial_X - zp_0^2\partial_P \right) F_z(\mathbf{R}), \tag{66c}$$

$$\hat{p}\rho \to \left(P - i\frac{\hbar}{2}\partial_X - zp_0^2\partial_P \right) F_z(\mathbf{R}), \tag{66d}$$

where we have collected the stochastic position and momentum in a single vector $\mathbf{R} = (X, P)^T$ for future convenience.

As an important remark, note that for $z = 0$ the correspondences do not depend on the choice of harmonic oscillator basis, x_0. This means that only in the Wigner representation one has a unique way of defining evolution equations in the phase space spanned by position and momentum.

Using these correspondence rules, we then obtain

$$\left[-\frac{i}{2m\hbar}\hat{P}^2, \rho \right] \to \left[\partial_X\left(-\frac{P}{m} \right) + \partial_X\partial_P\left(z\frac{p_0^2}{m} \right) \right] F_z(\mathbf{R}). \tag{67}$$

We have second order derivatives for $z \neq 0$. Moreover, in such case the matrix D is not positive semidefinite, since it is given by

$$D = z\frac{p_0^2}{m}\begin{pmatrix} 0 & 1 \\ 1 & 0 \end{pmatrix}, \tag{68}$$

with eigenvalues $\pm zp_0^2/m$, one of which is negative for all $z \neq 0$.

Hence, in this case, we don't obtain a Fokker-Planck equation in the P or Q representations. So it seems that to describe the system with a set of stochastic Langevin equations we should use the Wigner distribution for which the diffusion term vanishes ($z = 0$). However, as we show next, the optomechanical interaction destroys the Fokker-Planck form for the Wigner distribution, unless we introduce some approximations. Nevertheless, we will introduce in section 3.5 a generalization of the Glauber-Sudarshan distribution called the positive P distribution, which will allow the desired stochastic mapping without any approximations.

3.3.5 Optomechanical interaction

Finally we analyse the term in (26) accounting for the optomechanical interaction. Combining the correspondence rules (54) and (66), we get

$$
\begin{aligned}
\left[-i\hat{X}a^\dagger a, \rho\right] = -i &\left[\left(X + i\frac{\hbar}{2}\partial_P - zx_0^2\partial_X\right)\left(\alpha^* - \frac{z+1}{2}\partial_\alpha\right)\left(\alpha - \frac{z-1}{2}\partial_{\alpha^*}\right)\right. \\
&\left. - \left(\alpha - \frac{z+1}{2}\partial_{\alpha^*}\right)\left(\alpha^* - \frac{z-1}{2}\partial_\alpha\right)\left(X - i\frac{\hbar}{2}\partial_P - zx_0^2\partial_X\right)\right] F_z(\alpha, \mathbf{R}) \\
= &\left[\partial_\alpha(-i\alpha X) + \partial_{\alpha^*}(i\alpha^* X) + \partial_P\left(-\hbar|\alpha|^2 + \hbar\frac{z-1}{2}\right)\right. \\
&+ \partial_P\partial_\alpha\left(\hbar\frac{z}{2}\alpha\right) + \partial_P\partial_{\alpha^*}\left(\hbar\frac{z}{2}\alpha^*\right) + \partial_X\partial_\alpha\left(izx_0^2\alpha\right) - \partial_X\partial_{\alpha^*}\left(izx_0^2\alpha^*\right) \\
&\left. -\hbar\frac{z^2-1}{4}\partial_P\partial_\alpha\partial_{\alpha^*}\right] F_z(\alpha, \mathbf{R}).
\end{aligned}
\tag{69}
$$

We see that there is a term involving third order derivatives in the Wigner representation. As mentioned above, we will have to neglect it if we want to get a Fokker-Planck equation. This is what we will call the truncated Wigner approximation. In contrast, the P and Q distributions provide only up to second order derivatives. Unfortunately, the corresponding diffusion matrix is not positive semidefinite. In order to show this, we have to go to a real (quadrature) representation again using (59). Specifically, we need to transform the following terms:

$$
\partial_\alpha\alpha + \partial_{\alpha^*}\alpha^* = \frac{1}{2}(\partial_x - i\partial_p)(x + ip) + \frac{1}{2}(\partial_x + i\partial_p)(x - ip) = \partial_x x + \partial_p p, \tag{70a}
$$

$$
\partial_\alpha\alpha - \partial_{\alpha^*}\alpha^* = \frac{1}{2}(\partial_x - i\partial_p)(x + ip) - \frac{1}{2}(\partial_x + i\partial_p)(x - ip) = i\partial_x p - i\partial_p x. \tag{70b}
$$

The diffusion terms can now be written as

$$
\begin{aligned}
&\partial_P\partial_\alpha\left(\hbar\frac{z}{2}\alpha\right) + \partial_P\partial_{\alpha^*}\left(\hbar\frac{z}{2}\alpha^*\right) + \partial_X\partial_\alpha\left(izx_0^2\alpha\right) + \partial_X\partial_{\alpha^*}\left(izx_0^2\alpha^*\right), \\
&= \partial_P\partial_x\left(\hbar\frac{z}{2}x\right) + \partial_P\partial_p\left(\hbar\frac{z}{2}p\right) + \partial_X\partial_x\left(-zx_0^2p\right) + \partial_X\partial_p\left(zx_0^2x\right),
\end{aligned}
\tag{71}
$$

leading to the diffusion matrix

$$
D = z\begin{pmatrix} 0 & 0 & -x_0^2 p & \hbar\frac{x}{2} \\ 0 & 0 & x_0^2 x & \hbar\frac{p}{2} \\ -x_0^2 p & x_0^2 x & 0 & 0 \\ \hbar\frac{x}{2} & \hbar\frac{p}{2} & 0 & 0 \end{pmatrix}.
\tag{72}
$$

The eigenvalues of this matrix are $\pm z\frac{\hbar}{2}\sqrt{p^2 + x^2}$ and $\pm x_0^2\sqrt{p^2 + x^2}$, which show that, indeed, the matrix is not positive semidefinite.

3.3.6 Phase-space evolution equation for the single-mode case

Combining all terms together as they appear in the master equation (53), we obtain the equivalent evolution equation for the phase-space representations:

$$
\begin{aligned}
\partial_t F_z(\alpha, \mathbf{R}, t) = \Bigg[&\partial_\alpha\Big((\gamma + i\omega - iGX)\alpha\Big) + \partial_{\alpha^*}\Big((\gamma - i\omega + iGX)\alpha^*\Big) \\
&+ \partial_X\left(-\frac{P}{m}\right) + \partial_P\left(-\hbar G\left(|\alpha|^2 + \frac{1-z}{2}\right)\right) \\
&+ \partial_\alpha\partial_{\alpha^*}\Big((2\bar{n} + 1 - z)\gamma\Big) + \partial_X\partial_P\left(z\frac{p_0^2}{m}\right) \\
&+ \partial_P\partial_\alpha\left(\hbar G\frac{z}{2}\alpha\right) + \partial_P\partial_{\alpha^*}\left(\hbar G\frac{z}{2}\alpha^*\right) + \partial_X\partial_\alpha\left(iGzx_0^2\alpha\right) - \partial_X\partial_{\alpha^*}\left(iGzx_0^2\alpha^*\right) \\
&\qquad\qquad\qquad\qquad\qquad\qquad - \hbar G\frac{z^2-1}{4}\partial_P\partial_\alpha\partial_{\alpha^*} \Bigg] F_z(\alpha, \mathbf{R}, t).
\end{aligned}
\tag{73}
$$

3.3.7 Phase-space evolution equations for our most general models

We are now in conditions to present the phase-space evolution equations equivalent to our most general models with two cavities (43) and (44). Apart from the ingredients introduced above, we need to apply the correspondence rules to beam-splitter interaction term, which leads to

$$
\left[-i(ab^\dagger + a^\dagger b), \rho\right] \to \left[\partial_\alpha(i\beta) + \partial_{\alpha^*}(-i\beta^*) + \partial_\beta(i\alpha) + \partial_{\beta^*}(-i\alpha^*)\right] F_z(\alpha, \beta),
\tag{74}
$$

where we have denoted by β the complex stochastic variable associated to the second cavity.

Taking this into account, the phase-space evolution equation associated to the most general piston model (43) reads

$$
\begin{aligned}
\partial_t F_z(\alpha, \beta, \mathbf{R}, t) = \Bigg[&\partial_\alpha\Big((\gamma + i\omega - iGX)\alpha + i\lambda\beta\Big) + \partial_{\alpha^*}\Big((\gamma - i\omega + iGX)\alpha^* - i\lambda\beta^*\Big) \\
&+ \partial_\beta\Big((\gamma + i\omega + iGX)\alpha + i\lambda\alpha\Big) + \partial_{\beta^*}\Big((\gamma - i\omega - iGX)\alpha^* - i\lambda\alpha^*\Big) \\
&+ \partial_X\left(-\frac{P}{m}\right) + \partial_P\left(-\hbar G\left(|\alpha|^2 - |\beta|^2\right)\right) \\
&+ \partial_\alpha\partial_{\alpha^*}\Big((2\bar{n}_a + 1 - z)\gamma\Big) + \partial_\beta\partial_{\beta^*}\Big((2\bar{n}_b + 1 - z)\gamma\Big) + \partial_X\partial_P\left(z\frac{p_0^2}{m}\right) \\
+ &\partial_P\partial_\alpha\left(\hbar G\frac{z}{2}\alpha\right) + \partial_P\partial_{\alpha^*}\left(\hbar G\frac{z}{2}\alpha^*\right) + \partial_X\partial_\alpha\left(iGzx_0^2\alpha\right) - \partial_X\partial_{\alpha^*}\left(iGzx_0^2\alpha^*\right) \\
- &\partial_P\partial_\beta\left(\hbar G\frac{z}{2}\beta\right) - \partial_P\partial_{\beta^*}\left(\hbar G\frac{z}{2}\beta^*\right) - \partial_X\partial_\beta\left(iGzx_0^2\beta\right) + \partial_X\partial_{\beta^*}\left(iGzx_0^2\beta^*\right) \\
&\qquad\qquad - \hbar G\frac{z^2-1}{4}\partial_P\partial_\alpha\partial_{\alpha^*} + \hbar G\frac{z^2-1}{4}\partial_P\partial_\beta\partial_{\beta^*} \Bigg] F_z(\alpha, \beta, \mathbf{R}, t).
\end{aligned}
\tag{75}
$$

On the other hand, the phase-space evolution equation for the most general membrane model (44) is easily obtained from the previous one as follows. First, we replace the terms related to the free piston motion by terms related to the mechanical harmonic oscillator Hamiltonian. This amounts to $\partial_X(-P/m) + \partial_X\partial_P(zp_0^2/m) \longrightarrow \partial_\chi(i\Omega\chi) + \partial_{\chi^*}(-i\Omega\chi^*)$, where we denote by χ the

complex stochastic variabble associated to the membrane. Second, we use the change of variables and derivatives

$$
\begin{cases} \partial_X = (\partial_\chi + \partial_{\chi^*})/2x_0 \\ \partial_P = i(\partial_\chi - \partial_{\chi^*})/2p_0 \end{cases} , \quad \begin{cases} X = x_0(\chi + \chi^*) \\ P = -ip_0(\chi - \chi^*) \end{cases} \tag{76}
$$

finally leading to

$$
\begin{aligned}
\partial_t F_z(\alpha, \beta, \chi, t) = \Big[& \partial_\alpha \Big((\gamma + i\omega - ig(\chi + \chi^*))\alpha + i\lambda\beta \Big) + \partial_{\alpha^*} \Big((\gamma - i\omega + ig(\chi + \chi^*))\alpha^* - i\lambda\beta^* \Big) \\
& + \partial_\beta \Big((\gamma + i\omega + ig(\chi + \chi^*))\alpha + i\lambda\alpha \Big) + \partial_{\beta^*} \Big((\gamma - i\omega - ig(\chi + \chi^*))\alpha^* - i\lambda\alpha^* \Big) \\
& + \partial_\chi \Big(i\Omega\chi - ig \left(|\alpha|^2 - |\beta|^2 \right) \Big) + \partial_{\chi^*} \Big(- i\Omega\chi^* + ig \left(|\alpha|^2 - |\beta|^2 \right) \Big) \\
& + \partial_\alpha \partial_{\alpha^*} \Big((2\bar{n}_a + 1 - z)\gamma \Big) + \partial_\beta \partial_{\beta^*} \Big((2\bar{n}_b + 1 - z)\gamma \Big) \\
& + \partial_\chi \partial_\alpha (izg\alpha) + \partial_{\chi^*} \partial_{\alpha^*} (-izg\alpha^*) + \partial_\chi \partial_\beta (-izg\beta) + \partial_{\chi^*} \partial_{\beta^*} (izg\beta^*) \\
& - ig\frac{z^2 - 1}{4}(\partial_\chi - \partial_{\chi^*})\partial_\alpha \partial_{\alpha^*} + ig\frac{z^2 - 1}{4}(\partial_\chi - \partial_{\chi^*})\partial_\beta \partial_{\beta^*} \Big] F_z(\alpha, \beta, \chi, t).
\end{aligned} \tag{77}
$$

3.4   Truncated Wigner

As we showed above, in order to obtain a positive semidefinite diffusion matrix we have to use the Wigner distribution which contains third order derivatives. Neglecting those terms, gives a Fokker Planck equation which is the truncated Wigner evolution equation. There is strong evidence pointing out that this is the same as considering a sort of classical limit, with quantum noise replaced by a source of classical noise that tries to mimic quantum uncertainties, a scenario known as stochastic electrodynamics [13]. We will see this correspondence explicitly in the form of our final stochastic equations. Let us introduce this approach by considering the single-cavity model (73). Setting $z = 0$ in Eq (73) and truncating up to second order derivatives yields

$$
\begin{aligned}
\partial_t W(\alpha, \mathbf{R}, t) = \Big[& \partial_\alpha \Big((\gamma + i\omega - iGX)\alpha \Big) + \partial_{\alpha^*} \Big((\gamma - i\omega + iGX)\alpha^* \Big) \\
& + \partial_X (-P/m) + \partial_P \Big(- \hbar G \left(|\alpha|^2 + 1/2 \right) \Big) + \partial_\alpha \partial_{\alpha^*} \Big(\gamma(2\bar{n} + 1) \Big) \Big] W(\alpha, \mathbf{R}, t).
\end{aligned} \tag{78}
$$

Keeping the complex representation (see below for a proof of why we can do that), using equation (63) and ordering the variables as (α, α^*, X, P), the diffusion matrix reads

$$
D = (2\bar{n} + 1)\gamma \begin{pmatrix} 0 & 1 & 0 & 0 \\ 1 & 0 & 0 & 0 \\ 0 & 0 & 0 & 0 \\ 0 & 0 & 0 & 0 \end{pmatrix}, \tag{79}
$$

leading to a noise matrix

$$
B = \sqrt{(2\bar{n} + 1)\gamma} \begin{pmatrix} 1 & i \\ 1 & -i \\ 0 & 0 \\ 0 & 0 \end{pmatrix}. \tag{80}
$$

Hence, using (50) we find the system of stochastic equations

$$\dot{\alpha} = -(\gamma + i\omega_c - iGX)\alpha + \sqrt{(2\bar{n}+1)\gamma}\xi(t), \tag{81a}$$

$$\dot{X} = P/m, \tag{81b}$$

$$\dot{P} = \hbar G \left(|\alpha|^2 + 1/2 \right), \tag{81c}$$

where $\xi(t)$ is a complex, white, Gaussian noise, with $\overline{\xi(t)} = 0 = \overline{\xi(t)\xi(t')}$ and $\overline{\xi(t)\xi^*(t')} = \delta(t-t')$.

Note here that for $\gamma = 0$ the equations are fully deterministic. On the other hand, a complex additive noise term is what one expects from classical thermal noise. Hence, this shows that, as mentioned above, these equations are very close to the classical limit. There are a couple of subtle differences though. First, because of the symmetric order of the Wigner representation, the equations have small differences with respect to the fully classical ones, for example the factor $1/2$ in the last equation. On the other hand, even when the heat bath is at zero temperature ($\bar{n} = 0$), the noise term is different than zero. This comes from the fact that the truncated Wigner accounts for the quantum vacuum fluctuations, which are present even at zero temperature. Note however that all these differences are negligible in the limit $|\alpha|^2, \bar{n} \gg 1$, which one may regard as the true classical limit.

Let us now discuss why we can stay with the complex variables $\{\alpha, \alpha^*\}$ when writing the stochastic equations, instead of moving to the quadrature representation $\{x, p\}$, as we did in the previous section when analyzing the positivity of the diffusion matrix. To this aim, let us first define the matrix that connects these representations:

$$\underbrace{\begin{pmatrix} \alpha \\ \alpha^* \end{pmatrix}}_{\boldsymbol{\alpha}} = \underbrace{\frac{1}{2}\begin{pmatrix} 1 & 1 \\ i & -i \end{pmatrix}}_{R} \underbrace{\begin{pmatrix} x \\ p \end{pmatrix}}_{\mathbf{r}}. \tag{82}$$

Note that this matrix also allows us to connect the derivatives as $\boldsymbol{\partial} = R^T \bar{\boldsymbol{\partial}}$, where we have defined $\boldsymbol{\partial} = (\partial_x, \partial_p)^T$ and $\bar{\boldsymbol{\partial}} = (\partial_\alpha, \partial_{\alpha^*})^T$. Plugging these relations into the real Fokker-Planck equation (we show only the differential operator),

$$-\sum_j \partial_j A_j + \frac{1}{2}\sum_{jk} \partial_j \partial_k D_{jk} = -\sum_m \bar{\partial}_m \underbrace{\sum_j R_{mj} A_j}_{\bar{A}_m} + \frac{1}{2}\sum_{mn} \bar{\partial}_m \bar{\partial}_n \underbrace{\sum_{jk} R_{mj} R_{nk} D_{jk}}_{\bar{D}_{mn}}, \tag{83}$$

provides the relation between the drift vector and the diffusion matrix in the real and complex representations:

$$\bar{\mathbf{A}} = R\mathbf{A}, \qquad \bar{D} = RDR^T. \tag{84}$$

Since R is not orthogonal ($RR^T \neq \mathbb{1}$), it is clear that the eigenvalues of $\bar{D}$ and D are different. On the other hand, given a noise matrix for the real case, $D = BB^T$, the noise matrix $\bar{B} = RB$ decomposes the complex diffusion matrix, since $\bar{D} = RDR^T = RBB^T R^T = \bar{B}\bar{B}^T$. Moreover, given the stochastic equations in real form, $\dot{\mathbf{r}} = \mathbf{A} + B\boldsymbol{\eta}(t)$, the complex form reads $\dot{\boldsymbol{\alpha}} = R\dot{\mathbf{r}} = R\mathbf{A} + RB\boldsymbol{\eta}(t)$. This shows that the complex drift vector $\bar{\mathbf{A}}$ and noise matrix $\bar{B}$ defined above are indeed the ones appearing in the complex form of the stochastic equations.

Let us finally write down the truncated-Wigner stochastic equations associated to the general two-cavity models (75) and (77). Based on the previous derivations, it is straightforward to write the following stochastic equation associated to the piston model (75):

$$\dot{\alpha} = -(\gamma + i\omega_c - iGX)\alpha - i\lambda\beta + \sqrt{(2\bar{n}_a + 1)\gamma}\xi_a(t), \tag{85a}$$

$$\dot{\beta} = -(\gamma + i\omega_c + iGX)\beta - i\lambda\alpha + \sqrt{(2\bar{n}_b + 1)\gamma}\xi_b(t), \tag{85b}$$

$$\dot{X} = P/m, \tag{85c}$$

$$\dot{P} = \hbar G \left(|\alpha|^2 - |\beta|^2 \right), \tag{85d}$$

where the noises are complex, white, Gaussian, and independent, hence obeying the following statistics:

$$\overline{\xi_j(t)} = 0 = \overline{\xi_j(t)\xi_l(t')}, \qquad \overline{\xi_j(t)\xi_l^*(t')} = \delta_{jl}\delta(t - t'). \tag{86}$$

Similarly, for the membrane model (77) we obtain

$$\dot{\alpha} = -\big(\gamma + i\omega_c - ig(\chi + \chi^*)\big)\alpha - i\lambda\beta + \sqrt{(2\bar{n}_a + 1)\gamma}\,\xi_a(t), \tag{87a}$$

$$\dot{\beta} = -\big(\gamma + i\omega_c + ig(\chi + \chi^*)\big)\beta - i\lambda\alpha + \sqrt{(2\bar{n}_b + 1)\gamma}\,\xi_b(t), \tag{87b}$$

$$\dot{\chi} = -i\Omega\chi + ig\left(|\alpha|^2 - |\beta|^2\right). \tag{87c}$$

3.5 Positve P representation

The positive P distribution is a generalization of the Glauber-Sudarshan P distribution [7, 12]. Let us introduce it through the example of the single-cavity model (73). We will generalize the result to our models of interest (75) and (77) at the end of the section.

Remember that the good thing of the P distribution is that we didn't get third order derivatives, see (73) with $z = 1$. It had a problem though: the diffusion matrix is not positive semidefinite. Anyhow, suppose that we ignore the negativity of the diffusion matrix and we try to find a noise matrix satisfying the required diffusion matrix decomposition, $D = BB^T$. Indeed, it is possible to find such a noise matrix, but the remaining equations would not lead to complex-conjugate trajectories for α and α^*, signaling that something went wrong. This, on the other hand, can be interpreted as the oscillator trying to go out of its true phase space, into an extended one, where α^* is not the conjugate of α. The positive P distribution formally generates a representation where the oscillator is allowed to move in such an extended phase space. The drawback is that this means using two independent complex variables for each mode, instead of one. However, we will see that the payout is big: now we will be able to find stochastic equations representing the quantum dynamics without any approximations.

The rigorous definition of the positive P distribution in terms of a quantum characteristic function, as well as the corresponding correspondence rules to find phase-space equations from master equations, can be consulted in [6]. For our purposes, it is enough to point out that the phase-space equation can be retrieved from the Glauber-Sudarshan one simply by replacing α^* by a complex variable independent of α, which we usually denote by α^+.

Here, we also need to extend the phase space in the mechanical mode. Using the correspondences (76), the complex form of the evolution equation (73) for the Glauber-Sudarshan case ($z = 1$) takes the form

$$\partial_t P(\alpha, \chi, t) = \bigg[\partial_\alpha\Big(\big(\gamma + i\omega_c - iGx_0(\chi + \chi^*)\big)\alpha\Big) + \partial_{\alpha^*}\Big(\big(\gamma - i\omega_c + iGx_0(\chi + \chi^*)\big)\alpha^*\Big) \tag{88}$$

$$+ (\partial_\chi + \partial_{\chi^*})\left(\frac{ip_0}{2x_0 m}(\chi - \chi^*)\right) + (\partial_\chi - \partial_{\chi^*})\left(\frac{-i\hbar G}{2p_0}|\alpha|^2\right) + (\partial_\chi + \partial_{\chi^*})(\partial_\chi - \partial_{\chi^*})\left(\frac{ip_0}{4mx_0}\right)$$

$$+ \partial_\alpha\partial_{\alpha^*}(2\bar{n}\gamma) + (\partial_\chi - \partial_{\chi^*})(\partial_\alpha + \partial_{\alpha^*})\left(\frac{i\hbar G}{4p_0}\alpha\right) + (\partial_\chi + \partial_{\chi^*})(\partial_\alpha - \partial_{\alpha^*})\left(\frac{iGx_0}{2}\alpha\right)\bigg]P(\alpha, \chi, t).$$

From this equation, the evolution equation of the positive P distribution is found simply by

replacing χ^* and α^* by the independent complex variables χ^+ and α^+, respectively, obtaining

$$
\partial_t P^+(\boldsymbol{\alpha}, t) = \left[\partial_\alpha \underbrace{\left((\gamma + i\omega_c - iGx_0(\chi + \chi^+))\alpha \right)}_{-A_\alpha} + \partial_{\alpha^+} \underbrace{\left((\gamma - i\omega_c + iGx_0(\chi + \chi^+))\alpha^+ \right)}_{-A_{\alpha^+}} \right.
$$

$$
+ \partial_\chi \underbrace{\left(\frac{ip_0^2}{m\hbar} (\chi - \chi^+) - iGx_0\alpha^+\alpha \right)}_{-A_\chi} + \partial_{\chi^+} \underbrace{\left(\frac{ip_0^2}{m\hbar} (\chi - \chi^+) + iGx_0\alpha^+\alpha \right)}_{-A_{\chi^+}}
$$

$$
\left. + \partial_\chi^2 \left(\frac{ip_0^2}{2m\hbar} \right) + \partial_{\chi^+}^2 \left(\frac{-ip_0^2}{2m\hbar} \right) + \partial_\alpha\partial_{\alpha^+}(2\bar{n}\gamma) + \partial_\chi\partial_\alpha(iGx_0\alpha) + \partial_{\chi^+}\partial_{\alpha^+}(-iGx_0\alpha^+) \right] P^+(\boldsymbol{\alpha}, t),
$$

where we have gathered all the complex stochastic variables into $\boldsymbol{\alpha} = (\alpha, \alpha^+, \chi, \chi^+)^T$ and denoted by P^+ the positive P distribution. Note that the complex-conjugate of these variables do not appear anywhere in the equation or the distribution, and therefore, everything is analytic (in the complex sense) in this equation. This means that we can choose the direction of derivation in the complex plane at will (e.g., $\partial_\alpha = \partial_{\mathrm{Re}\{\alpha\}} = -i\partial_{\mathrm{Im}\{\alpha\}}$), and it is possible to show [7, 12, 14] that there is always a choice that turns this equation into a true Fokker-Planck equation. Therefore, P^+ stays a probability density function if it is so initially (we will show later in Section 4.3.2 that it is indeed a true probability density function for all quantum state). This is the virtue of the positive P representation.

Let's proceed now to find the corresponding set of stochastic equations. Ordering the variables as in $\boldsymbol{\alpha}$, the (complex) diffusion matrix reads

$$
D = \begin{pmatrix} 0 & 2\bar{n}\gamma & iGx_0\alpha & 0 \\ 2\bar{n}\gamma & 0 & 0 & -iGx_0\alpha^+ \\ iGx_0\alpha & 0 & ip_0^2/m\hbar & 0 \\ 0 & -iGx_0\alpha^+ & 0 & -ip_0^2/m\hbar \end{pmatrix}.
\tag{90}
$$

Finding a 4×4 noise matrix that satisfies $D = BB^T$ is not easy. We use the following trick. First, we write the diffusion matrix as the sum of two matrices, $D = D_1 + D_2$, with

$$
D_1 = \begin{pmatrix} 0 & 2\bar{n}\gamma & 0 & 0 \\ 2\bar{n}\gamma & 0 & 0 & 0 \\ 0 & 0 & ip_0^2/m\hbar & 0 \\ 0 & 0 & 0 & -ip_0^2/m\hbar \end{pmatrix},
\tag{91a}
$$

$$
D_2 = \begin{pmatrix} 0 & 0 & iGx_0\alpha & 0 \\ 0 & 0 & 0 & -iGx_0\alpha^+ \\ iGx_0\alpha & 0 & 0 & 0 \\ 0 & -iGx_0\alpha^+ & 0 & 0 \end{pmatrix}.
\tag{91b}
$$

Each of these matrices is easy to decompose as $D_1 = B_1 B_1^T$ and $D_2 = B_2 B_2^T$, specifically with

$$
B_1 = \begin{pmatrix} \sqrt{\bar{n}\gamma} & i\sqrt{\bar{n}\gamma} & 0 & 0 \\ \sqrt{\bar{n}\gamma} & -i\sqrt{\bar{n}\gamma} & 0 & 0 \\ 0 & 0 & \sqrt{ip_0^2/m\hbar} & 0 \\ 0 & 0 & 0 & \sqrt{-ip_0^2/m\hbar} \end{pmatrix},
\tag{92a}
$$

$$
B_2 = \sqrt{\frac{iGx_0}{2}} \begin{pmatrix} i\sqrt{\alpha} & \sqrt{\alpha} & 0 & 0 \\ 0 & 0 & -\sqrt{\alpha^+} & i\sqrt{\alpha^+} \\ -i\sqrt{\alpha} & \sqrt{\alpha} & 0 & 0 \\ 0 & 0 & \sqrt{\alpha^+} & i\sqrt{\alpha^+} \end{pmatrix}.
\tag{92b}
$$

Then if we use a noise matrix $B = (B_1 \ B_2)$ with dimensions 4×8, we get the desired decomposition

$$BB^T = (B_1 \ B_2) \begin{pmatrix} B_1^T \\ B_2^T \end{pmatrix} = B_1 B_1^T + B_2 B_2^T = D_1 + D_2 = D.$$

The fact that the 'internal' dimension of B is larger than the dimension of D, means that the stochastic representation will be more expensive (in terms of number of noises required for the simulation) than it could be.

The system of stochastic equations equivalent to the Fokker-Planck equation (89) is then given by:

$$\underset{4\times 1}{\dot{\boldsymbol{\alpha}}} = \underset{4\times 1}{\mathbf{A}(\alpha)} + \underset{4\times 8}{B(\alpha)} \underset{8\times 1}{\boldsymbol{\eta}(t)}, \tag{93}$$

where the components of $\boldsymbol{\eta}(t)$ are real, white, independent, Gaussian noises satisfying the statistics (51). It is interesting to note at this point that the positive P distribution allows to evaluate expectation values in normal order, similarly to the Glauber-Sudarshan representation. For example, considering a single oscillator for simplicity, we have

$$\langle a^{\dagger m} a^n \rangle = \int_{\mathbb{C}^2} d^2\alpha \, d^2\alpha^+ P^+(\alpha, \alpha^+) \alpha^{+m} \alpha^n = \overline{\alpha^{+m} \alpha^n}. \tag{94}$$

Let us now write down the explicitly form of the stochastic equations. We start by identifying the form of the noise terms:

$$\dot{\alpha} = A_\alpha + \sqrt{\bar{n}\gamma}\big(\eta_1(t) + i\eta_2(t)\big) + \sqrt{iGx_0\alpha/2}\,\big(i\eta_5(t) + \eta_6(t)\big), \tag{95a}$$

$$\dot{\alpha}^+ = A_{\alpha^+} + \sqrt{\bar{n}\gamma}\big(\eta_1(t) - i\eta_2(t)\big) + \sqrt{iGx_0\alpha^+/2}\,\big(-\eta_7(t) + i\eta_8(t)\big), \tag{95b}$$

$$\dot{\chi} = A_\chi + \sqrt{ip_0^2/m\hbar}\,\eta_3(t) + \sqrt{iGx_0\alpha/2}\,\big(-i\eta_5(t) + \eta_6(t)\big), \tag{95c}$$

$$\dot{\chi}^+ = A_{\chi^+} + \sqrt{-ip_0^2/m\hbar}\,\eta_4(t) + \sqrt{iGx_0\alpha^+/2}\,\big(\eta_7(t) + i\eta_8(t)\big). \tag{95d}$$

Instead of working with 8 real noises, it feels then natural to define 4 independent complex noises,

$$\xi_1(t) = \big(\eta_1(t) + i\eta_2(t)\big)/\sqrt{2}, \tag{96a}$$

$$\xi_2(t) = \big(\eta_3(t) + i\eta_4(t)\big)\sqrt{2}, \tag{96b}$$

$$\xi_3(t) = \big(\eta_6(t) + i\eta_5(t)\big)\sqrt{2}, \tag{96c}$$

$$\xi_4(t) = \big(\eta_8(t) + i\eta_7(t)\big)\sqrt{2}, \tag{96d}$$

which satisfy the statistics (125). Let us also define position and momentum variables defined by

$$X = x_0(\chi + \chi^+), \tag{97a}$$

$$P = -ip_0(\chi - \chi^+), \tag{97b}$$

which we remark are in general not the real position and momentum of the piston, but complex variables (χ and χ^+ are not complex-conjugate) living in the extended positive-P phase space.

The final system of stochastic equations associated to the master equation (26) is then given by

$$\dot{\alpha} = -(\gamma + i\omega_c - iGX)\alpha + \sqrt{2\gamma\bar{n}}\xi_1(t) + \sqrt{iGx_0\alpha}\xi_3(t), \tag{98a}$$

$$\dot{\alpha}^+ = -(\gamma - i\omega_c + iGX)\alpha^+ + \sqrt{2\gamma\bar{n}}\xi_1^*(t) + \sqrt{-iGx_0\alpha^+}\xi_4(t), \tag{98b}$$

$$\dot{X} = \frac{P}{m} + \sqrt{\frac{i\hbar}{2m}}\xi_2(t) + \sqrt{iGx_0^3}\left(i\sqrt{\alpha^+}\xi_4^*(t) + \sqrt{\alpha}\xi_3^*(t)\right), \tag{98c}$$

$$\dot{P} = \hbar G\alpha^+\alpha - i\sqrt{\frac{2ip_0^4}{m\hbar}}\xi_2^*(t) + \sqrt{-iGx_0p_0^2}\left(i\sqrt{\alpha^+}\xi_4^*(t) - \sqrt{\alpha}\xi_3^*(t)\right). \tag{98d}$$

Note that, as mentioned above, even if we set (α, χ) and (α^+, χ^+) complex conjugate initially, the equations will quickly destroy those relations. This is easy to see, for example, by realizing that the noise terms of $\dot{\alpha}$ and $\dot{\alpha}^+$ are not complex-conjugate.

Note that each noise term comes from a well-defined physical process that can be identified from the nature of the coefficients: $\xi_1(t)$ is the thermal noise entering the cavity from the environment, while $\xi_2(t)$ and $\xi_{3,4}(t)$ are associated to the free motion of the piston and the optomechanical interaction, respectively.

Let us finally provide the positive-P stochastic equations associated to the most general model (75) and (77). The generalization is straightforward. In the case of the piston (75) we get:

$$\dot{\alpha} = -(\gamma + i\omega_c - iGX)\alpha - i\lambda\beta + \sqrt{2\gamma\bar{n}_a}\xi_a(t) + \sqrt{iGx_0\alpha}\xi_1(t), \tag{99a}$$

$$\dot{\alpha}^+ = -(\gamma - i\omega_c + iGX)\alpha^+ + i\lambda\beta^+ + \sqrt{2\gamma\bar{n}_a}\xi_a^*(t) + \sqrt{-iGx_0\alpha^+}\xi_2(t), \tag{99b}$$

$$\dot{\beta} = -(\gamma + i\omega_c + iGX)\beta - i\lambda\alpha + \sqrt{2\gamma\bar{n}_b}\xi_b(t) + \sqrt{-iGx_0\beta}\xi_3(t), \tag{99c}$$

$$\dot{\beta}^+ = -(\gamma - i\omega_c - iGX)\beta^+ + i\lambda\alpha^+ + \sqrt{2\gamma\bar{n}_b}\xi_b^*(t) + \sqrt{iGx_0\beta^+}\xi_4(t), \tag{99d}$$

$$\dot{X} = \frac{P}{m} + \sqrt{\frac{i\hbar}{2m}}\xi_m(t) + \sqrt{iGx_0^3}\left(i\sqrt{\alpha^+}\xi_2^*(t) + \sqrt{\alpha}\xi_1^*(t) + i\sqrt{-\beta^+}\xi_4^*(t) + \sqrt{-\beta}\xi_3^*(t)\right), \tag{99e}$$

$$\dot{P} = \hbar G(\alpha^+\alpha - \beta^+\beta) - i\sqrt{\frac{2ip_0^4}{m\hbar}}\xi_m^*(t) \tag{99f}$$
$$+ \sqrt{-iGx_0p_0^2}\left(i\sqrt{\alpha^+}\xi_2^*(t) - \sqrt{\alpha}\xi_1^*(t) + i\sqrt{-\beta^+}\xi_4^*(t) - \sqrt{-\beta}\xi_3^*(t)\right),$$

where all the noises are independent, complex, white, and Gaussian.

In the case of the membrane, replacing $(\alpha^*, \beta^*, \chi^*)$ by $(\alpha^+, \beta^+, \chi^+)$ in (77), we obtain

$$\partial_t P^+(\boldsymbol{\alpha}, t) = \left[\partial_\alpha \left((\gamma + i\omega - ig(\chi + \chi^+))\alpha + i\lambda\beta \right) + \partial_{\alpha^+} \left((\gamma - i\omega + ig(\chi + \chi^+))\alpha^+ - i\lambda\beta^+ \right) \right.$$
$$+ \partial_\beta \left((\gamma + i\omega + ig(\chi + \chi^+))\alpha + i\lambda\alpha \right) + \partial_{\beta^+} \left((\gamma - i\omega - ig(\chi + \chi^+))\alpha^+ - i\lambda\alpha^+ \right)$$
$$+ \partial_\chi \left(i\Omega\chi - ig\left(\alpha^+\alpha - \beta\beta^+\right) \right) + \partial_{\chi^+} \left(-i\Omega\chi^+ + ig\left(\alpha^+\alpha - \beta\beta^+\right) \right) \tag{100}$$
$$+ \partial_\alpha\partial_{\alpha^+}\left(2\bar{n}_a\gamma\right) + \partial_\beta\partial_{\beta^+}\left(2\bar{n}_b\gamma\right) + \partial_\chi\partial_\alpha(ig\alpha) + \partial_{\chi^+}\partial_{\alpha^+}(-ig\alpha^+)$$
$$\left. + \partial_\chi\partial_\beta(-ig\beta) + \partial_{\chi^+}\partial_{\beta^+}(ig\beta^+) \right] P^+(\boldsymbol{\alpha}, t),$$

where we have again collected in a single vector $\boldsymbol{\alpha} = (\alpha, \alpha^+, \beta, \beta^+, \chi, \chi^+)$ all the complex stochastic

variables. The diffusion matrix can be written in this case as $D = D_1 + D_2 + D_3$, with

$$D_1 = \begin{pmatrix} 0 & 2\bar{n}_a\gamma & 0 & 0 & 0 & 0 \\ 2\bar{n}_a\gamma & 0 & 0 & 0 & 0 & 0 \\ 0 & 0 & 0 & 2\bar{n}_b\gamma & 0 & 0 \\ 0 & 0 & 2\bar{n}_b\gamma & 0 & 0 & 0 \\ 0 & 0 & 0 & 0 & 0 & 0 \\ 0 & 0 & 0 & 0 & 0 & 0 \end{pmatrix}, \tag{101a}$$

$$D_2 = \begin{pmatrix} 0 & 0 & 0 & 0 & ig\alpha & 0 \\ 0 & 0 & 0 & 0 & 0 & -ig\alpha^+ \\ 0 & 0 & 0 & 0 & 0 & 0 \\ 0 & 0 & 0 & 0 & 0 & 0 \\ ig\alpha & 0 & 0 & 0 & 0 & 0 \\ 0 & -ig\alpha^+ & 0 & 0 & 0 & 0 \end{pmatrix}, \tag{101b}$$

$$D_3 = \begin{pmatrix} 0 & 0 & 0 & 0 & 0 & 0 \\ 0 & 0 & 0 & 0 & 0 & 0 \\ 0 & 0 & 0 & 0 & -ig\beta & 0 \\ 0 & 0 & 0 & 0 & 0 & ig\beta^+ \\ 0 & 0 & -ig\beta & 0 & 0 & 0 \\ 0 & 0 & 0 & ig\beta^+ & 0 & 0 \end{pmatrix}. \tag{101c}$$

Each of these matrices can be easily decomposed as $D_j = B_j B_j^T$ similarly to what we did above:

$$B_1 = \begin{pmatrix} \sqrt{\bar{n}_a\gamma} & i\sqrt{\bar{n}_a\gamma} & 0 & 0 \\ \sqrt{\bar{n}_a\gamma} & -i\sqrt{\bar{n}_a\gamma} & 0 & 0 \\ 0 & 0 & \sqrt{\bar{n}_b\gamma} & i\sqrt{\bar{n}_b\gamma} \\ 0 & 0 & \sqrt{\bar{n}_b\gamma} & -i\sqrt{\bar{n}_b\gamma} \\ 0 & 0 & 0 & 0 \\ 0 & 0 & 0 & 0 \end{pmatrix}, \tag{102a}$$

$$B_2 = \sqrt{\frac{ig}{2}} \begin{pmatrix} i\sqrt{\alpha} & \sqrt{\alpha} & 0 & 0 \\ 0 & 0 & -\sqrt{\alpha^+} & i\sqrt{\alpha^+} \\ 0 & 0 & 0 & 0 \\ 0 & 0 & 0 & 0 \\ -i\sqrt{\alpha} & \sqrt{\alpha} & 0 & 0 \\ 0 & 0 & \sqrt{\alpha^+} & i\sqrt{\alpha^+} \end{pmatrix}, \tag{102b}$$

$$B_3 = \sqrt{-\frac{ig}{2}} \begin{pmatrix} 0 & 0 & 0 & 0 \\ 0 & 0 & 0 & 0 \\ i\sqrt{\beta} & \sqrt{\beta} & 0 & 0 \\ 0 & 0 & -\sqrt{\beta^+} & i\sqrt{\beta^+} \\ -i\sqrt{\beta} & \sqrt{\beta} & 0 & 0 \\ 0 & 0 & \sqrt{\beta^+} & i\sqrt{\beta^+} \end{pmatrix}. \tag{102c}$$

The total noise matrix is then built as $B = (B_1 \; B_2 \; B_3)$, leading to the stochastic equations

$$\dot{\alpha} = -\big(\gamma + i\omega_c - ig(\chi + \chi^+)\big)\alpha - i\lambda\beta + \sqrt{2\bar{n}_a\gamma}\xi_a(t) + \sqrt{ig\alpha}\xi_1(t), \tag{103a}$$

$$\dot{\alpha}^+ = -\big(\gamma - i\omega_c + ig(\chi + \chi^+)\big)\alpha^+ + i\lambda\beta^+ + \sqrt{2\bar{n}_a\gamma}\xi_a^*(t) + \sqrt{-ig\alpha^+}\xi_2(t), \tag{103b}$$

$$\dot{\beta} = -\big(\gamma + i\omega_c + ig(\chi + \chi^+)\big)\beta - i\lambda\alpha + \sqrt{2\bar{n}_b\gamma}\xi_b(t) + \sqrt{-ig\beta}\xi_3(t), \tag{103c}$$

$$\dot{\beta}^+ = -\big(\gamma - i\omega_c - ig(\chi + \chi^+)\big)\beta^+ + i\lambda\alpha^+ + \sqrt{2\bar{n}_b\gamma}\xi_b^*(t) + \sqrt{ig\beta^+}\xi_4(t), \tag{103d}$$

$$\dot{\chi} = -i\Omega\chi + ig\big(\alpha^+\alpha - \beta\beta^+\big) + \sqrt{ig\alpha}\xi_1^*(t) + \sqrt{-ig\beta}\xi_3^*(t), \tag{103e}$$

$$\dot{\chi}^+ = i\Omega\chi^+ - ig\big(\alpha^+\alpha - \beta\beta^+\big) + \sqrt{-ig\alpha^+}\xi_2^*(t) + \sqrt{ig\beta^+}\xi_4^*(t). \tag{103f}$$

3.6 Relation between the covariance matrix and stochastic averages

In the previous sections we have found the stochastic equations that we will use to simulate the dynamics of the system numerically. Reconstructing the full state (density operator) from the stochastically sampled variables is in most situations impossible. Instead, we have to focus on the evaluation of expectation values of specific observables. For Gaussian states, the first and second order moments of the basic bosonic operators of the system would indeed suffice to characterize the full state [4, 5]. Even for non-Gaussian states, these lowest order moments are usually the most interesting ones, as they are related to the expectation value and uncertainty of the electromagnetic field or the mechanical variables. Higher-order moments can be evaluated to check how much the state differs from a Gaussian one. In this section we explain how to find these important first and second order moments from the different phase-space stochastic representations that we have developed (truncated Wigner in Section 3.4 and positive P in Section 3.5).

3.6.1 The covariance matrix

Let us start with some definitions (for clarity, in this section we bring back the 'hat' notation for operators so we don't confuse them with their associated stochastic variables). We define the vector of quadratures $\hat{\mathbf{r}} = (\hat{x}_a, \hat{p}_a, \hat{x}_b, \hat{p}_b, \hat{x}_c, \hat{p}_c)$, where $\hat{x}_m = \hat{m} + \hat{m}^\dagger$ and $\hat{p}_m = -i(\hat{m} - \hat{m}^\dagger)$. Note that in the piston case, we have $\hat{x}_c = \hat{X}/x_0$ and $\hat{p}_c = \hat{P}/p_0$. The first and second order moments of these modes are then compactly expressed through the mean vector $\mathbf{d}$ and the covariance matrix V, with elements

$$d_j = \langle \hat{r}_j \rangle, \qquad V_{jl} = \frac{1}{2}\langle \delta\hat{r}_j \delta\hat{r}_l + \delta\hat{r}_l \delta\hat{r}_j \rangle, \tag{104}$$

where given any operator $\hat{A}$ we denote its fluctuations around the mean by $\delta\hat{A} = \hat{A} - \langle\hat{A}\rangle$.

Sometimes it is useful to work with a different representation for the moments, a complex one defined through annihilation and creation operators. Let us introduce it now as well. Define the vector operator $\hat{\boldsymbol{\alpha}} = (\hat{a}, \hat{a}^\dagger, \hat{b}, \hat{b}^\dagger, \hat{c}, \hat{c}^\dagger)$, where the relations $\hat{m} = (\hat{x}_m + i\hat{p}_m)/2$ with the quadratures hold. Then, we define the complex mean vector $\boldsymbol{\Delta}$ and covariance matrix Λ, with elements

$$\Delta_j = \langle \hat{\alpha}_j \rangle, \qquad \Lambda_{jl} = \langle \delta\hat{\alpha}_j \delta\hat{\alpha}_l \rangle, \tag{105}$$

Our goal now is to connect these expressions to stochastic averages. Because the Wigner and positive P representations correspond to different orderings of quantum expectation values (symmetric and normal order, respectively), we have to be careful.

Before we proceed, it is useful to remark that the commutation relations can be written in the compact form

$$[\hat{r}_j, \hat{r}_l] = 2i\Omega_{jl}, \qquad [\hat{\alpha}_j, \hat{\alpha}_l] = \Omega_{jl}, \tag{106}$$

where we have defined the so-called symplectic form

$$\Omega = \begin{pmatrix} \mathbb{w} & \mathbb{0} & \mathbb{0} \\ \mathbb{0} & \mathbb{w} & \mathbb{0} \\ \mathbb{0} & \mathbb{0} & \mathbb{w} \end{pmatrix}, \quad \text{with } \mathbb{w} = \begin{pmatrix} 0 & 1 \\ -1 & 0 \end{pmatrix}, \tag{107}$$

and $\mathbb{0}$ is a matrix of zeros.

3.6.2 Connection with Wigner stochastic averages

Let us define the vector of stochastic quadratures $\mathbf{r} = (x_\alpha, p_\alpha, x_\beta, p_\beta, x_\chi, p_\chi)$, with $x_\mu = \mu + \mu^*$ and $p_\mu = -i(\mu - \mu^*)$ within the Wigner representation. From it, we define the stochastic mean vector

$\mathbf{d}^{(W)}$ and covariance matrix $V^{(W)}$ with elements

$$d_j^{(W)} = \overline{r_j}, \qquad V_{jl}^{(W)} = \overline{\delta r_j \delta r_l}, \tag{108}$$

where for any stochastic variable A we define a corresponding fluctuation $\delta A = A - \overline{A}$. Now, recalling that within the Wigner representation stochastic averages correspond to symmetrically ordered quantum expectation values, and noting that expressions (104) are already in symmetric order, we then get the simple relation

$$\mathbf{d} = \mathbf{d}^{(W)}, \qquad V = V^{(W)}. \tag{109}$$

Let us now define the complex vector $\boldsymbol{\alpha} = (\alpha, \alpha^*, \beta, \beta^*, \chi, \chi^*)$, and the corresponding complex stochastic mean vector $\boldsymbol{\Delta}^{(W)}$ and covariance matrix $\Lambda^{(W)}$, with elements

$$\Delta_j^{(W)} = \overline{\alpha_j}, \qquad \Lambda_{jl}^{(W)} = \overline{\delta\alpha_j \delta\alpha_l}. \tag{110}$$

In order to relate these with (105), we first need to write the covariance matrix in symmetric order. This is easy using the commutation relations (106), specifically

$$\Lambda_{jl} = \langle \delta\hat{\alpha}_j \delta\hat{\alpha}_l \rangle = \frac{1}{2} \left(\langle \delta\hat{\alpha}_j \delta\hat{\alpha}_l \rangle + \langle \delta\hat{\alpha}_l \delta\hat{\alpha}_j \rangle + \Omega_{jl} \right) = \overline{\delta\alpha_j \delta\alpha_l} + \Omega_{jl}/2. \tag{111}$$

Hence, we obtain the relations

$$\boldsymbol{\Delta} = \boldsymbol{\Delta}^{(W)}, \qquad \Lambda = \Lambda^{(W)} + \frac{\Omega}{2}. \tag{112}$$

As interesting specific relations, note that (109) tells us that the variance of any quadrature is directly related to the corresponding stochastic expression, $\langle \delta\hat{x}_a^2 \rangle = \overline{\delta x_\alpha^2}$, while (112) shows that the mean photon numbers are related by a $1/2$ shift, $\langle \delta\hat{a}^\dagger \delta\hat{a} \rangle = \overline{\delta\alpha^* \delta\alpha} - 1/2$.

3.6.3 Connection with positive-P stochastic averages

Let's proceed similarly now with the stochastic variables associated to the positive P representation. We define again the vector of stochastic quadratures $\mathbf{r} = (x_\alpha, p_\alpha, x_\beta, p_\beta, x_\chi, p_\chi)$, but now with $x_\mu = \mu + \mu^+$ and $p_\mu = -i(\mu - \mu^+)$. From it, we define the stochastic mean vector $\mathbf{d}^{(P)}$ and covariance matrix $V^{(P)}$ with elements

$$d_j^{(P)} = \overline{r_j}, \qquad V_{jl}^{(P)} = \overline{\delta r_j \delta r_l}. \tag{113}$$

Before connecting these with (104), we need to bring the covariance matrix to normal order. This is very easy, because in the expression of the covariance matrix only terms of the form $\hat{a}\hat{a}^\dagger = 1 + \hat{a}^\dagger \hat{a}$ (and similarly for the other modes) are not in normal order. But these appear only in the diagonal, e.g., $\hat{x}_a^2 = \hat{a}^2 + \hat{a}^{\dagger 2} + \hat{a}^\dagger \hat{a} + \hat{a}\hat{a}^\dagger = 1 + : \hat{x}_a^2 :$, where the notation '$: :$' means arranging in normal order as if operators would commute, e.g., $: \hat{a}\hat{a}^\dagger := \hat{a}^\dagger \hat{a}$. Hence, we find the relations

$$\mathbf{d} = \mathbf{d}^{(P)}, \qquad V = \mathbb{1} + V^{(P)}, \tag{114}$$

where $\mathbb{1}$ is the identity matrix.

We define next the complex vector $\boldsymbol{\alpha} = (\alpha, \alpha^+, \beta, \beta^+, \chi, \chi^+)$, and the corresponding complex stochastic mean vector $\boldsymbol{\Delta}^{(P)}$ and covariance matrix $\Lambda^{(P)}$, with elements

$$\Delta_j^{(P)} = \overline{\alpha_j}, \qquad \Lambda_{jl}^{(P)} = \overline{\delta\alpha_j \delta\alpha_l}. \tag{115}$$

In order to relate these with (105), we first need to write the complex covariance matrix in normal order. Note that only the upper triangular of Λ contains terms that are not in normal order.

Specifically, it contains antinormal terms such as $\hat{a}\hat{a}^\dagger = \hat{a}^\dagger\hat{a} + 1$ (and similarly for the other modes). Defining the matrix Υ containing only the upper triangular of Ω and zeros everywhere else, we then obtain

$$\boldsymbol{\Delta} = \boldsymbol{\Delta}^{(P)}, \qquad \Lambda = \Lambda^{(P)} + \Upsilon, \tag{116}$$

with

$$\Upsilon = \begin{pmatrix} \mathbb{s} & \mathbb{0} & \mathbb{0} \\ \mathbb{0} & \mathbb{s} & \mathbb{0} \\ \mathbb{0} & \mathbb{0} & \mathbb{s} \end{pmatrix}, \quad \text{with } \mathbb{s} = \begin{pmatrix} 0 & 1 \\ 0 & 0 \end{pmatrix}. \tag{117}$$

Equations (109), (112), (114), and (116) provide us with the relations we need to evaluate any desired quantum moments up to second order from the corresponding phase-space stochastic representation.

4 Benchmarking stochastic simulations: isolated systems

In the previous chapters we introduced the tools and the mathematical description of the autonomous thermodynamical machines we are interested in: two cavities interacting with heat baths, and coupled to a mechanical element that can be a piston or a membrane. In both cases we have developed stochastic Langevin equations that should allow us to sample both the classical and quantum dynamics of the system, see, respectively, (85) and (99) for the piston, or (87) and (103) for the membrane. In order to benchmark the simulation of these stochastic equations, we would like to have some analytic results to which we can compare to. As we show in Section 4.2, this is indeed possible if we forget about the environments and the beam splitter, setting $\gamma = 0 = \lambda$. Then, in Section 4.3 we solve numerically the corresponding stochastic equations, and compare with the exact results. This will also provide the first opportunity to analyze the effects of entanglement by comparing separable with entangled initial conditions.

4.1 Dimensionless equations

Before performing numerical simulations, it is important to identify the relevant free parameters of the equations. In this section we introduce some variable changes that will allow us to find these easily. For starters, we move to a picture rotating at the cavity frequency for the optical variables, that is, we make the variable change $\bar{\alpha} = e^{i\omega_c t}\alpha$, and similarly for the rest of optical variables. Since the noises are delta-correlated (white), this change does not affect the form of the equations, except for now the terms with ω_c go away. Moreover, in order to ease the notation, we don't add the 'bar' in the variables.

4.1.1 Classical limit: dimensionless truncated Wigner equations

In the absence of coupling to the environment ($\gamma = 0$), the stochastic equations of the piston model within the truncated Wigner representation (85) read

$$\dot{\alpha} = iGX\alpha - i\lambda\beta, \tag{118a}$$

$$\dot{\beta} = -iGX\beta - i\lambda\alpha, \tag{118b}$$

$$\dot{X} = P/m, \tag{118c}$$

$$\dot{P} = \hbar G\left(|\alpha|^2 - |\beta|^2\right). \tag{118d}$$

In order to make the equations dimensionless, we simply introduce arbitrary length scales for position and momentum, x_0 and $p_0 = \hbar/2x_0$, and then define the mechanical quadratures $x = X/x_0$ and $p = P/p_0$. Note these quadratures were called x_χ and p_χ in Section 3.6, but here we drop the subindex χ since we don't need to distinguish them from the optical quadratures. A comment on x_0: while it is arbitrary, in our case it will be chosen to match the width of the initial wavefunction of the piston, as we will see later. Introducing this change, we get

$$\dot{\alpha} = iGx_0 x\alpha - i\lambda\beta, \tag{119a}$$

$$\dot{\beta} = -iGx_0 x\beta - i\lambda\alpha, \tag{119b}$$

$$\dot{x} = (p_0/mx_0)p, \tag{119c}$$

$$\dot{p} = \hbar Gp_0\left(|\alpha|^2 - |\beta|^2\right). \tag{119d}$$

Hence, defining the frequency $\Omega = p_0/mx_0 = \hbar/2mx_0^2$ and the optomechanical coupling rate $g = Gx_0$, we get

$$\dot{\alpha} = igx\alpha - i\lambda\beta, \tag{120a}$$

$$\dot{\beta} = -igx\beta - i\lambda\alpha, \tag{120b}$$

$$\dot{x} = \Omega p, \tag{120c}$$

$$\dot{p} = 2g\left(|\alpha|^2 - |\beta|^2\right). \tag{120d}$$

Finally, we see that defining a new dimensionless time $\bar{t} = \Omega t$, and normalizing all the rates to Ω, that is, $\bar{g} = g/\Omega$ and $\bar{\lambda} = \lambda/\Omega$, we obtain the equations

$$\dot{\alpha} = i\bar{g}x\alpha - i\bar{\lambda}\beta, \tag{121a}$$

$$\dot{\beta} = -i\bar{g}x\beta - i\bar{\lambda}\alpha, \tag{121b}$$

$$\dot{x} = p, \tag{121c}$$

$$\dot{p} = 2\bar{g}\left(|\alpha|^2 - |\beta|^2\right), \tag{121d}$$

where now the 'dot' must be understood as derivative with respect to $\bar{t}$. These equations depend only on two parameters, the normalized optomechanical interaction $\bar{g}$ and beam-splitter coupling $\bar{\lambda}$. Of course, we will also have any parameters that may come from the initial condition, e.g., the width of the piston's wavefunction, the photon number of the cavities if we consider thermal states, or the entanglement if we consider entangled states, etc. Later we will provide specific examples.

Note that we could even remove $\bar{g}$ from the equations by normalizing all the stochastic variables to it. However, we prefer not to do this, because this is specific to the truncated Wigner, and moreover makes the limit $\bar{g} \to 0$ rather obscure.

Applying the same changes to the membrane equations (87), we obtain

$$\dot{\alpha} = i\bar{g}(\chi + \chi^*)\alpha - i\bar{\lambda}\beta, \tag{122a}$$

$$\dot{\beta} = -ig(\chi + \chi^*)\beta - i\bar{\lambda}\alpha, \tag{122b}$$

$$\dot{\chi} = -i\chi + i\bar{g}\left(|\alpha|^2 - |\beta|^2\right), \tag{122c}$$

which, as it turns out, depend on exactly the same parameters as (121).

4.1.2 Quantum dynamics: postive P equations

Let us now do a similar derivation for the stochastic equations associated with the positive P representation, which should capture the full quantum dynamics. As in the previous section, let us start with the piston equations (99). In terms of the mechanical quadratures $x = X/x_0$ and

$p = P/p_0$, which we remind are complex in this representation, the equations read

$$\dot{\alpha} = iGx_0x\alpha - i\lambda\beta + \sqrt{iGx_0\alpha}\xi_1(t), \tag{123a}$$

$$\dot{\alpha}^+ = -iGx_0x\alpha^+ + i\lambda\beta^+ + \sqrt{-iGx_0\alpha^+}\xi_2(t), \tag{123b}$$

$$\dot{\beta} = -iGx_0x\beta - i\lambda\alpha + \sqrt{-iGx_0\beta}\xi_3(t), \tag{123c}$$

$$\dot{\beta}^+ = iGx_0x\beta^+ + i\lambda\alpha^+ + \sqrt{iGx_0\beta^+}\xi_4(t), \tag{123d}$$

$$\dot{x} = \left(\frac{p_0}{mx_0}\right)p + \sqrt{\frac{i\hbar}{2mx_0^2}}\xi_m(t), \tag{123e}$$

$$+ \sqrt{iGx_0}\Big(i\sqrt{\alpha^+}\xi_2^*(t) + \sqrt{\alpha}\xi_1^*(t) + i\sqrt{-\beta^+}\xi_4^*(t) + \sqrt{-\beta}\xi_3^*(t)\Big),$$

$$\dot{p} = \frac{\hbar G}{p_0}(\alpha^+\alpha - \beta^+\beta) - i\sqrt{\frac{2ip_0^2}{m\hbar}}\xi_m^*(t) \tag{123f}$$

$$+ \sqrt{-iGx_0}\Big(i\sqrt{\alpha^+}\xi_2^*(t) - \sqrt{\alpha}\xi_1^*(t) + i\sqrt{-\beta^+}\xi_4^*(t) - \sqrt{-\beta}\xi_3^*(t)\Big).$$

Using $x_0p_0 = \hbar/2$, we see that the frequency $\Omega = \hbar/2mx_0^2$ appears rather naturally in the equations, together with the optomechanical coupling rate $g = Gx_0$. In terms of these, the equations read

$$\dot{\alpha} = igx\alpha - i\lambda\beta + \sqrt{ig\alpha}\xi_1(t), \tag{124a}$$

$$\dot{\alpha}^+ = -igx\alpha^+ + i\lambda\beta^+ + \sqrt{-ig\alpha^+}\xi_2(t), \tag{124b}$$

$$\dot{\beta} = -igx\beta - i\lambda\alpha + \sqrt{-ig\beta}\xi_3(t), \tag{124c}$$

$$\dot{\beta}^+ = igx\beta^+ + i\lambda\alpha^+ + \sqrt{ig\beta^+}\xi_4(t), \tag{124d}$$

$$\dot{x} = \Omega p + \sqrt{i\Omega}\xi_m(t) + \sqrt{ig}\Big(i\sqrt{\alpha^+}\xi_2^*(t) + \sqrt{\alpha}\xi_1^*(t) + i\sqrt{-\beta^+}\xi_4^*(t) + \sqrt{-\beta}\xi_3^*(t)\Big), \tag{124e}$$

$$\dot{p} = 2g(\alpha^+\alpha - \beta^+\beta) - i\sqrt{i\Omega}\xi_m^*(t) \tag{124f}$$

$$+ \sqrt{-ig}\Big(i\sqrt{\alpha^+}\xi_2^*(t) - \sqrt{\alpha}\xi_1^*(t) + i\sqrt{-\beta^+}\xi_4^*(t) - \sqrt{-\beta}\xi_3^*(t)\Big).$$

As before, we can use Ω to define a dimensionless time $\bar{t} = \Omega t$. However, in this case it becomes then convenient to define new noises $\bar{\xi}(\bar{t}) = \xi(t)/\sqrt{\Omega}$, so that the two-time correlators remain the usual ones (125), but now with respect to the dimensionless time,

$$\overline{\bar{\xi}_j(\bar{t})\bar{\xi}_l(\bar{t}')} = 0, \qquad \overline{\bar{\xi}_j(\bar{t})\bar{\xi}_l^*(\bar{t}')} = \delta_{jl}\delta(\bar{t} - \bar{t}'). \tag{125}$$

In the following, we remove the hats from the noises though, in order to ease the notation. With this change, the final dimensionless equations for the piston read

$$\dot{\alpha} = i\bar{g}x\alpha - i\bar{\lambda}\beta + \sqrt{i\bar{g}\alpha}\xi_1(\bar{t}), \tag{126a}$$

$$\dot{\alpha}^+ = -i\bar{g}x\alpha^+ + i\bar{\lambda}\beta^+ + \sqrt{-i\bar{g}\alpha^+}\xi_2(\bar{t}), \tag{126b}$$

$$\dot{\beta} = -i\bar{g}x\beta - i\bar{\lambda}\alpha + \sqrt{-i\bar{g}\beta}\xi_3(\bar{t}), \tag{126c}$$

$$\dot{\beta}^+ = i\bar{g}x\beta^+ + i\bar{\lambda}\alpha^+ + \sqrt{i\bar{g}\beta^+}\xi_4(\bar{t}), \tag{126d}$$

$$\dot{x} = p + \sqrt{i}\xi_m(\bar{t}) + \sqrt{i\bar{g}}\Big(i\sqrt{\alpha^+}\xi_2^*(\bar{t}) + \sqrt{\alpha}\xi_1^*(\bar{t}) + i\sqrt{-\beta^+}\xi_4^*(\bar{t}) + \sqrt{-\beta}\xi_3^*(\bar{t})\Big), \tag{126e}$$

$$\dot{p} = 2\bar{g}(\alpha^+\alpha - \beta^+\beta) - i\sqrt{i}\xi_m^*(\bar{t}) \tag{126f}$$

$$+ \sqrt{-i\bar{g}}\Big(i\sqrt{\alpha^+}\xi_2^*(\bar{t}) - \sqrt{\alpha}\xi_1^*(\bar{t}) + i\sqrt{-\beta^+}\xi_4^*(\bar{t}) - \sqrt{-\beta}\xi_3^*(\bar{t})\Big).$$

Remarkably, even though in this case we have many more (noise) terms, these equations depend on the same dimensionless parameters as their truncated Wigner counterparts, $\bar{g} = g/\Omega$ and $\bar{\lambda} = \lambda/\Omega$.

We can apply the same changes to the membrane equations (103), obtaining

$$\dot{\alpha} = i\bar{g}(\chi + \chi^+)\alpha - i\bar{\lambda}\beta + \sqrt{i\bar{g}\alpha}\,\xi_1(\bar{t}), \tag{127a}$$

$$\dot{\alpha}^+ = -i\bar{g}(\chi + \chi^+)\alpha^+ + i\bar{\lambda}\beta^+ + \sqrt{-i\bar{g}\alpha^+}\,\xi_2(\bar{t}), \tag{127b}$$

$$\dot{\beta} = -i\bar{g}(\chi + \chi^+)\beta - i\bar{\lambda}\alpha + \sqrt{-i\bar{g}\beta}\,\xi_3(\bar{t}), \tag{127c}$$

$$\dot{\beta}^+ = -i\bar{g}(\chi + \chi^+)\beta^+ + i\bar{\lambda}\alpha^+ + \sqrt{i\bar{g}\beta^+}\,\xi_4(\bar{t}), \tag{127d}$$

$$\dot{\chi} = -i\chi + i\bar{g}\left(\alpha^+\alpha - \beta\beta^+\right) + \sqrt{i\bar{g}\alpha}\,\xi_1^*(\bar{t}) + \sqrt{-i\bar{g}\beta}\,\xi_3^*(\bar{t}), \tag{127e}$$

$$\dot{\chi}^+ = i\chi^+ - i\bar{g}\left(\alpha^+\alpha - \beta\beta^+\right) + \sqrt{-i\bar{g}\alpha^+}\,\xi_2^*(\bar{t}) + \sqrt{i\bar{g}\beta^+}\,\xi_4^*(\bar{t}). \tag{127f}$$

Unlike in the truncated Wigner case, we see that now normalizing the stochastic variables to $\bar{g}$ doesn't remove the latter from the equations, as the noise terms would get a factor $\bar{g}$.

4.2 Analytic solutions for $\lambda = 0$

We now proceed to the derivation of some analytic solutions. This can only be done in the absence of beam-splitter coupling between the cavities, so we set $\lambda = 0$. Also, for the first time in the thesis, we will work in the Heisenberg picture. The analytic expressions for $\hat{X}(t)$, $\hat{P}(t)$, $\hat{a}(t)$, and $\hat{b}(t)$ will allow us to find any desired observables, and use them to benchmark the stochastic equations that we have developed. Note that in the reminder of the section we remove hats from operators, since being in the Heisenberg picture, no confusion is possible (we always refer to operators).

4.2.1 The piston model

The Hamiltonian for the piston model can be written as

$$H = \frac{P^2}{2m} - \hbar GX(\underbrace{a^\dagger a}_{n_a} - \underbrace{b^\dagger b}_{n_b}) = \frac{P^2}{2m} - \hbar GX\Delta n, \tag{128}$$

where we have denoted the photon number difference operator by $\Delta n = n_a - n_b$. Using the Heisenberg equation of motion $dA(t)/dt = [A(t), H/i\hbar]$ (valid for any operator A), we obtain the conservation of the number of photons of each cavity

$$\frac{dn_a}{dt} = 0 = \frac{dn_b}{dt} \quad \Rightarrow \quad n_a(t) = n_a(0), \;\; n_b(t) = n_b(0), \tag{129}$$

which of course implies the conservation of the photon number difference

$$\Delta n(t) = \Delta n(0). \tag{130}$$

Since this photon number difference is a constant of motion, the equations for position and momentum are trivial to solve. Specifically, we get for the momentum

$$\frac{dP}{dt} = [P, iGX\Delta n] = \hbar G\Delta n(t) \quad \Rightarrow \quad P(t) = P(0) + \hbar G\Delta n(0)t, \tag{131}$$

which leads to a position

$$\frac{dX}{dt} = \left[X, \frac{P^2}{2i\hbar m}\right] = \frac{P(t)}{m} \quad \Rightarrow \quad X(t) = X(0) + \frac{P(0)}{m}t + \frac{G\hbar}{2m}\Delta n(0)t^2. \tag{132}$$

With this equations at hand, it is easy to evaluate the expectation value of any mechanical observable. We will focus on the first and second order moments, that is, the mechanical mean vector and covariance matrix. As discussed in Section 3.6, we consider normalized versions of the position and momentum, $x = X/x_0$ and $p = P/p_0$, with $x_0 p_0 = \hbar/2$. In terms of these, the solutions read

$$x(\bar{t}) = x(0) + p(0)\bar{t} + \bar{g}\Delta n(0)\bar{t}^2, \tag{133a}$$
$$p(\bar{t}) = p(0) + 2\bar{g}\Delta n(0)\bar{t}, \tag{133b}$$

where we have introduced dimensionless time $\bar{t}$ and optomechanical rate $\bar{g}$ as introduced in the previous section. Taking the expectation value of these expressions, the mechanical mean vector $\mathbf{d} = (d_x, d_p)$ is found to be

$$d_x(\bar{t}) = \langle x(\bar{t}) \rangle = d_x(0) + d_p(0)\bar{t} + \bar{g}d_{\Delta n}\bar{t}^2, \tag{134a}$$
$$d_p(\bar{t}) = \langle p(\bar{t}) \rangle = d_p(0) + 2\bar{g}d_{\Delta n}\bar{t}, \tag{134b}$$

where we have defined the average photon number difference $d_{\Delta n} = \langle \Delta n(0) \rangle$. As a first thing to see here, note that the momentum will increase or decrease in time at a constant rate, which makes sense since the force applied to the piston is proportional to the radiation pressure, which is constant as $n(t) = n(0)$. If the piston is initially at rest, this leads to unidirectional motion, with constant acceleration, describing a parabola over time.

Let us now compute the mechanical covariance matrix, which we write as

$$V = \begin{pmatrix} V_{xx} & V_{xp} \\ V_{xp} & V_{pp} \end{pmatrix} = \begin{pmatrix} \langle \delta x^2 \rangle & \langle \{\delta x, \delta p\} \rangle/2 \\ \langle \{\delta x, \delta p\} \rangle/2 & \langle \delta p^2 \rangle \end{pmatrix}. \tag{135}$$

where we remind that, for any operator A, its fluctuation reads $\delta A = A - \langle A \rangle$. Note that, in our case, the position and momentum fluctuations at time t can be written in terms of the fluctuations at time zero as

$$\delta x(\bar{t}) = \delta x(0) + \delta p(0)\bar{t} + \bar{g}\delta\Delta n(0)\bar{t}^2, \tag{136a}$$
$$\delta p(\bar{t}) = \delta p(0) + 2\bar{g}\delta\Delta n(0)\bar{t}. \tag{136b}$$

This allows to trivially connect the covariance matrix at time t with that at time zero as

$$V_{xx}(\bar{t}) = V_{xx}(0) + 2V_{xp}(0)\bar{t} + V_{pp}(0)\bar{t}^2 + \bar{g}^2 V_{\Delta n}\bar{t}^4, \tag{137a}$$
$$V_{pp}(\bar{t}) = V_{pp}(0) + 4\bar{g}^2 V_{\Delta n}\bar{t}^2, \tag{137b}$$
$$V_{xp}(\bar{t}) = V_{xp}(0) + V_{pp}(0)\bar{t} + 2\bar{g}^2 V_{\Delta n}\bar{t}^3, \tag{137c}$$

where we have defined the variance of the photon number difference $V_{\Delta n} = \langle \delta\Delta n^2(0) \rangle$, and we have assumed that initially the optical cavities and the piston are uncorrelated, such that $\langle \delta x\Delta n \rangle = 0 = \langle \delta p\Delta n \rangle$.

For concreteness, we will assume that the piston starts with a Gaussian wave function of width x_0 and centered at $X = 0$. This corresponds then to the vacuum state of the annihilation operator $c = (x + ip)/2$, such that the initial mean vector and covariance matrix are

$$\mathbf{d}(0) = \begin{pmatrix} 0 \\ 0 \end{pmatrix}, \qquad V(0) = \begin{pmatrix} 1 & 0 \\ 0 & 1 \end{pmatrix}, \tag{138}$$

leading to

$$d_x(\bar{t}) = \bar{g}d_{\Delta n}\bar{t}^2, \tag{139a}$$
$$d_p(\bar{t}) = 2\bar{g}d_{\Delta n}\bar{t}, \tag{139b}$$
$$V_{xx}(\bar{t}) = 1 + \bar{t}^2 + \bar{g}^2 V_{\Delta n}\bar{t}^4, \tag{139c}$$
$$V_{pp}(\bar{t}) = 1 + 4\bar{g}^2 V_{\Delta n}\bar{t}^2, \tag{139d}$$
$$V_{xp}(\bar{t}) = \bar{t} + 2\bar{g}^2 V_{\Delta n}\bar{t}^3, \tag{139e}$$

41

As for the state of the cavities, we will use this opportunity to show that quantum correlations can make a huge difference. Specifically, we consider two different families of states, both characterized by the average photon number in the cavities, which we take the same, and call $\bar{n}$. The first family then corresponds to separable thermal states $\rho = \rho_{th}(\bar{n}) \otimes \rho_{th}(\bar{n})$. Note that for this state

$$\langle n_a \rangle = \bar{n} = \langle n_b \rangle, \tag{140a}$$

$$\langle n_a^2 \rangle = \langle a^\dagger a a^\dagger a \rangle \underset{\substack{\text{Gaussian} \\ \text{with } \langle a \rangle = 0}}{=} \langle a^\dagger a \rangle \langle a^\dagger a \rangle + \langle a^\dagger a \rangle \underbrace{\langle a a^\dagger \rangle}_{\langle a^\dagger a \rangle + 1} + \underbrace{\langle a^{\dagger 2} \rangle \langle a^2 \rangle}_{0} = 2\bar{n}^2 + \bar{n} = \langle n_b^2 \rangle. \tag{140b}$$

And hence, we get

$$d_{\Delta n} = 0, \tag{141a}$$

$$V_{\Delta n} = \langle (\delta n_a - \delta n_b)^2 \rangle = \langle \delta n_a^2 \rangle + \langle \delta n_b^2 \rangle - 2\underbrace{\langle \delta n_a \delta n_b \rangle}_{\langle \delta n_a \rangle \langle \delta n_b \rangle} = 2\bar{n}(\bar{n} + 1), \tag{141b}$$

leading to

$$d_x(\bar{t}) = 0 = d_p(\bar{t}) \tag{142a}$$

$$V_{xx}(\bar{t}) = 1 + \bar{t}^2 + 2\bar{g}^2 \bar{n}(\bar{n} + 1)\bar{t}^4, \tag{142b}$$

$$V_{pp}(\bar{t}) = 1 + 8\bar{g}^2 \bar{n}(\bar{n} + 1)\bar{t}^2, \tag{142c}$$

$$V_{xp}(\bar{t}) = \bar{t} + 4\bar{g}^2 \bar{n}(\bar{n} + 1)\bar{t}^3. \tag{142d}$$

On average, the position and momentum of the piston do not change, since the average photon number difference is zero. However, the variance of the photon number difference is different than zero (since the thermal photon-number fluctuations of each cavity are uncorrelated), which is revealed as a strong modification of the mechanical covariance matrix as time goes by.

In contrast with the previous case, we then consider now a family of states in which the cavities have perfect photon-number correlations: two-mode squeezed vacuum states. These are defined as [4, 5]

$$|\text{TMSV}\rangle = e^{r(a^\dagger b^\dagger - ab)}|0\rangle = \frac{1}{\cosh r} \sum_{n=0}^{\infty} \tanh^n r |n, n\rangle, \quad \text{with } r \in [0, \infty[. \tag{143}$$

Note that the reduced state of each cavity is just a thermal state,

$$\text{tr}_b\{|\text{TMSV}\rangle\langle\text{TMSV}|\} = \sum_{n=0}^{\infty} \frac{\tanh^{2n} r}{\cosh^2 r} |n\rangle\langle n| = \sum_{n=0}^{\infty} \frac{(\sinh^2 r)^n}{(1 + \sinh^2 r)^{n+1}} |n\rangle\langle n| = \rho_{th}(\sinh^2 r). \tag{144}$$

Hence, taking $\sinh^2 r = \bar{n}$, locally $|\text{TMSV}\rangle$ is indistinguishable from the the product of thermal states considered before. The difference lays now in the correlations between the cavities. In particular, note that (143) is an eigenstate of the photon number difference operator Δn, with zero eigenvalue. Hence, in this case all the moments of these operator are identically zero, $\langle \Delta n^m \rangle = 0$ $\forall m$ (signaling perfect photon number correlations between the cavities), leading to

$$d_{\Delta n} = 0, \quad V_{\Delta n} = 0. \tag{145}$$

Hence, in this case the optomechanical interaction plays absolutely no role in the dynamics of the piston, that is,

$$d_x(\bar{t}) = 0 = d_p(\bar{t}) \tag{146a}$$

$$V_{xx}(\bar{t}) = 1 + \bar{t}^2, \tag{146b}$$

$$V_{pp}(\bar{t}) = 1, \tag{146c}$$

$$V_{xp}(\bar{t}) = \bar{t}. \tag{146d}$$

42

4.2.2 The membrane model

Now, let's see what happens in the case of the membrane. We remind that the Hamiltonian reads in this case

$$H = \hbar\Omega c^\dagger c - \hbar g(c + c^\dagger)\Delta n. \tag{147}$$

As before, the photon number difference is a conserved quantity, $\Delta n(t) = \Delta n(0)$. Hence, the Heisenberg equation of motion of the mechanical annihilation operator reads

$$\frac{dc}{dt} = -i\Omega c + ig\Delta n(0), \quad \Rightarrow \quad c(\bar{t}) = e^{-i\bar{t}}\big(c(0) - \bar{g}\Delta n(0)\big) + \bar{g}\Delta n(0), \tag{148}$$

where we have introduced the dimensionless time and optomechanical coupling. In this case, it is more natural to evaluate the complex mean vector and covariance matrix, whose relevant elements we define as

$$\Delta = \langle c \rangle, \quad \Lambda_{c^\dagger c} = \langle \delta c^\dagger \delta c \rangle, \quad \Lambda_{cc} = \langle \delta c \delta c \rangle. \tag{149}$$

We can easily evaluate these from (148). In the case of the mean vector, we get

$$\Delta(\bar{t}) = e^{-it}\big(\Delta(0) - \bar{g}d_{\Delta n}\big) + \bar{g}d_{\Delta n}. \tag{150}$$

As for the covariance matrix elements, first we note that we can write the fluctuation operator as

$$\delta c(\bar{t}) = e^{-i\bar{t}}\big(\delta c(0) - \bar{g}\delta\Delta n(0)\big) + \bar{g}\delta\Delta n(0), \tag{151}$$

from which we easily obtain

$$\Lambda_{c^\dagger c}(\bar{t}) = \Lambda_{c^\dagger c}(0) + 2\bar{g}^2(1 - \cos\bar{t})V_{\Delta n}, \tag{152a}$$

$$\Lambda_{cc}(t) = e^{-2i\bar{t}}\Lambda_{cc}(0) - 2\bar{g}^2 e^{-i\bar{t}}(1 - \cos\bar{t}), \tag{152b}$$

again assuming that the cavities and the membrane are uncorrelated initially.

If we assume that the membrane is on its ground state initially, characterized by $\Delta = 0 = \Lambda_{c^\dagger c} = \Lambda_{cc}$, we then get

$$\Delta(\bar{t}) = \bar{g}\left(1 - e^{-it}\right)d_{\Delta n}, \tag{153a}$$

$$\Lambda_{c^\dagger c}(\bar{t}) = 2\bar{g}^2(1 - \cos\bar{t})V_{\Delta n}, \tag{153b}$$

$$\Lambda_{cc}(\bar{t}) = -2\bar{g}^2 e^{-i\bar{t}}(1 - \cos\bar{t})V_{\Delta n}. \tag{153c}$$

Finally, we consider the same initial states for the cavities as we did for the piston. For the separable thermal state, we obtain

$$\Delta(\bar{t}) = 0, \tag{154a}$$

$$\Lambda_{c^\dagger c}(\bar{t}) = 4\bar{g}^2\bar{n}(\bar{n} + 1)(1 - \cos\bar{t}), \tag{154b}$$

$$\Lambda_{cc}(\bar{t}) = -4\bar{g}^2\bar{n}(\bar{n} + 1)e^{-i\bar{t}}(1 - \cos\bar{t})V_{\Delta n}. \tag{154c}$$

whereas for the two mode squeezed vacuum state we have

$$\Delta(\bar{t}) = 0 = \Lambda_{c^\dagger c}(\bar{t}) = \Lambda_{cc}(\bar{t}). \tag{155}$$

Hence, again, the optomechanical interaction has no effect when the photon-number correlated state is considered, while thermal cavity fluctuations show up in the mechanical covariance matrix.

4.3   Stochastic Simulations

In this section we solve the system of stochastic Langevin equations numerically, comparing with the analytical expressions that we derived in the previous section. While we have developed very carefully the stochatic equations that describe the evolution of the system, we still haven't said anything about how to sample the required initial states within each representation (Wigner or positive P). In the first part of this section we address this issue for the initial states considered in the previous section: thermal states and two-mode squeezed vacuum states. Then we perform numerical simulations using the XMDS2 package [15], which is the leading numerical software in the field of stochastic equations.

4.3.1   Initial state sampling with the Wigner distribution

Let us start explaining how to sample with the Wigner distribution the initial states we are interested in. Since we consider Gaussian initial states, this is particularly easy with the Wigner distribution. Specifically, the Wigner function of a Gaussian state with covariance matrix V (we take zero mean vector, since that's the case in both initial states we consider) is [4, 5, 10]

$$W(\mathbf{r}) = \frac{1}{\sqrt{(2\pi)^N \det V}} e^{-\frac{1}{2}\mathbf{r}^T V^{-1}\mathbf{r}}, \tag{156}$$

where N is the number of modes we consider, and $\mathbf{r} = (x_1, p_1, ..., x_N, p_N)^T$ is a column vector collecting all the phase space variables. The general idea to sample Gaussian states is simple: since the covariance matrix is real and symmetric, it can be diagonalized with an orthogonal transformation. Then, moving to the phase-space coordinates defined by such transformation, the Wigner function turns into a product of simple one-dimensional Gaussians that can be sampled with independent variables normally distributed. Let's see this in our specific cases.

Let us remark that in the following we use the notation η_j for real independent random numbers normally distributed with unit variance, that is,

$$\overline{\eta_j} = 0, \qquad \overline{\eta_j \eta_l} = \delta_{jl}. \tag{157}$$

In the case of a single-mode thermal state, the covariance matrix is [4, 5, 10]

$$V_{th}(\bar{n}) = (2\bar{n} + 1) \begin{pmatrix} 1 & 0 \\ 0 & 1 \end{pmatrix}, \tag{158}$$

which is already diagonal. The Wigner function reads then (we omit normalization factors in the following)

$$W(\mathbf{r}) = e^{-x^2/2(2\bar{n}+1)} e^{-p^2/2(2\bar{n}+1)}. \tag{159}$$

which is the product of two Gaussians with variance $2\bar{n}+1$. These can be sampled from stochastic position and momentum as

$$x = \sqrt{2\bar{n} + 1}\, \eta_1, \qquad p = \sqrt{2\bar{n} + 1}\, \eta_2, \tag{160}$$

or in terms of a single complex stochastic variable $\alpha = (x + ip)/2$ as

$$\alpha = \sqrt{\bar{n} + \frac{1}{2}}\, \frac{\eta_1 + i\eta_2}{\sqrt{2}}. \tag{161}$$

Note that vacuum is sampled in this exact way with $\bar{n} = 0$.

Next we consider the two-mode squeezed vacuum state, with covariance matrix [5, 4]

$$V_{\text{TMSV}} = \begin{pmatrix} \cosh(2r)\mathbb{1} & \sinh(2r)\mathbb{Z} \\ \sinh(2r)\mathbb{Z} & \cosh(2r)\mathbb{1} \end{pmatrix}, \tag{162}$$

where $\mathbb{Z} = \begin{pmatrix} 1 & 0 \\ 0 & -1 \end{pmatrix}$, $\mathbb{1}$ is the identity matrix, and we order the phase space variables as $\mathbf{r} = (x_a, p_a, x_b, p_b)^T$. This covariance matrix is readily diagonalized with an orthogonal transformation,

$$B^T V_{\text{TMSV}} B = \begin{pmatrix} e^{2r} & 0 & 0 & 0 \\ 0 & e^{-2r} & 0 & 0 \\ 0 & 0 & e^{-2r} & 0 \\ 0 & 0 & 0 & e^{2r} \end{pmatrix}, \quad \text{with } B = \frac{1}{\sqrt{2}} \begin{pmatrix} 1 & 0 & 1 & 0 \\ 1 & 0 & -1 & 0 \\ 0 & 1 & 0 & 1 \\ 0 & 1 & 0 & -1 \end{pmatrix}. \tag{163}$$

Hence, defining the transformed phase space variables

$$\mathbf{x} = \begin{pmatrix} \hat{x}_+ \\ \hat{x}_- \\ \hat{p}_+ \\ \hat{p}_- \end{pmatrix} = B\mathbf{r}, \tag{164}$$

the Wigner function is decomposed into a product of four one-dimensional Gaussians,

$$W(\mathbf{x}) = e^{-x_+/2e^{2r}} e^{-x_-/2e^{-2r}} e^{-p_+/2e^{-2r}} e^{-p_-/2e^{2r}}. \tag{165}$$

These variables are then sampled as

$$x_+ = e^r \eta_1, \tag{166a}$$
$$x_- = e^{-r} \eta_2, \tag{166b}$$
$$p_+ = e^{-r} \eta_3, \tag{166c}$$
$$p_- = e^r \eta_4, \tag{166d}$$

or transforming back to the original variables, and defining the complex stochastic variables as usual,

$$\alpha = \frac{1}{2\sqrt{2}}(x_+ + x_- + ip_+ + ip_-) = \frac{1}{\sqrt{8}}(e^r \eta_1 + e^{-r}\eta_2 + ie^{-r}\eta_3 + ie^r\eta_4), \tag{167a}$$

$$\beta = \frac{1}{2\sqrt{2}}(x_+ - x_- + ip_+ - ip_-) = \frac{1}{\sqrt{8}}(e^r \eta_1 - e^{-r}\eta_2 + ie^{-r}\eta_3 - ie^r\eta_4). \tag{167b}$$

4.3.2 Initial state sampling with the positive P distribution

Sampling with the positive P distribution is in general more complicated. For Gaussian states, however, one can still find Gaussian functional forms for P^+, which make the task relatively simple. One important thing worth remarking here is that, contrary to the Wigner distribution (or any of the other quasi-probability distributions defined in the standard phase space), the positive P distribution is not unique [7, 12]. In other words, different functional forms of the distribution can sample the same quantum state. In order to see this, let us introduce two important properties connecting the positive P distribution with quantum states. First, any quantum state can be expanded as [7, 12]

$$\hat{\rho} = \int_{\mathbb{C}^{2N}} d^{2N}\boldsymbol{\alpha} d^{2N}\boldsymbol{\alpha}^+ P^+(\boldsymbol{\alpha}, \boldsymbol{\alpha}^+) \frac{|\boldsymbol{\alpha}\rangle\langle\boldsymbol{\alpha}^{+*}|}{\langle\boldsymbol{\alpha}^{+*}|\boldsymbol{\alpha}\rangle}, \tag{168}$$

where N is again the number of modes, $\boldsymbol{\alpha} = (\alpha_1,...,\alpha_N)^T$ and $\boldsymbol{\alpha}^+ = (\alpha_1^+,...,\alpha_N^+)^T$ collect the complex extended phase-space variables, and $|\boldsymbol{\alpha}\rangle$ refer to multi-mode coherent states [6, 10]. The second expression goes in the opposite direction: P^+ can be written in terms of the state as

$$P^+(\boldsymbol{\alpha}, \boldsymbol{\alpha}^+) = \frac{1}{4\pi} e^{-\frac{|\boldsymbol{\alpha}^* - \boldsymbol{\alpha}^+|}{4}} \left\langle \frac{\boldsymbol{\alpha}^* + \boldsymbol{\alpha}^+}{2} \middle| \rho \middle| \frac{\boldsymbol{\alpha}^* + \boldsymbol{\alpha}^+}{2} \right\rangle. \tag{169}$$

Consider now the vacuum state for a single mode, $\rho = |0\rangle\langle 0|$. Expression (168) tells us that $P^+(\alpha, \alpha^+) = \delta(\alpha)\delta(\alpha^+ - \alpha^*)$. On the other hand, plugging $\rho = |0\rangle\langle 0|$ in (169) we get a very different expression, involving a product of Gaussian functions for $\alpha^* - \alpha^+$ and $\alpha^* + \alpha^+$. Hence, if both expressions are to hold, this shows that the positive P distribution is not unique.

But let's move on now to more practical matters: how to sample the initial states we are interested in. Let us start with thermal states of a single mode. Expression (168) tells us that whenever a well-behaved Glauber-Sudarshan $P(\alpha)$ distribution exists, a valid choice of positive P is

$$P^+(\alpha, \alpha^+) = P(\alpha)\delta(\alpha^+ - \alpha^*). \tag{170}$$

Now, since the P distribution of a thermal state $\rho_{th}(\bar{n})$ is the Gaussian [6] (as before, we omit normalizations)

$$P_{\rho_{th}(\bar{n})}(\alpha) = e^{-2|\alpha|^2/\bar{n}} = e^{-x^2/2\bar{n}} e^{-p^2/2\bar{n}}, \tag{171}$$

where as usual $\alpha = (x + ip)/2$, we can easily sample a thermal state within the positive P representation based on the following stochastic variables:

$$\alpha = \sqrt{\bar{n}} \, \frac{\eta_1 + i\eta_2}{\sqrt{2}}, \quad \alpha^+ = \alpha^*. \tag{172}$$

In the $\bar{n} \to 0$ limit, the distribution (171) tends to a delta function $\delta(\alpha)$ as corresponds to vacuum. Hence, the vacuum state is sampled as

$$\alpha = 0 = \alpha^+. \tag{173}$$

Sampling the two-mode squeezed vacuum state is a bit more involved. We cannot use the relation (170), since the P distribution of the two-mode squeezed state has negativities and divergences beyond a delta function. Nevertheless, since the overlap of Gaussian states with coherent states is always a quadratic form of the coherent-state amplitudes [10], expression (169) always allows us to write the corresponding positive P distribution as a Gaussian probability distribution that can be sampled similarly to how we sampled in the Wigner case. This is the route that we follow here. Indeed, we follow a shortcut. In [16], the authors already used this expression to sample a single-mode squeezed state $|e^{i\theta}r\rangle = \exp[r(e^{i\theta}a^{\dagger 2} + e^{-i\theta}a^2)]|0\rangle$ as

$$\alpha = \sqrt{\frac{\cosh r}{2}} e^{i\frac{\theta}{2}} \left(e^{\frac{r}{2}}\eta_1 + ie^{-\frac{r}{2}}\eta_2 \right) + \frac{1}{\sqrt{2}}(\eta_3 + i\eta_4), \tag{174a}$$

$$\alpha^+ = \sqrt{\frac{\cosh r}{2}} e^{-i\frac{\theta}{2}} \left(e^{\frac{r}{2}}\eta_1 - ie^{-\frac{r}{2}}\eta_2 \right) - \frac{1}{\sqrt{2}}(\eta_3 - i\eta_4). \tag{174b}$$

On the other hand, we use the fact that a two mode squeezed vacuum state can be written as a 50/50 beam splitter acting on two single mode-squeezed states [5]

$$|\text{TMSV}\rangle = \hat{B}\left(|-r\rangle \otimes |r\rangle\right), \tag{175}$$

where $B = e^{\frac{\pi}{4}(\hat{a}^\dagger \hat{b} - \hat{a} \hat{b}^\dagger)}$. Next, we use

$$P^+_{\hat{B}\hat{\rho}\hat{B}^\dagger}(\boldsymbol{\alpha}, \boldsymbol{\alpha}^+) = P^+_{\hat{\rho}}(\tilde{B}\boldsymbol{\alpha}, \tilde{B}\boldsymbol{\alpha}^+), \tag{176}$$

where we have defined the matrix $\tilde{B} = \frac{1}{\sqrt{2}}\begin{pmatrix} 1 & 1 \\ -1 & 1 \end{pmatrix}$. We prove this expression at the end of this section. Identifying ρ in this expression with the state $|-r\rangle \otimes |r\rangle$, and noting that

$$P^+_{|-r\rangle \otimes |r\rangle}(\boldsymbol{\alpha}, \boldsymbol{\alpha}^+) = P^+_{|-r\rangle}\left(\alpha, \alpha^+\right) P^+_{|r\rangle}\left(\beta, \beta^+\right), \tag{177}$$

(175) leads to

$$\begin{aligned} P^+_{|\text{TMSV}\rangle}(\boldsymbol{\alpha}, \boldsymbol{\alpha}^+) &= P^+_{\hat{B}(|-r\rangle \otimes |r\rangle)}(\boldsymbol{\alpha}, \boldsymbol{\alpha}^+) \\ &= P^+_{|-r\rangle}\left(\frac{\alpha + \beta}{\sqrt{2}}, \frac{\alpha^+ + \beta^+}{\sqrt{2}}\right) P^+_{|r\rangle}\left(\frac{\beta - \alpha}{\sqrt{2}}, \frac{\beta^+ - \alpha^+}{\sqrt{2}}\right), \end{aligned} \tag{178}$$

which based on (174) can be sampled as

$$\frac{\alpha + \beta}{\sqrt{2}} = i\sqrt{\frac{\cosh r}{2}}\left(e^{\frac{r}{2}}\eta_1 + ie^{-\frac{r}{2}}\eta_2\right) + \frac{1}{\sqrt{2}}(\eta_3 + i\eta_4), \tag{179a}$$

$$\frac{\alpha^+ + \beta^+}{\sqrt{2}} = -i\sqrt{\frac{\cosh r}{2}}\left(e^{\frac{r}{2}}\eta_1 - ie^{-\frac{r}{2}}\eta_2\right) - \frac{1}{\sqrt{2}}(\eta_3 - i\eta_4), \tag{179b}$$

$$\frac{\beta - \alpha}{\sqrt{2}} = \sqrt{\frac{\cosh r}{2}}\left(e^{\frac{r}{2}}\eta_5 + ie^{-\frac{r}{2}}\eta_6\right) + \frac{1}{\sqrt{2}}(\eta_7 + i\eta_8), \tag{179c}$$

$$\frac{\beta^+ - \alpha^+}{\sqrt{2}} = \sqrt{\frac{\cosh r}{2}}\left(e^{\frac{r}{2}}\eta_5 - ie^{-\frac{r}{2}}\eta_6\right) - \frac{1}{\sqrt{2}}(\eta_7 - i\eta_8). \tag{179d}$$

Solving for the independent complex variables, we finally get

$$\alpha = \frac{\sqrt{\cosh r}}{2}\left(i\left(e^{\frac{r}{2}}\eta_1 + ie^{-\frac{r}{2}}\eta_2\right) - \left(e^{\frac{r}{2}}\eta_5 + ie^{-\frac{r}{2}}\eta_6\right)\right) + \frac{1}{2}(\eta_3 - \eta_7 + i\eta_4 - i\eta_8), \tag{180a}$$

$$\beta = \frac{\sqrt{\cosh r}}{2}\left(i\left(e^{\frac{r}{2}}\eta_1 + ie^{-\frac{r}{2}}\eta_2\right) + \left(e^{\frac{r}{2}}\eta_5 + ie^{-\frac{r}{2}}\eta_6\right)\right) + \frac{1}{2}(\eta_3 + \eta_7 + i\eta_4 + i\eta_8), \tag{180b}$$

$$\alpha^+ = \frac{\sqrt{\cosh r}}{2}\left(-i\left(e^{\frac{r}{2}}\eta_1 - ie^{-\frac{r}{2}}\eta_2\right) - \left(e^{\frac{r}{2}}\eta_5 - ie^{-\frac{r}{2}}\eta_6\right)\right) + \frac{1}{2}(\eta_7 - \eta_3 + i\eta_4 - i\eta_8), \tag{180c}$$

$$\beta^+ = \frac{\sqrt{\cosh r}}{2}\left(-i\left(e^{\frac{r}{2}}\eta_1 - ie^{-\frac{r}{2}}\eta_2\right) + \left(e^{\frac{r}{2}}\eta_5 - ie^{-\frac{r}{2}}\eta_6\right)\right) + \frac{1}{2}(-\eta_3 - \eta_7 + i\eta_4 + i\eta_8). \tag{180d}$$

Let us finally prove expression (176). We will use the following property of a beam-splitter acting on a coherent state coherent:

$$\begin{aligned} \hat{B}|\boldsymbol{\alpha}\rangle &= \hat{B}e^{\alpha a^\dagger + \beta b^\dagger - \text{H.c.}}|0\rangle = \hat{B}e^{\alpha a^\dagger + \beta b^\dagger - \text{H.c.}}\hat{B}^\dagger \hat{B}|0\rangle = e^{\alpha \hat{B}a^\dagger \hat{B}^\dagger + \beta \hat{B}b^\dagger \hat{B}^\dagger - \text{H.c.}}|0\rangle \\ &= e^{\left(\frac{\alpha - \beta}{\sqrt{2}}\right)a^\dagger + \left(\frac{\alpha + \beta}{\sqrt{2}}\right)b^\dagger - \text{H.c.}}|0\rangle = |\tilde{B}^T \boldsymbol{\alpha}\rangle, \end{aligned} \tag{181}$$

where we have used $\hat{B}a\hat{B}^\dagger = (a + b)/\sqrt{2}$ and $\hat{B}b\hat{B}^\dagger = (b - a)/\sqrt{2}$. Using then expression (168),

we get

$$
\begin{aligned}
\hat{B}\rho\hat{B}^{\dagger} &= \int_{\mathbb{C}^4} d^4\boldsymbol{\alpha}\, d^4\boldsymbol{\alpha}^+ P_\rho^+(\boldsymbol{\alpha},\boldsymbol{\alpha}^+)\frac{\hat{B}|\boldsymbol{\alpha}\rangle\langle\boldsymbol{\alpha}^{+*}|\hat{B}^{\dagger}}{\langle\boldsymbol{\alpha}^{+*}|\boldsymbol{\alpha}\rangle} \\
&= \int_{\mathbb{C}^4} d^4\boldsymbol{\alpha}\, d^4\boldsymbol{\alpha}^+ P_\rho^+(\boldsymbol{\alpha},\boldsymbol{\alpha}^+)\frac{|\tilde{B}^T\boldsymbol{\alpha}\rangle\langle\tilde{B}^T\boldsymbol{\alpha}^{+*}|}{\langle\boldsymbol{\alpha}^{+*}|\boldsymbol{\alpha}\rangle} \\
&\underbrace{=}_{\boldsymbol{\alpha}=\tilde{B}\boldsymbol{u}} \int_{\mathbb{C}^4} d^4\boldsymbol{u}\, d^4\boldsymbol{u}^+ P_\rho^+(\tilde{B}\boldsymbol{u},\tilde{B}\boldsymbol{u}^+)\frac{|\boldsymbol{u}\rangle\langle\boldsymbol{u}^{+*}|}{\underbrace{\langle\tilde{B}\boldsymbol{u}^{+*}|\tilde{B}\boldsymbol{u}\rangle}_{\langle\boldsymbol{u}^{+*}|\hat{B}\hat{B}^{\dagger}|\boldsymbol{u}\rangle=\langle\boldsymbol{u}^{+*}|\boldsymbol{u}\rangle}} \\
&\equiv \int_{\mathbb{C}^4} d^4\boldsymbol{\alpha}\, d^4\boldsymbol{\alpha}^+ P_{\hat{B}\rho\hat{B}^{\dagger}}^+(\boldsymbol{\alpha},\boldsymbol{\alpha}^+)\frac{|\boldsymbol{\alpha}\rangle\langle\boldsymbol{\alpha}^{+*}|}{\langle\boldsymbol{\alpha}^{+*}|\boldsymbol{\alpha}\rangle}, \\
&\qquad\qquad\qquad\Downarrow \\
P_{\hat{B}\rho\hat{B}^{\dagger}}^+(\boldsymbol{\alpha},\boldsymbol{\alpha}^+) &= P_\rho^+(\tilde{B}\boldsymbol{\alpha},\tilde{B}\boldsymbol{\alpha}^+),
\end{aligned}
\tag{182}
$$

which is the expression we wanted to prove.

4.3.3 Stochastic simulations I: comparison with the analytic case $\lambda = 0$

We proceed now to the simulation of the stochastic equations discussed in Section 4.1, and their comparison with the exact results of Section 4.2. We have performed the numerical simulations using the XMDS2 package [15][6]. The choice of this package is justified by its user-friendliness since it uses an XML-based code generator, and also by its efficiency since it generates C++ code, which is a low-level language much more efficient than Matlab. Additionally, let us note that we have compared it with our own codes written in Matlab from scratch following [14, 17], and with the XSPDE Matlab package, also developed by Peter Drummond and collaborators [18]. We found these were outperformed by XMDS2 in all the instances we studied.

The goal of this section is checking the validity of our derivation of the stochastic equations and the related codes, which we give in Appendix C. As representative cases, we present 8 simulations, corresponding to all the possible combination of mechanical element (membrane or piston), phase-space representation (positive P or truncated Wigner), and initial optical state (uncorrelated thermal $\rho_{th}(\bar{n}) \otimes \rho_{th}(\bar{n})$, or entangled $|\text{TMSV}\rangle$). In all cases we set[7] $\lambda = 0$ (in order to compare with the analytic solution), $\bar{g} = 0.001$, and $\bar{n} = 1000$. We choose these parameters because they are close to the classical limit (large photon number and small optomechanical coupling), so that the truncated Wigner representation should be close to the analytical results. For the piston we simulate until $\bar{t} = 2$, since according to (142a), deviations from the $g = 0$ can only be appreciated if $\bar{g}\bar{n}t \geq 1$. For the membrane, we consider up to $t = 2\pi$, based on the periodicity of the analytical solution (154a). Note that XMDS2 outputs the data in an h5 file, which we convert to the desired plots with Octave (codes also provided at the end of Section C).

Before showing the results of the simulations, let us also introduce some more general remarks. When $\gamma = 0$, the truncated Wigner equations of Section 4.1 are completely deterministic, which allows for a very big number of stochastic paths with high tolerance[8] on the order of 10^{-15}. On the other hand, the positive P equations have multiplicative noise terms and are therefore much harder to simulate. Thus, we perform less paths for this simulations, and set a much larger tolerance of 10^{-7}.

We present the results in a total of 4 figures: membrane within the truncated Wigner (Fig. 3) and positive P (Fig. 4), and piston within the truncated Wigner (Fig. 5) and positive P (Fig. 6). We consider both initial conditions within the same figure: uncorrelated thermal on the left column and entangled state on the right column. Each column has six plots: the top one shows the number of photons ($\langle n_a \rangle$ in dashed red, and $\langle n_b \rangle$ in dashed-dotted green), while the next two ones show the first order moments and the last three the second order moments forming the covariance matrix (Re$\{\Delta\}$, Im$\{\Delta\}$, $\Lambda_{c^\dagger c}$, Re$\{\Lambda_{cc}\}$, and Im$\{\Lambda_{cc}\}$ for the membrane; d_x, d_p, V_{xx}, V_{pp}, and V_{xp} for the piston). All the stochastic curves are shown in dashed red, and we also show the analytic solution in solid blue for comparison.

We start with the membrane model, specifically with its truncated Wigner simulation in Figure 3. As expected, the number of photons in the cavities stay constant in time. As the number of paths is quite large (10^6), they average very close to the exact value of $\bar{n} = 1000$. We also see that the mean vector (represented through Re$\{\Delta\}$) stays close to 0. It's interesting though, to note that the truncated Wigner simulation gives a very small (but well-defined) oscillation around 0. This is due to the fact that $d_{\Delta n}$ is not perfectly sampled to 0 initially, and thus equation (153a) gives a slight oscillation. For thermal initial conditions, the stochastic covariance matrix matches perfectly the exact one. In the case of the entangled initial condition, all (complex) second order

---

[6]This package was created by Peter Drummond and Greg Collecutt in 1997. Let us remark that Peter Drummond is one of the leading figures in the field of quantum noise in nonlinear optical systems, and hence the use of this package seems pretty adequate.

[7]In real experiments $\bar{g}$ is usually even smaller [8].

[8]The program uses adaptive stepsize algorithm which requires a tolerance attribute that defines the tolerated relative error per integration step

moments should be 0. However, again because $V_{\Delta n}$ is not exactly sampled to 0 initially, we find oscillations around zero that follow the form of equations (153b), and become smaller and smaller the larger the number of stochastic paths is.
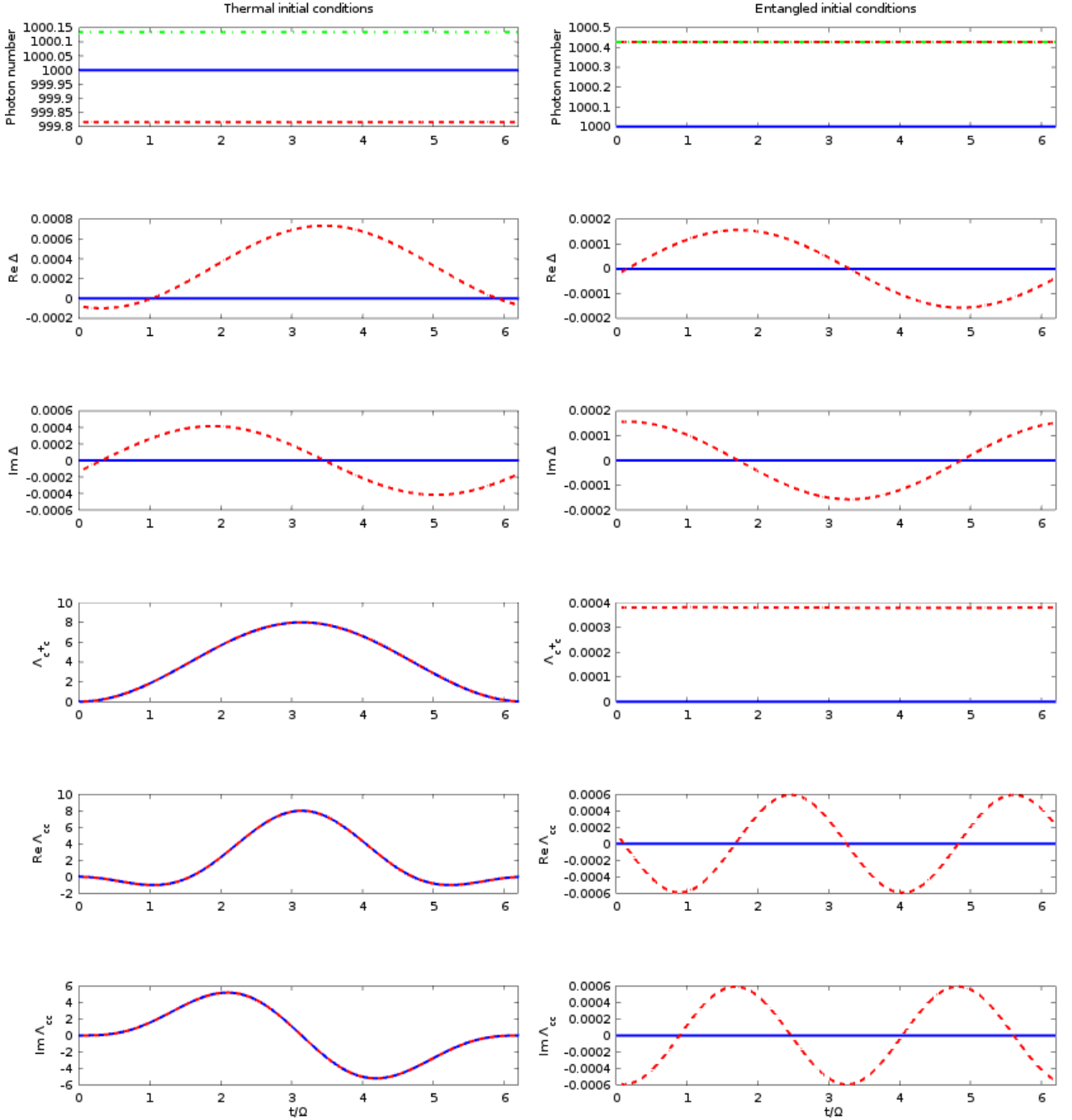

Figure 3: Result of the simulations of Eqs. (122), corresponding to the membrane model within the truncated Wigner representation. We consider initial uncorrelated thermal optical states (right column) and an entangled state (left column). The parameters are $\bar{g} = 0.001$, $\bar{n} = 1000$, and $\lambda = 0$. We average over 10^6 stochastic paths, and show the simulations in dashed red and the analytical solutions of section 4.2 in blue.

In Figure 4 we show the positive P simulations. The results are similar to those of the truncated Wigner. Even the oscillating behaviour around 0 seems to be displayed, although the number of paths is not big enough to see it clearly. Thus, in this idealized case with $\gamma = 0$ and a relatively large photon number, there is not much difference between the quasi-classical truncated Wigner and the fully quantum positive P, as expected.
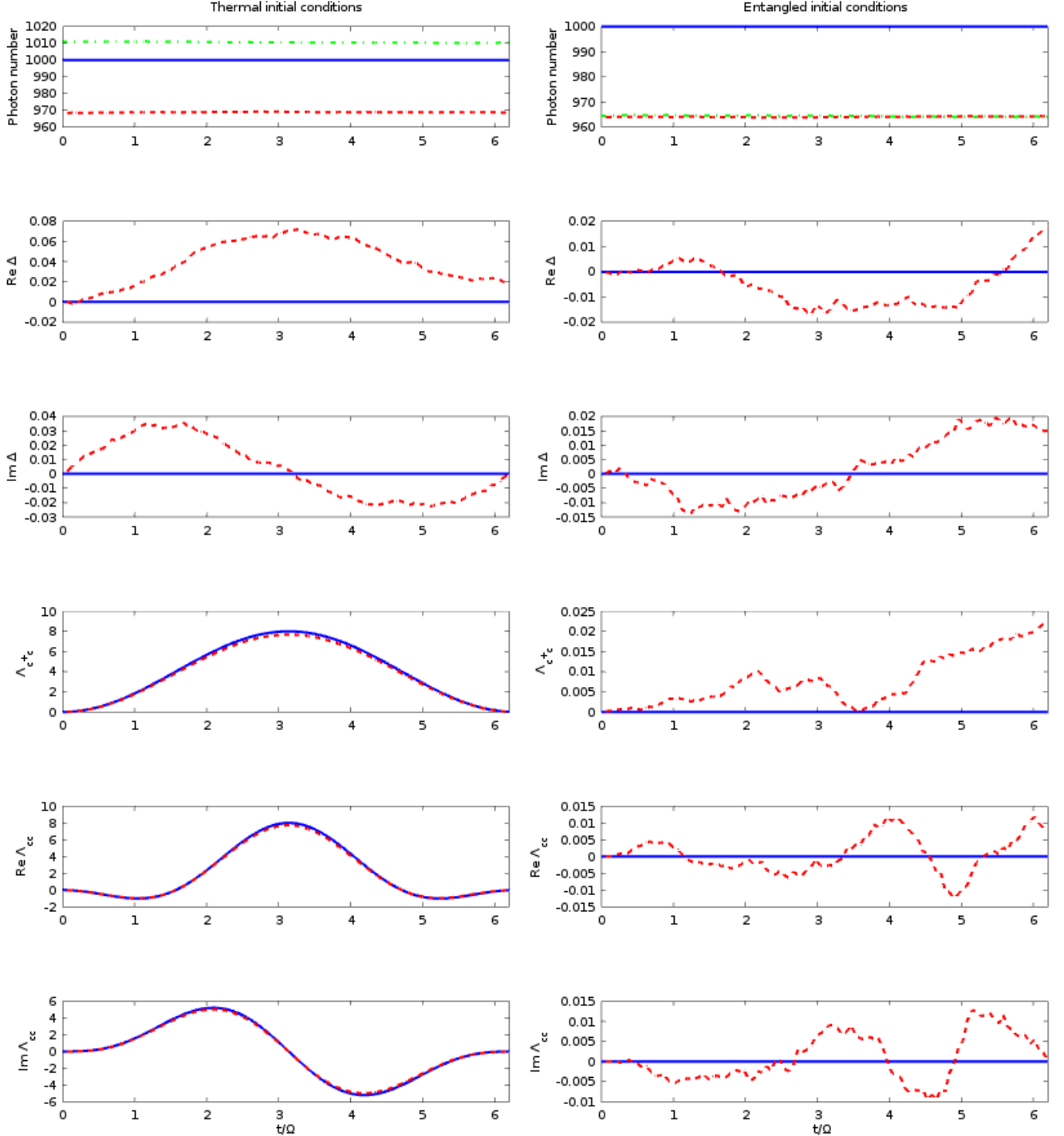

Figure 4: Same as in the previous figure, but for Eqs. (127), corresponding to the membrane model within the positive P representation. Again, we consider initial uncorrelated thermal optical states (right column) and an entangled state (left column), and the parameters are $\bar{g} = 0.001$, $\bar{n} = 1000$, and $\lambda = 0$. In this case we average over 10^3 stochastic paths, with the simulations shown in dashed red and the analytical solutions of section 4.2 in blue.

Next we present the simulations for the piston, starting again with the truncated Wigner in Figure 5 and the positive P in Figure 6. The results are comparable to the ones of the membrane. In particular, we see that all the predictions of the analytic result are matched, within the accuracy with which we sample the initial state: again, any small deviations are explained by the form of equations (134) and (137), and the fact that $d_{\Delta n}$ and $V_{\Delta n}$ are not sampled perfectly to their analytical values.
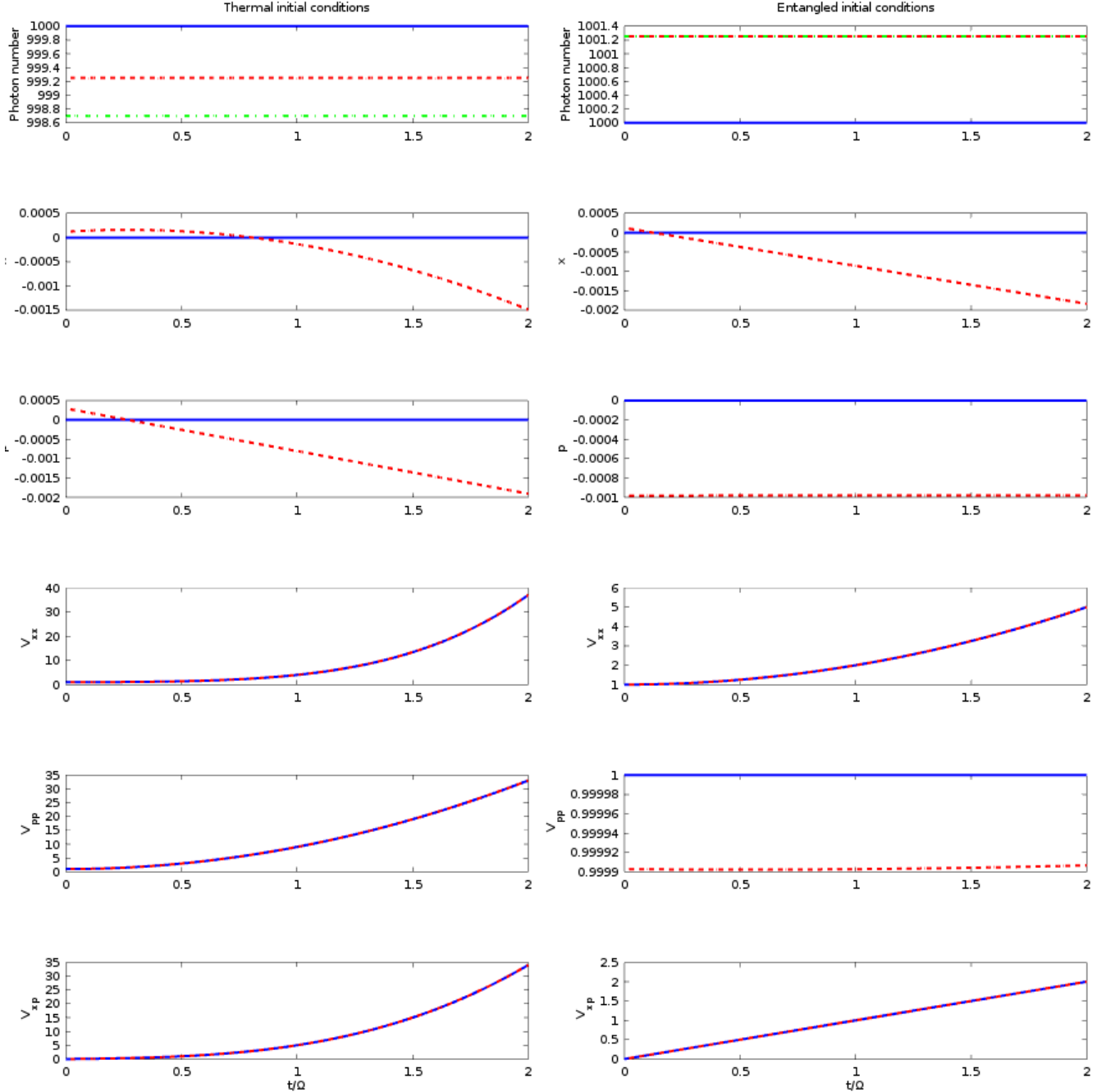

Figure 5: Result of the simulations of Eqs. (121), corresponding to the piston model within the truncated Wigner representation. As in previous plots, we consider initial uncorrelated thermal optical states (right column) and an entangled state (left column). The parameters are $\bar{g} = 0.001$, $\bar{n} = 1000$, and $\lambda = 0$. We average over 10^6 stochastic paths, and show the simulations in dashed red and the analytical solutions of section 4.2 in blue.
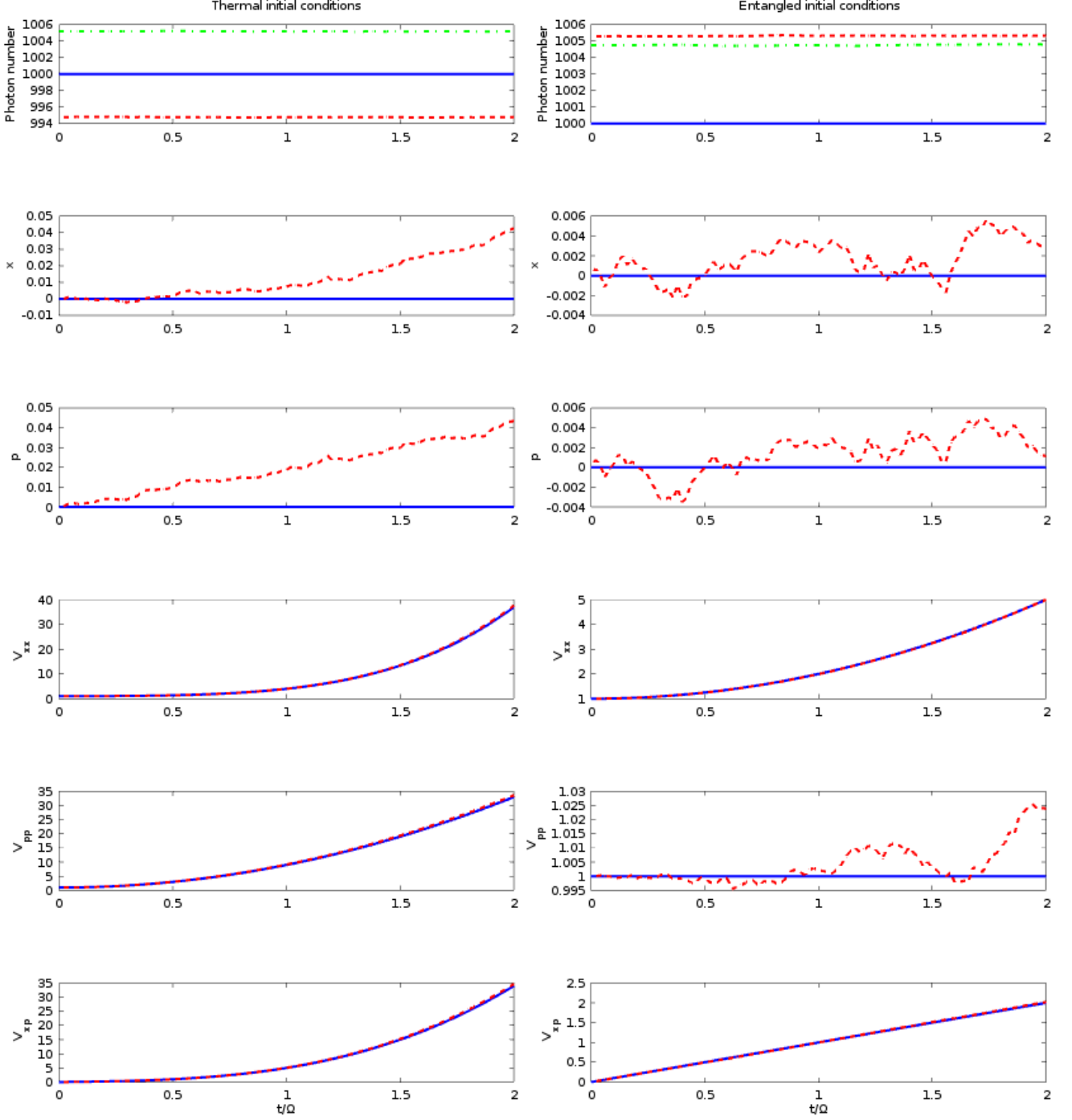
Figure 6: Result of the simulations of Eqs. (126), corresponding to the piston model within the positive P representation. Once again, we consider initial uncorrelated thermal optical states (right column) and an entangled state (left column). The parameters are $\bar{g} = 0.001$, $\bar{n} = 1000$, and $\lambda = 0$. We average over 2×10^4 stochastic paths, and show the simulations in dashed red and the analytical solutions of Section 4.2 in blue.

4.3.4 Stochastic simulations II: beyond the $\lambda = 0$ case

Now that we have tested he accuracy of the stochastic simulations, we can analyze cases without analytic solution. As a warm up, we still consider the closed-system limit ($\gamma = 0$), but now add a beam-splitter coupling between the cavities ($\lambda \neq 0$).

We have checked that if we set $\lambda = 0.01$ or smaller, the previous results are virtually unaffected (see Appendix B). Going to larger values, we start seeing differences, and we present here results for $\lambda = 0.2$. Note that we keep the $\lambda = 0$ plots in the figure in order to appreciate the effect introduced by the beam-splitter.

In Figures 7 and 8 we present the results for the membrane model, within the truncated Wigner and positive P representations, respectively. Let us first note that the thermal state $\rho_{th}(\bar{n}) \otimes \rho_{th}(\bar{n})$ is invariant under the beam-splitter operation, contrary to the entanglement of the two-mode squeezed vacuum state $|\text{TMSV}\rangle$, which is very sensitive [5]. Hence, we would expect a larger impact of the beam splitter in the case of initial entangled conditions. However, note that in both cases the beam-splitter leaves the number of photons on each cavity invariant, and hence we still expect the force felt by the membrane to be zero on average. Indeed, we appreciate in the plots photon numbers and a Δ that oscillate in time with a very small amplitude that can be attributed to the sampling error of the initial states. Moreover, we have checked that the amplitude decreases as we increase the number of stochastic paths.

On the other hand, differences between the thermal and entangled initial states are more noticeable in the covariance matrix. Specifically, while we can appreciate a change with respect to the $\lambda = 0$ case for both initial conditions, the change is far more dramatic in the entangled case. Nevertheless, in both cases we see that the addition of the beam splitter breaks the simple periodic behavior that the system was showing for $\lambda = 0$.

The robustness of the thermal initial state against the beam-splitter interaction is even more evident in the case of the piston, shown in Figures 9 and 10 for the truncated Wigner and the positive P, respectively. For the thermal state (left columns) the effect of the beam-splitter remains almost negligible in the observed time interval, although we can see how it starts deviating for longer times. On the other hand, beam-splitter effects appear much faster for the entangled initial state.

Let us also note that in all cases there doesn't seem to be much differences between the truncated Wigner and the positive P representations, as expected from the fact that we are working in the classical limit of large photon number and small optomechanical coupling.
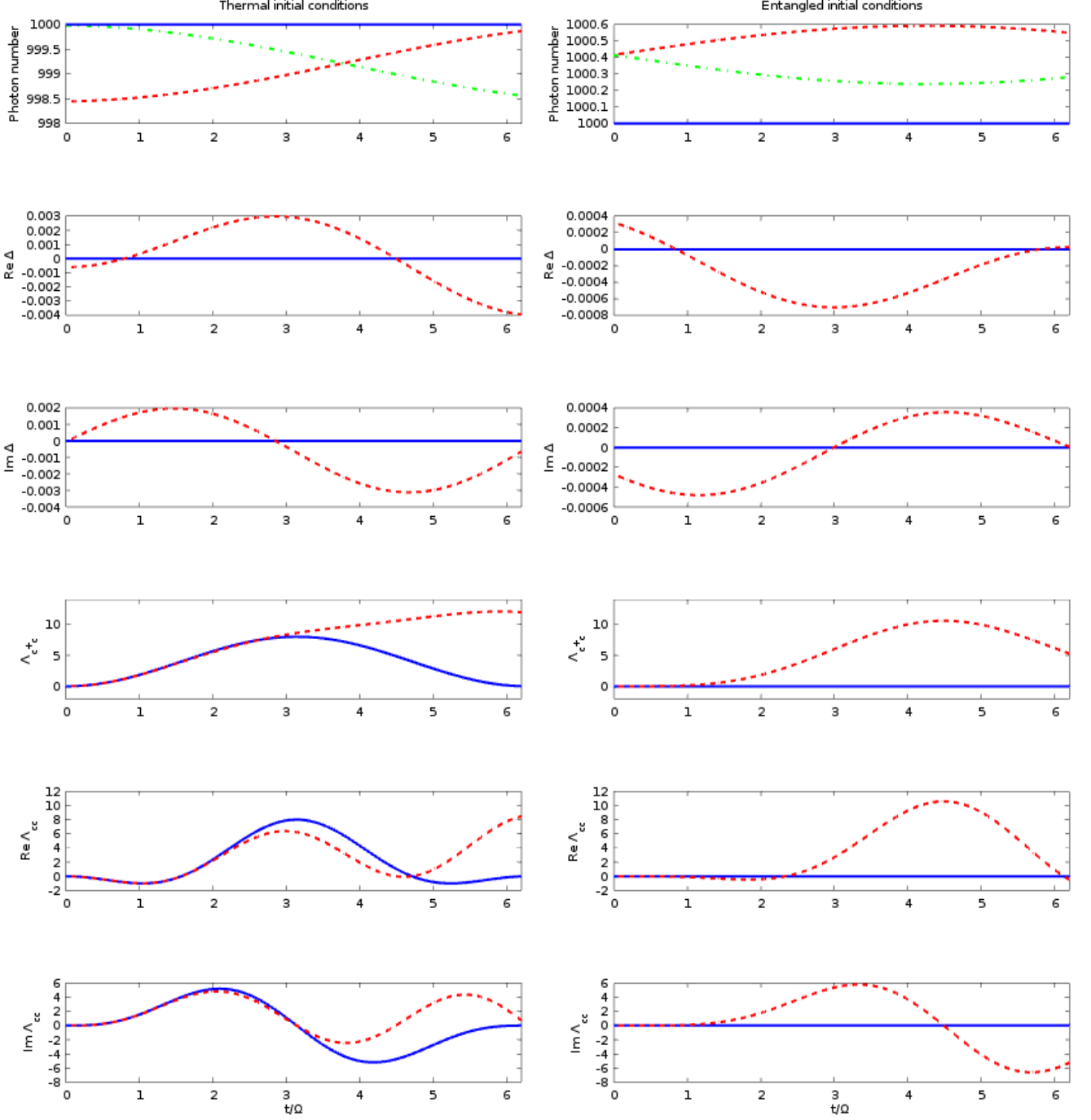
Figure 7: Result of the simulations of Eqs. (122), corresponding to the membrane model within the truncated Wigner representation, with $\bar{\lambda} = 0.2$, and the rest of parameters as in the previous section: $\bar{g} = 0.001$ and $\bar{n} = 1000$. Once again, we consider initial uncorrelated thermal optical states (right column) and an entangled state (left column). We average over 10^7 stochastic paths, and show the simulations in dashed red and the $\lambda = 0$ analytical solutions of Section 4.2 in blue.

Figure 8: Result of the simulations of Eqs. (127), corresponding to the membrane model within the positive P representation, with $\bar{\lambda} = 0.2$, and the rest of parameters as in the previous section: $\bar{g} = 0.001$ and $\bar{n} = 1000$. As usual, we consider initial uncorrelated thermal optical states (right column) and an entangled state (left column). We average over 10^4 stochastic paths, and show the simulations in dashed red and the $\lambda = 0$ analytical solutions of Section 4.2 in blue.

Figure 9: Result of the simulations of Eqs. (126), corresponding to the piston model within the truncated Wigner representation, with $\bar{\lambda} = 0.2$, and the rest of parameters as in the previous section: $\bar{g} = 0.001$ and $\bar{n} = 1000$. We consider initial uncorrelated thermal optical states (right column) and an entangled state (left column). We average over 10^6 stochastic paths, and show the simulations in dashed red and the $\lambda = 0$ analytical solutions of Section 4.2 in blue.
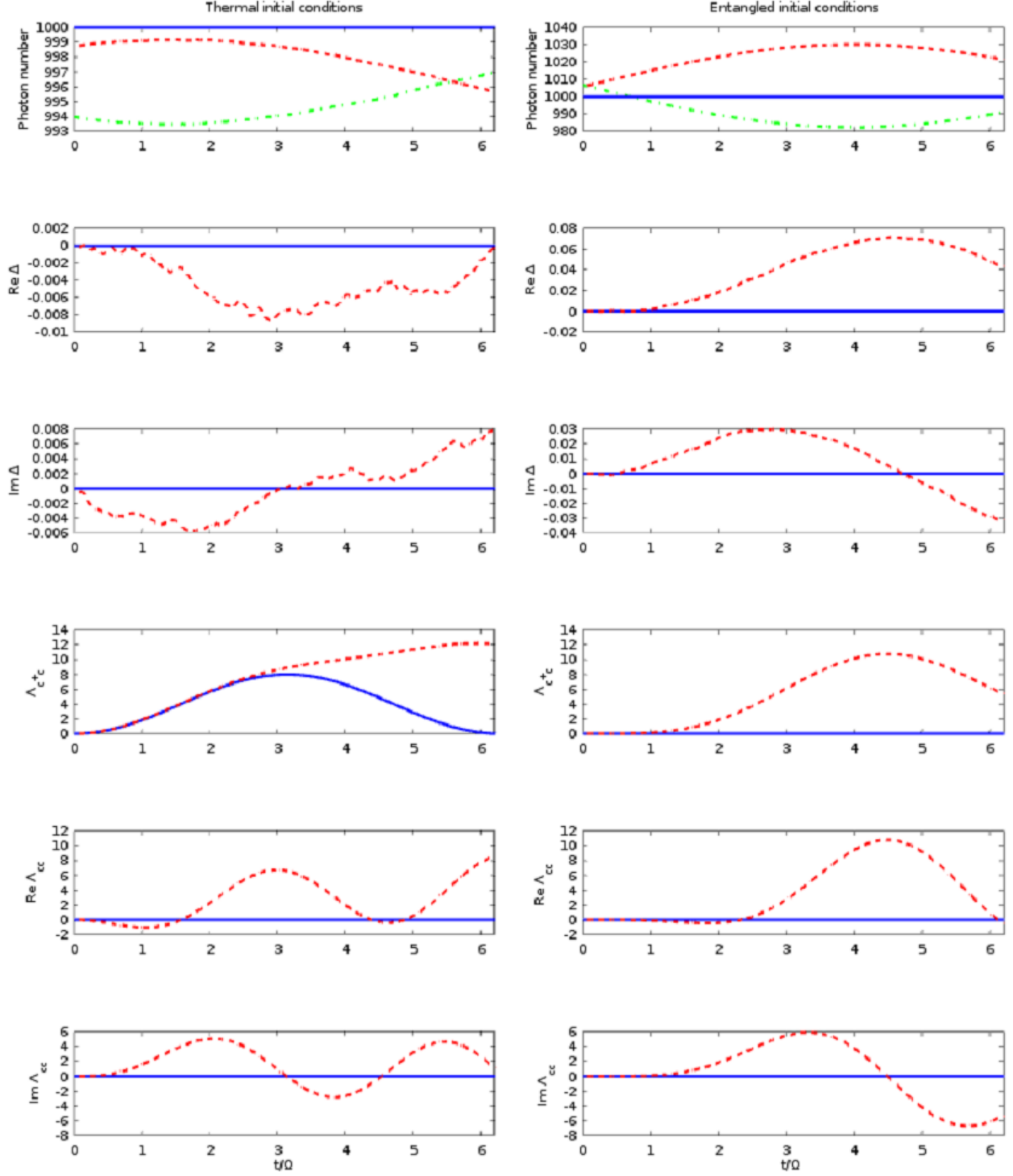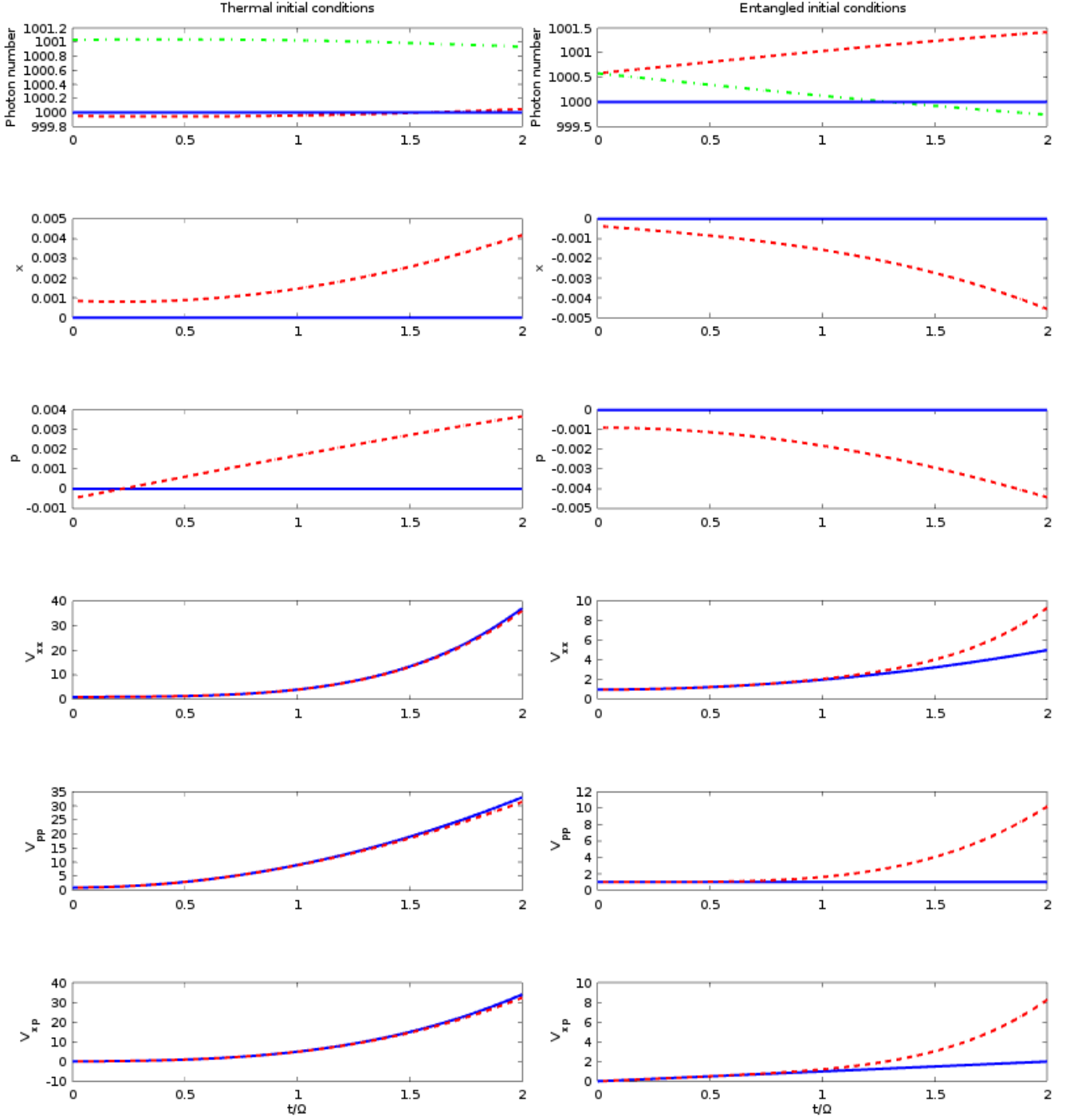
Figure 10: Result of the simulations of Eqs. (126), corresponding to the piston model within the positive P representation, with $\bar{\lambda} = 0.2$, and the rest of parameters as in the previous section: $\bar{g} = 0.001$ and $\bar{n} = 1000$. Once again, we consider initial uncorrelated thermal optical states (right column) and an entangled state (left column). We average over 3×10^4 stochastic paths, and show the simulations in dashed red and the $\lambda = 0$ analytical solutions of Section 4.2 in blue.
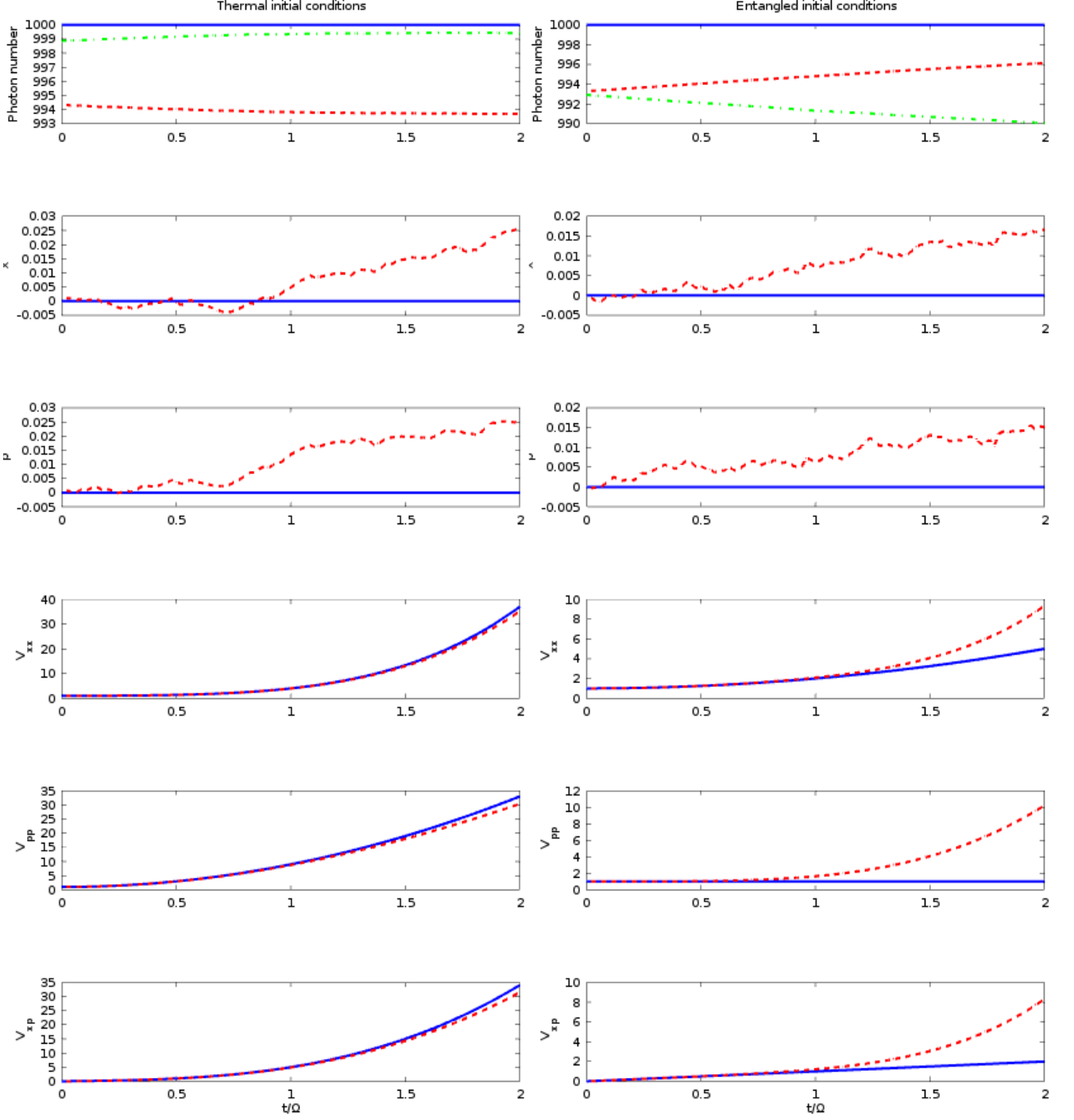
In order to confirm that our simulations do not contain errors, we consider now a limit in which we can analytically solve the problem: the large λ limit. Let us first prove that for large enough values of λ, the effects of the optomechanical coupling should be effectively suppressed, irrespective of the initial state. In order to show this, let us move to the eigenmodes of the beam-splitter Hamiltonian, which we introduced in (34):

$$H = H_m - \hbar g x (a^\dagger a - b^\dagger b) + \hbar \lambda (a^\dagger b + a b^\dagger) = H_m + \hbar g x (A B^\dagger + A^\dagger B) + \hbar \lambda (A^\dagger A - B^\dagger B), \quad (183)$$

where $H_m = \hbar \Omega c^\dagger c$ for the membrane and $H_m = P^2/2m = \Omega p^2/4$ for the piston. Let us consider first the membrane. Moving to the interaction picture defined by the transformation $U = \exp[-i(\Omega c^\dagger c + \lambda a^\dagger a - \lambda b^\dagger b)t]$, the transformed state evolves according to the Hamiltonian

$$H_I = \hbar g \left(e^{-i\Omega t} c + e^{i\Omega t} c^\dagger \right) \left(e^{-2i\lambda t} A B^\dagger + \text{H.C} \right). \quad (184)$$

For $\lambda \gg \Omega$, we obtain a rotation at frequency 2λ, which will make the interaction negligible when it becomes much larger than the interaction strength (rotating-wave approximation). While it is difficult to evaluate the strength of the interaction in general, we can provide the conservative limit $\lambda \gg g\bar{n}$ for our case (interaction dressed by the number of photons). In this limit, the optomechanical interaction is effectively suppressed, so that the evolution of the membrane should follow the free case $g = 0$.

Similarly, in the case of piston we obtain in the interaction picture

$$H_I = \hbar g (x + p\Omega t) \left(e^{-2i\lambda t} A B^\dagger + \text{H.C} \right). \quad (185)$$

Now the effective strength of the interaction increases linearly with time. Hence, in this case the rotating-wave approximation in the limit $\lambda \gg g$ tells us that the optomechanical interaction will be suppressed only until a certain time, that (being conservative again) we can bound by $\bar{t} < \lambda/g\bar{n}$. Staying within this time limit should ensure that the optomechanical interaction is effectively suppressed. We have verified that this is the case by simulating the piston model for the same parameters as before ($\bar{g} = 0.001$ and $\bar{n} = 1000$), except for $\bar{\lambda} = 10$, see Figures 11 and 12 for the truncated Wigner and the positive P, respectively. It can be appreciated how both simulations (dashed red curves) agree very well within the stochastic accuracy with the analytic result with $\bar{g} = 0$ (solid blue curves).

Figure 11: Result of the simulations of Eqs. (121), corresponding to the piston model within the truncated Wigner representation, with $\bar{\lambda} = 10$, and the rest of parameters as in the previous cases: $\bar{g} = 0.001$ and $\bar{n} = 1000$. Once again, we consider initial uncorrelated thermal optical states (right column) and an entangled state (left column). We average over 10^6 stochastic paths, and show the simulations in dashed red and the analytical solutions of Section 4.2 in blue for $\bar{g} = 0 = \bar{\lambda}$.
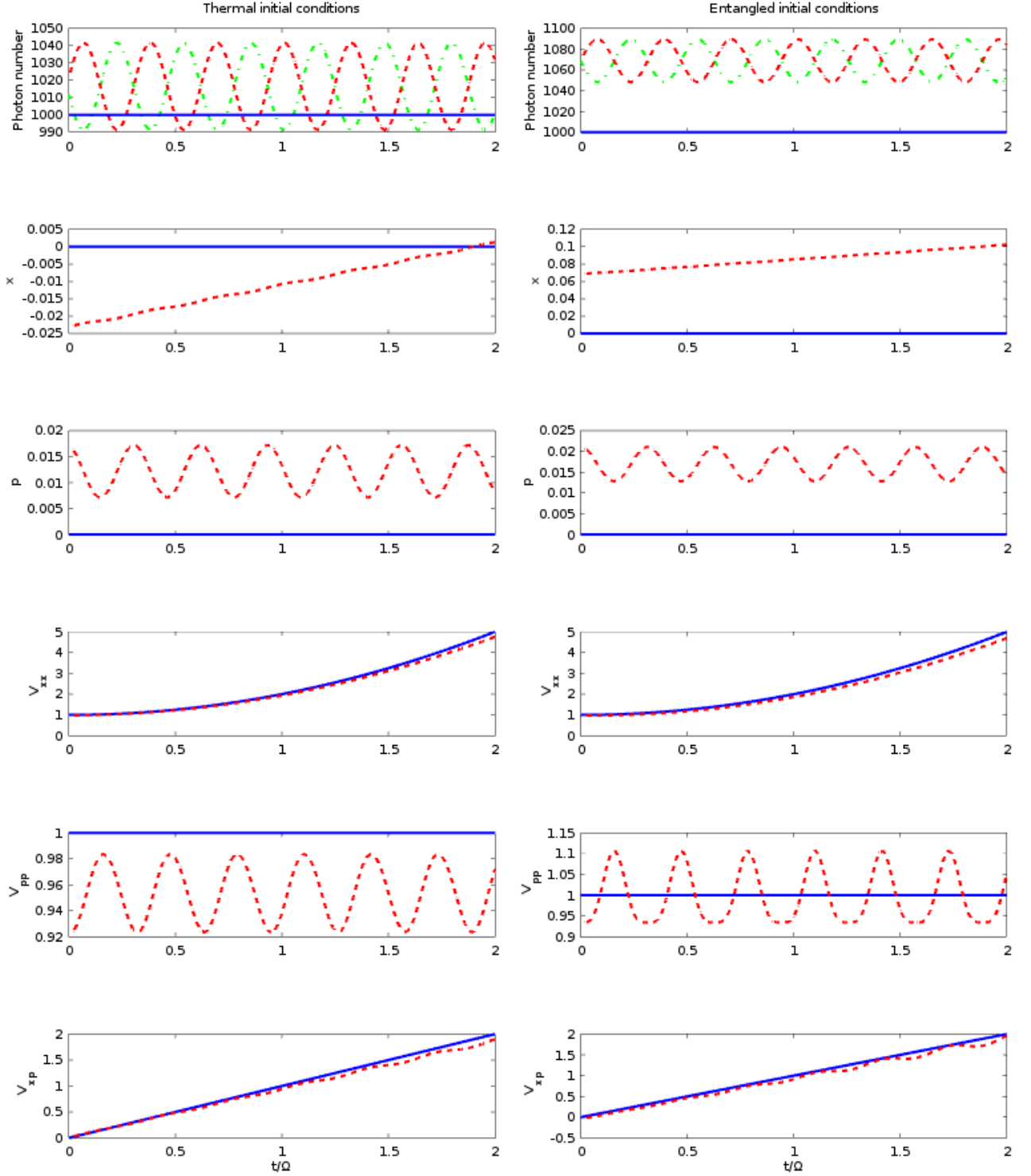
Figure 12: Result of the simulations of Eqs. (126), corresponding to the piston model within the positive P representation, with $\bar{\lambda} = 10$, and the rest of parameters as in the previous cases: $\bar{g} = 0.001$ and $\bar{n} = 1000$. Once again, we consider initial uncorrelated thermal optical states (right column) and an entangled state (left column). We average over 10^3 stochastic paths, and show the simulations in dashed red and the analytical solutions of Section 4.2 in blue for $\bar{g} = 0 = \bar{\lambda}$.
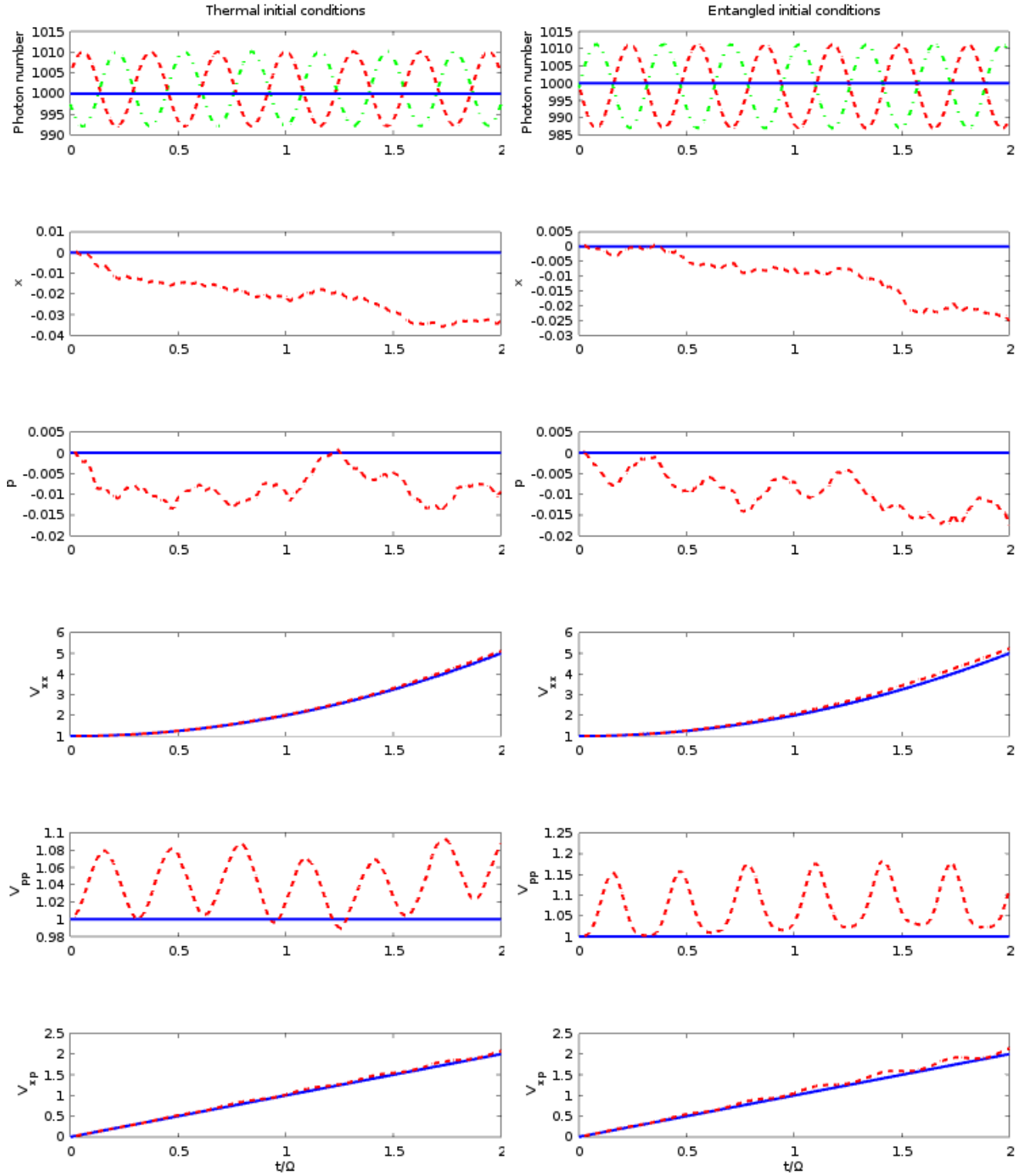
5 Conclusions and outlook

In this thesis we have made a step forward towards the long term goal of finding an autonomous quantum heat engine based solely on linear degrees of freedom. Specifically, we have introduced the two models of Fig. 2, which in spite of not being useful as thermodynamical machines (in the sense of having a well-defined thermodynamical cycle in which heat is transformed into work), contain all the basic ingredients that the final heat engine should have: a mechanical element coupled to cavities, with heat baths providing the energy required to extract work, making them autonomous.

These examples have allowed us to develop in depth the techniques that we will use for the analysis of quantum thermodynamical machines based on linear degrees of freedom. We have proceeded in three steps. First, by tracing out the heat baths under the Born-Markov approximation, we have derived the master equation governing the evolution of the state of the system. Then, we have introduced the concept of phase-space quasiprobability distributions, and have turned the master equation into a partial differential equation for such distributions. Finally, we have put this in correspondence with a set of stochastic dynamical equations for the phase space variables. We have shown that this last step is only possible either by using a truncated Wigner representation equivalent to stochastic electrodynamics (which for high-temperature is nothing but the classical limit), or by using the positive P representation that reproduces the full quantum dynamics, but making use of an extended phase space with twice the number of variables.

In order to benchmark the simulations based on these stochastic equations, we have considered the limit of zero coupling to the environments, which is analytically solvable. We considered two different initial conditions for the cavities: separable and entangled. In both cases, the reduced state of each cavity is thermal, and we have worked in the large photon number and small optomechanical coupling limit (classical regime), where both the truncated Wigner and the positive P representations should work. We showed that indeed the simulations agree with the analytics, but a large number of stochastic paths is usually required for accurate results, typically on the tens of millions or beyond. This means that future analysis will require the use of parallel computing facilities.

As a case that cannot be treated analytically, we consider the addition of the beam-splitter coupling between the cavities (but still without environments). We showed that the stochastic simulations provide results that agree with intuitive expectations, and even with an analytical prediction in the large beam-splitter coupling regime: the optomechanical coupling gets effectively suppressed.

Looking forward, there is still a lot of interesting work to do in the models that we have introduced here. Specifically, from the point of view of quantum optomechanical phenomena it will be very interesting to understand the asymptotic state reached by the system when we introduce coupling to the environments. Specifically, since we assume that the mechanical element is free of friction, it is not yet clear under which conditions the system will reach a steady state, and also, whether the initial state of the cavities will play an important role (usually, it is washed out by the dissipation).

Once this warm up models are fully understood, together with the limits of our stochastic simulations, we will move forward towards our long term goal: developing an autonomous heat engine. While it's still early to devise the exact model that will be required, we want to mention here two possibilities. The first one consists in using a similar strategy as that considered in [2], that is, introducing mechanical-position dependent couplings to the environments. This is known in the optomechanics community as dissipative optomechanical coupling, which has indeed become available in experiments in recent times [19]. A second route would consist on introducing more mechanical or optical elements, something that our stochastic techniques allow because their complexity scales only linearly or quadratically with the number of elements (in contrast to Hilbert-

space based techniques, which scale exponentially). This would allow to consider more complicated scenarios in which entanglement between optical modes coupled to different mechanical elements, or even between the mechanical elements themselves could play a role in boosting the efficiency of the thermodynamical machine.

Overall, we believe that the tools developed in this master thesis will be of great relevance for the analysis of thermal machines working in the quantum regime.

References

[1] J. Goold, M. Huber, A. Riera, L. del Rio, and P. Skrzypczyk, "The role of quantum information in thermodynamics—a topical review," *Journal of Physics A: Mathematical and Theoretical*, vol. 49, p. 143001, 2016.

[2] A. Roulet, S. Nimmrichter, J. M. Arrazola, S. Seah, and V. Scarani, "Autonomous rotor heat engine," *Phys. Rev. E*, vol. 95, p. 062131, 2017.

[3] C. Navarrete-Benlloch, "Open systems dynamics: Simulating master equations in the computer," *arXiv:1504.05266*.

[4] C. Weedbrook, S. Pirandola, R. García-Paton, N. J. Cerf, T. C. Ralph, J. H. Shapiro, and S. Lloyd, "Gaussian quantum information," *Rev. Mod. Phys.*, vol. 84, p. 621, 2012.

[5] C. Navarrete-Benlloch, *An introduction to the formalism of quantum information with continuous variables.* Institute of Physics and Morgan&Claypool publishers, 2015.

[6] H. J. Carmichael, *Statistical methods in quantum optics 1: Master equations and Fokker–Planck equations.* Springer Verlag, 1999.

[7] H. J. Carmichael, *Statistical methods in quantum optics 2: Non-classical fields.* Springer Verlag, 2008.

[8] M. Aspelmeyer, T. J. Kippenberg, and F. Marquardt, "Cavity optomechanics," *Rev. Mod. Phys.*, vol. 86, p. 1391, 2014.

[9] H. Breuer and F. Petruccione, *The Theory of Open Quantum Systems.* Oxford University Press, 2002.

[10] Carlos Navarrete-Benlloch, lecture notes on *Open Quantum Optical Systems*, 2018. https://goo.gl/o96XWP.

[11] C. W. Gardiner and M. J. Collett, "Input and output in damped quantum systems: Quantum stochastic differential equations and the master equation," *Phys. Rev. A*, vol. 31, p. 3761, 1985.

[12] P. D. Drummond and C. W. Gardiner, "Generalized P-representations in quantum optics," *J. Phys. A: math. gen.*, vol. 13, p. 2353, 1980.

[13] D. T. Pope, P. D. Drummond, and W. J. Munro, "Disagreement between correlations of quantum mechanics and stochastic electrodynamics in the damped parametric oscillator," *Phys. Rev. A*, vol. 62, p. 042108, 2000.

[14] C. Navarrete-Benlloch, "Contributions to the quantum optics of multi-mode optical parametric oscillators," *arXiv:1504.05917.*

[15] G. R. Dennis, J. J. Hope, and M. T. Johnsson, "XMDS2: Fast, scalable simulation of coupled stochastic partial differential equations," *Computer Physics Communications*, vol. 184, p. 201, 2013.

[16] M. Olsen and A. Bradley, "Numerical representation of quantum states in the positive-P and wigner representations," *Optics Communications*, vol. 282, p. 3924, 2009.

[17] P. Drummond and I. Mortimer, "Computer simulations of multiplicative stochastic differential equations," *Journal of Computational Physics*, vol. 93, p. 144, 1991.

[18] S. Kiesewetter, R. Polkinghorne, B. Opanchuk, and P. D. Drummond, "xSPDE: Extensible software for stochastic equations," *SoftwareX*, vol. 5, p. 12, 2016.

[19] A. Sawadsky, H. Kaufer, R. M. Nia, S. P. Tarabrin, F. Y. Khalili, K. Hammerer, and R. Schnabel, "Observation of generalized optomechanical coupling and cooling on cavity resonance," *Phys. Rev. Lett.*, vol. 114, p. 043601, 2015.

A Beam-splitter interaction

In this appendix we give further details on the calculations concerning the Beam-splitter interaction

A.1 Detailed initial conditions

This section contains the detailled initial conditions. The non vanishing initial terms are:

$$
\mathrm{tr}\left\{E(\omega')\rho_B E^\dagger(\omega)\right\} = \mathrm{tr}\left\{E^\dagger(\omega)E(\omega')\rho_B\right\} = \mathrm{tr}\left\{\frac{1}{\sqrt{2}}\big(e^\dagger(\omega)+d^\dagger(\omega)\big)\frac{1}{\sqrt{2}}\big(e(\omega')+d(\omega')\big)\rho_B\right\}
$$

$$
= \frac{1}{2}\,\mathrm{tr}\left\{e^\dagger(\omega)e(\omega')\rho_B\right\} + \frac{1}{2}\underset{0}{\mathrm{tr}}\left\{e^\dagger(\omega)d(\omega')\rho_B\right\} + \frac{1}{2}\underset{0}{\mathrm{tr}}\left\{d^\dagger(\omega)e(\omega')\rho_B\right\} + \frac{1}{2}\,\mathrm{tr}\left\{d^\dagger(\omega)d(\omega')\rho_B\right\}
$$

$$
= \frac{1}{2}(\bar{n}_a + \bar{n}_b)\delta(\omega - \omega'),\tag{186}
$$

$$
\mathrm{tr}\left\{E^\dagger(\omega)\rho_B E(\omega')\right\} = \mathrm{tr}\left\{E(\omega')E^\dagger(\omega)\rho_B\right\} = \mathrm{tr}\left\{\frac{1}{\sqrt{2}}\big(e(\omega')+d(\omega')\big)\frac{1}{\sqrt{2}}\big(e^\dagger(\omega)+d^\dagger(\omega)\big)\rho_B\right\}
$$

$$
= \frac{1}{2}\,\mathrm{tr}\left\{e(\omega')e^\dagger(\omega)\rho_B\right\} + \frac{1}{2}\underset{0}{\mathrm{tr}}\left\{d(\omega')e^\dagger(\omega)\rho_B\right\} + \frac{1}{2}\underset{0}{\mathrm{tr}}\left\{e(\omega')d^\dagger(\omega)\rho_B\right\} + \frac{1}{2}\,\mathrm{tr}\left\{d(\omega')d^\dagger(\omega)\rho_B\right\}
$$

$$
= \frac{1}{2}(\bar{n}_a + \bar{n}_b + 2)\delta(\omega - \omega'),\tag{187}
$$

$$
\mathrm{tr}\left\{D(\omega')\rho_B E^\dagger(\omega)\right\} = \mathrm{tr}\left\{E^\dagger(\omega)D(\omega')\rho_B\right\} = \mathrm{tr}\left\{\frac{1}{\sqrt{2}}\big(e^\dagger(\omega)+d^\dagger(\omega)\big)\frac{1}{\sqrt{2}}\big(-e(\omega')+d(\omega')\big)\rho_B\right\}
$$

$$
= -\frac{1}{2}\,\mathrm{tr}\left\{e^\dagger(\omega)e(\omega')\rho_B\right\} + \frac{1}{2}\underset{0}{\mathrm{tr}}\left\{e^\dagger(\omega)d(\omega')\rho_B\right\} - \frac{1}{2}\underset{0}{\mathrm{tr}}\left\{d^\dagger(\omega)e(\omega')\rho_B\right\} + \frac{1}{2}\,\mathrm{tr}\left\{d^\dagger(\omega)d(\omega')\rho_B\right\}
$$

$$
= \frac{1}{2}(-\bar{n}_a + \bar{n}_b)\delta(\omega - \omega'),\tag{188}
$$

$$
\mathrm{tr}\left\{E^\dagger(\omega)\rho_B D(\omega')\right\} = \mathrm{tr}\left\{D(\omega')E^\dagger(\omega)\rho_B\right\} = \mathrm{tr}\left\{\frac{1}{\sqrt{2}}\big(-e(\omega')+d(\omega')\big)\frac{1}{\sqrt{2}}\big(e^\dagger(\omega)+d^\dagger(\omega)\big)\rho_B\right\}
$$

$$
= -\frac{1}{2}\,\mathrm{tr}\left\{e(\omega')e^\dagger(\omega)\rho_B\right\} + \frac{1}{2}\underset{0}{\mathrm{tr}}\left\{d(\omega')e^\dagger(\omega)\rho_B\right\} - \frac{1}{2}\underset{0}{\mathrm{tr}}\left\{e(\omega')d^\dagger(\omega)\rho_B\right\} + \frac{1}{2}\,\mathrm{tr}\left\{d(\omega')d^\dagger(\omega)\rho_B\right\}
$$

$$
= \frac{1}{2}(-\bar{n}_a + \bar{n}_b)\delta(\omega - \omega'),\tag{189}
$$

$$
\mathrm{tr}\left\{E(\omega')\rho_B D^\dagger(\omega)\right\} = \mathrm{tr}\left\{D^\dagger(\omega)E(\omega')\rho_B\right\} = \mathrm{tr}\left\{\frac{1}{\sqrt{2}}\big(-e^\dagger(\omega)+d^\dagger(\omega)\big)\frac{1}{\sqrt{2}}\big(e(\omega')+d(\omega')\big)\rho_B\right\}
$$

$$
= -\frac{1}{2}\,\mathrm{tr}\left\{e^\dagger(\omega)e(\omega')\rho_B\right\} - \frac{1}{2}\underset{0}{\mathrm{tr}}\left\{e^\dagger(\omega)d(\omega')\rho_B\right\} + \frac{1}{2}\underset{0}{\mathrm{tr}}\left\{d^\dagger(\omega)e(\omega')\rho_B\right\} + \frac{1}{2}\,\mathrm{tr}\left\{d^\dagger(\omega)d(\omega')\rho_B\right\}
$$

$$
= \frac{1}{2}(-\bar{n}_a + \bar{n}_b)\delta(\omega - \omega'),\tag{190}
$$

$$\text{tr}\left\{D^\dagger(\omega)\rho_B E(\omega')\right\} = \text{tr}\left\{E(\omega')D^\dagger(\omega)\rho_B\right\} = \text{tr}\left\{\frac{1}{\sqrt{2}}\big(e(\omega') + d(\omega')\big)\frac{1}{\sqrt{2}}\big(-e^\dagger(\omega) + d^\dagger(\omega)\big)\rho_B\right\}$$

$$= -\frac{1}{2}\text{tr}\left\{e(\omega')e^\dagger(\omega)\rho_B\right\} - \underbrace{\frac{1}{2}\text{tr}\left\{d(\omega')e^\dagger(\omega)\rho_B\right\}}_{0} + \underbrace{\frac{1}{2}\text{tr}\left\{e(\omega')d^\dagger(\omega)\rho_B\right\}}_{0} + \frac{1}{2}\text{tr}\left\{d(\omega')d^\dagger(\omega)\rho_B\right\}$$

$$= \frac{1}{2}(-\bar{n}_a + \bar{n}_b)\delta(\omega - \omega'), \tag{191}$$

$$\text{tr}\left\{D(\omega')\rho_B D^\dagger(\omega)\right\} = \text{tr}\left\{D^\dagger(\omega)D(\omega')\rho_B\right\} = \text{tr}\left\{\frac{1}{\sqrt{2}}\big(-e^\dagger(\omega) + d^\dagger(\omega)\big)\frac{1}{\sqrt{2}}\big(-e(\omega') + d(\omega')\big)\rho_B\right\}$$

$$= \frac{1}{2}\text{tr}\left\{e^\dagger(\omega)e(\omega')\rho_B\right\} - \underbrace{\frac{1}{2}\text{tr}\left\{e^\dagger(\omega)d(\omega')\rho_B\right\}}_{0} - \underbrace{\frac{1}{2}\text{tr}\left\{d^\dagger(\omega)e(\omega')\rho_B\right\}}_{0} + \frac{1}{2}\text{tr}\left\{d^\dagger(\omega)d(\omega')\rho_B\right\}$$

$$= \frac{1}{2}(\bar{n}_a + \bar{n}_b)\delta(\omega - \omega'), \tag{192}$$

$$\text{tr}\left\{D^\dagger(\omega)\rho_B D(\omega')\right\} = \text{tr}\left\{D(\omega')D^\dagger(\omega)\rho_B\right\} = \text{tr}\left\{\frac{1}{\sqrt{2}}\big(-e(\omega') + d(\omega')\big)\frac{1}{\sqrt{2}}\big(-e^\dagger(\omega) + d^\dagger(\omega)\big)\rho_B\right\}$$

$$= \frac{1}{2}\text{tr}\left\{e(\omega')e^\dagger(\omega)\rho_B\right\} - \underbrace{\frac{1}{2}\text{tr}\left\{d(\omega')e^\dagger(\omega)\rho_B\right\}}_{0} - \underbrace{\frac{1}{2}\text{tr}\left\{e(\omega')d^\dagger(\omega)\rho_B\right\}}_{0} + \frac{1}{2}\text{tr}\left\{d(\omega')d^\dagger(\omega)\rho_B\right\}$$

$$= \frac{1}{2}(\bar{n}_a + \bar{n}_b + 2)\delta(\omega - \omega'). \tag{193}$$

The other initial conditions are of the form

$$\text{tr}\left\{E(\omega)E(\omega')\rho_B\right\} = \text{tr}\left\{\frac{1}{\sqrt{2}}\big(e(\omega) + d(\omega)\big)\frac{1}{\sqrt{2}}\big(e(\omega') + d(\omega')\big)\rho_B\right\}$$

$$= \frac{1}{2}\text{tr}\left\{e(\omega)e(\omega')\rho_B\right\} + \frac{1}{2}\text{tr}\left\{e(\omega)d(\omega')\rho_B\right\} + \frac{1}{2}\text{tr}\left\{d(\omega)e(\omega')\rho_B\right\} + \frac{1}{2}\text{tr}\left\{d(\omega)d(\omega')\rho_B\right\}$$

$$= 0 + 0 + 0 + 0 = 0, \tag{194}$$

and will all give zero.

A.2 Derivation of the master equation with beam-splitter

In this section we perform the detailled derivation of Eq (40) from the interaction Hamiltonian in the interaction picture of Eq (39), H_I.

To calculate the master equation, we have to calculate the terms in the commutator

$$\Big[H_I(t), [H_I(t - \tau), \tilde{\rho}(t - \tau)]\Big]. \tag{195}$$

In order to do this, we decompose the Hamiltonian into two parts: $H_I(t) = V(t) + V(t)^\dagger$, and we replace in (195):

$$\Big[V(t) + V^\dagger(t), \big[V^\dagger(t - \tau) + V(t - \tau), \tilde{\rho}(t - \tau)\big]\Big]$$

$$= \Big[V(t), \big[V^\dagger(t - \tau) + V(t - \tau), \tilde{\rho}(t - \tau)\big]\Big]$$

$$+ \Big[V(t)^\dagger, \big[V^\dagger(t - \tau) + V(t - \tau), \tilde{\rho}(t - \tau)\big]\Big]$$

$$= \Big[V(t), \big[V^\dagger(t - \tau) + V(t - \tau), \tilde{\rho}(t - \tau)\big]\Big]$$

$$+ \Big[V(t), \big[V^\dagger(t - \tau) + V(t - \tau), \tilde{\rho}(t - \tau)\big]\Big]^\dagger, \tag{196}$$

where in the last step we used the following property:

$$\begin{cases} \left[L, [K,\rho]\right]^{\dagger} = \left[[K,\rho]^{\dagger}, L^{\dagger}\right] \\ [K,\rho]^{\dagger} = [\rho^{\dagger}, K^{\dagger}] = [\rho, K] = -[K,\rho] \end{cases} \Rightarrow \left[L, [K,\rho]\right]^{\dagger} = \left[L^{\dagger}, [K,\rho]\right], \qquad (197)$$

where K is an Hermitian operator.

Now we observe that the terms in $\left[V(t), [V(t-\tau), \tilde{\rho}(t-\tau)]\right]$ are 0 since they only contain initial conditions of the form (194).
In other words, we only need to calculate

$$\left[V(t), \left[V^{\dagger}(t-\tau), \tilde{\rho}(t-\tau)\right]\right]. \qquad (198)$$

The other terms coming from $\left[V^{\dagger}(t), [V(t-\tau), \tilde{\rho}(t-\tau)]\right]$ will only be their complex conjugate[9]. The calculation of Q, where by definition

$$Q \equiv \left[V(t), \left[V^{\dagger}(t-\tau), \tilde{\rho}(t-\tau)\right]\right] = \left[E^{\dagger}(\omega)\tilde{A}e^{i\omega t} + D^{\dagger}(\omega)\tilde{B}e^{i\omega t}, \left[V^{\dagger}(t-\tau), \tilde{\rho}(t-\tau)\right]\right]$$

$$= \left[E^{\dagger}(\omega)\tilde{A}e^{i\omega t} + D^{\dagger}(\omega)\tilde{B}e^{i\omega t}, \left[\tilde{A}^{\dagger}E(\omega')e^{-i\omega'(t-\tau)} + \tilde{B}^{\dagger}D(\omega')e^{-i\omega'(t-\tau)}, \tilde{\rho}(t-\tau)\right]\right], \qquad (199)$$

gives 16 terms:

$$Q_1 = e^{i\omega t}e^{-i\omega'(t-\tau)}(\omega)\tilde{A}\tilde{A}^{\dagger}\tilde{\rho}_S(t-\tau) \otimes E^{\dagger}E(\omega')\tilde{\rho}_B, \qquad (200\text{a})$$

$$Q_2 = e^{i\omega t}e^{-i\omega'(t-\tau)}\tilde{A}\tilde{B}^{\dagger}\tilde{\rho}_S(t-\tau) \otimes E^{\dagger}(\omega)D(\omega')\tilde{\rho}_B, \qquad (200\text{b})$$

$$Q_3 = -e^{i\omega t}e^{-i\omega'(t-\tau)}\tilde{A}\tilde{\rho}_S(t-\tau)\tilde{A}^{\dagger} \otimes \tilde{\rho}_B E^{\dagger}(\omega)E(\omega'), \qquad (200\text{c})$$

$$Q_4 = -e^{i\omega t}e^{-i\omega'(t-\tau)}(\omega)\tilde{A}\tilde{\rho}_S(t-\tau)\tilde{B}^{\dagger} \otimes E^{\dagger}\tilde{\rho}_B D(\omega'), \qquad (200\text{d})$$

$$Q_5 = e^{i\omega t}e^{-i\omega'(t-\tau)}\tilde{B}\tilde{A}^{\dagger}\tilde{\rho}_S(t-\tau) \otimes D^{\dagger}(\omega)E(\omega')\tilde{\rho}_B, \qquad (200\text{e})$$

$$Q_6 = e^{i\omega t}e^{-i\omega'(t-\tau)}\tilde{B}\tilde{B}^{\dagger}\tilde{\rho}_S(t-\tau) \otimes D^{\dagger}(\omega)D(\omega')\tilde{\rho}_B, \qquad (200\text{f})$$

$$Q_7 = -e^{i\omega t}e^{-i\omega'(t-\tau)}\tilde{B}\tilde{\rho}_S(t-\tau)\tilde{A}^{\dagger} \otimes D^{\dagger}(\omega)\tilde{\rho}_B E(\omega'), \qquad (200\text{g})$$

$$Q_8 = -e^{i\omega t}e^{-i\omega'(t-\tau)}\tilde{B}\tilde{\rho}_S(t-\tau)\tilde{B}^{\dagger} \otimes D^{\dagger}(\omega)\tilde{\rho}_B D(\omega'), \qquad (200\text{h})$$

$$Q_9 = -e^{-i\omega'(t-\tau)}e^{i\omega t}\tilde{A}^{\dagger}\tilde{\rho}_S(t-\tau)\tilde{A} \otimes E(\omega')\tilde{\rho}_B E^{\dagger}(\omega), \qquad (200\text{i})$$

$$Q_{10} = -e^{-i\omega'(t-\tau)}e^{i\omega t}\tilde{A}^{\dagger}\tilde{\rho}_S(t-\tau)\tilde{B} \otimes E(\omega')\tilde{\rho}_B D^{\dagger}(\omega), \qquad (200\text{j})$$

$$Q_{11} = -e^{-i\omega'(t-\tau)}e^{i\omega t}\tilde{B}^{\dagger}\tilde{\rho}_S(t-\tau)\tilde{A} \otimes D(\omega')\tilde{\rho}_B E^{\dagger}(\omega), \qquad (200\text{k})$$

$$Q_{12} = -e^{-i\omega'(t-\tau)}e^{i\omega t}\tilde{B}^{\dagger}\tilde{\rho}_S(t-\tau)\tilde{B} \otimes D(\omega')\tilde{\rho}_B D^{\dagger}(\omega), \qquad (200\text{l})$$

$$Q_{13} = e^{-i\omega'(t-\tau)}e^{i\omega t}\tilde{\rho}_S(t-\tau)\tilde{A}^{\dagger}\tilde{A} \otimes \tilde{\rho}_B E(\omega')E^{\dagger}(\omega), \qquad (200\text{m})$$

$$Q_{14} = e^{-i\omega'(t-\tau)}e^{i\omega t}\tilde{\rho}_S(t-\tau)\tilde{A}^{\dagger}\tilde{B} \otimes \tilde{\rho}_B E(\omega')D^{\dagger}(\omega), \qquad (200\text{n})$$

$$Q_{15} = e^{-i\omega'(t-\tau)}e^{i\omega t}\tilde{\rho}_S(t-\tau)\tilde{B}^{\dagger}\tilde{A} \otimes \tilde{\rho}_B D(\omega')E^{\dagger}(\omega), \qquad (200\text{o})$$

$$Q_{16} = e^{-i\omega'(t-\tau)}e^{i\omega t}\tilde{\rho}_S(t-\tau)\tilde{B}^{\dagger}\tilde{B} \otimes \tilde{\rho}_B D(\omega')D^{\dagger}(\omega). \qquad (200\text{p})$$

$$(200\text{q})$$

---

[9] $\left[V, [V^{\dagger}, \rho]\right]^{\dagger} = \left[[V^{\dagger}, \rho]^{\dagger}, V^{\dagger}\right] = \left[[\rho^{\dagger}, V], V^{\dagger}\right] = \left[V^{\dagger}, [V, \rho]\right]$

As before, using the initial conditions we get:

$$\frac{\gamma_A}{\pi} \int_0^t d\tau \int_{-\infty}^{\infty} d\omega \int_{-\infty}^{\infty} d\omega' \, \text{tr}_B \{Q_1\} = \frac{1}{2}\gamma_A(\bar{n}_b + \bar{n}_a)\tilde{A}\tilde{A}^\dagger \tilde{\rho}_S, \tag{201a}$$

$$\frac{\sqrt{\gamma_A \gamma_B}}{\pi} \int_0^t d\tau \int_{-\infty}^{\infty} d\omega \int_{-\infty}^{\infty} d\omega' \, \text{tr}_B \{Q_2\} = \frac{1}{2}\sqrt{\gamma_A \gamma_B}(\bar{n}_b - \bar{n}_a)\tilde{A}\tilde{B}^\dagger \tilde{\rho}_S, \tag{201b}$$

$$\frac{\gamma_A}{\pi} \int_0^t d\tau \int_{-\infty}^{\infty} d\omega \int_{-\infty}^{\infty} d\omega' \, \text{tr}_B \{Q_3\} = -\frac{1}{2}\gamma_A(\bar{n}_b + \bar{n}_a + 2)\tilde{A}\tilde{\rho}_S\tilde{A}^\dagger, \tag{201c}$$

$$\frac{\sqrt{\gamma_A \gamma_B}}{\pi} \int_0^t d\tau \int_{-\infty}^{\infty} d\omega \int_{-\infty}^{\infty} d\omega' \, \text{tr}_B \{Q_4\} = -\frac{1}{2}\sqrt{\gamma_A \gamma_B}(\bar{n}_b - \bar{n}_a)\tilde{A}\tilde{\rho}_S\tilde{B}^\dagger, \tag{201d}$$

$$\frac{\sqrt{\gamma_A \gamma_B}}{\pi} \int_0^t d\tau \int_{-\infty}^{\infty} d\omega \int_{-\infty}^{\infty} d\omega' \, \text{tr}_B \{Q_5\} = \frac{1}{2}\sqrt{\gamma_A \gamma_B}(\bar{n}_b - \bar{n}_a)\tilde{B}\tilde{A}^\dagger \tilde{\rho}_S, \tag{201e}$$

$$\frac{\gamma_B}{\pi} \int_0^t d\tau \int_{-\infty}^{\infty} d\omega \int_{-\infty}^{\infty} d\omega' \, \text{tr}_B \{Q_6\} = \frac{1}{2}\gamma_B(\bar{n}_b + \bar{n}_a)\tilde{B}\tilde{B}^\dagger \tilde{\rho}_S, \tag{201f}$$

$$\frac{\sqrt{\gamma_A \gamma_B}}{\pi} \int_0^t d\tau \int_{-\infty}^{\infty} d\omega \int_{-\infty}^{\infty} d\omega' \, \text{tr}_B \{Q_7\} = -\frac{1}{2}\sqrt{\gamma_A \gamma_B}(\bar{n}_b - \bar{n}_a)\tilde{B}\tilde{\rho}_S\tilde{A}^\dagger, \tag{201g}$$

$$\frac{\gamma_B}{\pi} \int_0^t d\tau \int_{-\infty}^{\infty} d\omega \int_{-\infty}^{\infty} d\omega' \, \text{tr}_B \{Q_8\} = -\frac{1}{2}\gamma_B(\bar{n}_b + \bar{n}_a + 2)\tilde{B}\tilde{\rho}_S\tilde{B}^\dagger, \tag{201h}$$

$$\frac{\gamma_A}{\pi} \int_0^t d\tau \int_{-\infty}^{\infty} d\omega \int_{-\infty}^{\infty} d\omega' \, \text{tr}_B \{Q_9\} = -\frac{1}{2}\gamma_A(\bar{n}_b + \bar{n}_a)\tilde{A}^\dagger \tilde{\rho}_S\tilde{A}, \tag{201i}$$

$$\frac{\sqrt{\gamma_A \gamma_B}}{\pi} \int_0^t d\tau \int_{-\infty}^{\infty} d\omega \int_{-\infty}^{\infty} d\omega' \, \text{tr}_B \{Q_{10}\} = -\frac{1}{2}\sqrt{\gamma_A \gamma_B}(\bar{n}_b - \bar{n}_a)\tilde{A}^\dagger \tilde{\rho}_S\tilde{B}, \tag{201j}$$

$$\frac{\sqrt{\gamma_A \gamma_B}}{\pi} \int_0^t d\tau \int_{-\infty}^{\infty} d\omega \int_{-\infty}^{\infty} d\omega' \, \text{tr}_B \{Q_{11}\} = -\frac{1}{2}\sqrt{\gamma_A \gamma_B}(\bar{n}_b - \bar{n}_a)\tilde{B}^\dagger \tilde{\rho}_S\tilde{A}, \tag{201k}$$

$$\frac{\gamma_B}{\pi} \int_0^t d\tau \int_{-\infty}^{\infty} d\omega \int_{-\infty}^{\infty} d\omega' \, \text{tr}_B \{Q_{12}\} = -\frac{1}{2}\gamma_B(\bar{n}_b + \bar{n}_a)\tilde{B}^\dagger \tilde{\rho}_S\tilde{B}, \tag{201l}$$

$$\frac{\gamma_A}{\pi} \int_0^t d\tau \int_{-\infty}^{\infty} d\omega \int_{-\infty}^{\infty} d\omega' \, \text{tr}_B \{Q_{13}\} = \frac{1}{2}\gamma_A(\bar{n}_b + \bar{n}_a + 2)\tilde{\rho}_S\tilde{A}^\dagger \tilde{A}, \tag{201m}$$

$$\frac{\sqrt{\gamma_A \gamma_B}}{\pi} \int_0^t d\tau \int_{-\infty}^{\infty} d\omega \int_{-\infty}^{\infty} d\omega' \, \text{tr}_B \{Q_{14}\} = \frac{1}{2}\sqrt{\gamma_A \gamma_B}(\bar{n}_b - \bar{n}_a)\tilde{\rho}_S\tilde{A}^\dagger \tilde{B}, \tag{201n}$$

$$\frac{\sqrt{\gamma_A \gamma_B}}{\pi} \int_0^t d\tau \int_{-\infty}^{\infty} d\omega \int_{-\infty}^{\infty} d\omega' \, \text{tr}_B \{Q_{15}\} = \frac{1}{2}\sqrt{\gamma_A \gamma_B}(\bar{n}_b - \bar{n}_a)\tilde{\rho}_S\tilde{B}^\dagger \tilde{A}, \tag{201o}$$

$$\frac{\gamma_B}{\pi} \int_0^t d\tau \int_{-\infty}^{\infty} d\omega \int_{-\infty}^{\infty} d\omega' \, \text{tr}_B \{Q_{16}\} = \frac{1}{2}\gamma_B(\bar{n}_b + \bar{n}_a + 2)\tilde{\rho}_S\tilde{B}^\dagger \tilde{B}. \tag{201p}$$

$$\tag{201q}$$

Adding those terms (+H.C) we get:

$$\frac{d\tilde{\rho}_S}{dt} = \gamma_A \left(-\tilde{A}\tilde{\rho}_S\tilde{A}^\dagger + \tilde{\rho}_S\tilde{A}^\dagger\tilde{A} \right) + \gamma_B \left(-\tilde{B}\tilde{\rho}_S\tilde{B}^\dagger + \tilde{\rho}_S\tilde{B}^\dagger\tilde{B} \right)$$

$$+ \gamma_A \frac{\bar{n}_a + \bar{n}_b}{2} \left(\tilde{A}\tilde{A}^\dagger\tilde{\rho}_S - \tilde{A}^\dagger\tilde{\rho}_S\tilde{A} - \tilde{A}\tilde{\rho}_S\tilde{A}^\dagger + \tilde{\rho}_S\tilde{A}^\dagger\tilde{A} \right)$$

$$+ \gamma_B \frac{\bar{n}_a + \bar{n}_b}{2} \left(\tilde{B}\tilde{B}^\dagger\tilde{\rho}_S - \tilde{B}^\dagger\tilde{\rho}_S\tilde{B} - \tilde{B}\tilde{\rho}_S\tilde{B}^\dagger + \tilde{\rho}_S\tilde{B}^\dagger\tilde{B} \right)$$

$$+ \sqrt{\gamma_A\gamma_B}\frac{\bar{n}_a - \bar{n}_b}{2} \left(\tilde{A}\tilde{B}^\dagger\tilde{\rho}_S + \tilde{\rho}_S\tilde{B}^\dagger\tilde{A} + \tilde{B}\tilde{A}^\dagger\tilde{\rho}_S + \tilde{\rho}_S\tilde{A}^\dagger\tilde{B} - \tilde{A}^\dagger\tilde{\rho}_S\tilde{B} - \tilde{B}\tilde{\rho}_S\tilde{A}^\dagger - \tilde{B}^\dagger\tilde{\rho}_S\tilde{A} - \tilde{A}\tilde{\rho}_S\tilde{B}^\dagger \right)$$

$$+ H.C, \tag{202}$$

which can be written

$$\frac{d\tilde{\rho}_S}{dt} = \gamma_A \left(\frac{\bar{n}_a + \bar{n}_b}{2} + 1 \right) D_{\tilde{A}}[\tilde{\rho}_S] + \gamma_A\frac{\bar{n}_a + \bar{n}_b}{2} D_{\tilde{A}^\dagger}[\tilde{\rho}_S] + \left(\frac{\bar{n}_a + \bar{n}_b}{2} + 1 \right) \gamma_B D_{\tilde{B}}[\tilde{\rho}_S] + \gamma_B\frac{\bar{n}_a + \bar{n}_b}{2} D_{\tilde{B}^\dagger}[\tilde{\rho}_S]$$

$$+ \sqrt{\gamma_A\gamma_B}\frac{\bar{n}_a - \bar{n}_b}{2} \left(2\tilde{A}\tilde{\rho}_S\tilde{B}^\dagger - \left\{ \tilde{\rho}_S, \tilde{B}^\dagger\tilde{A} \right\} + 2\tilde{B}^\dagger\tilde{\rho}_S\tilde{A} - \left\{ \tilde{\rho}_S, \tilde{A}\tilde{B}^\dagger \right\} + \text{H.c.} \right), \tag{203}$$

which is Eq(40) .

B   Additional figures

We mentioned in the main text that our simulations show that the beam splitter interaction produces no effect when $\bar{\lambda}$ is too small. In the following figures we show that this is indeed the case for the case $\bar{\lambda} = 0.01$.
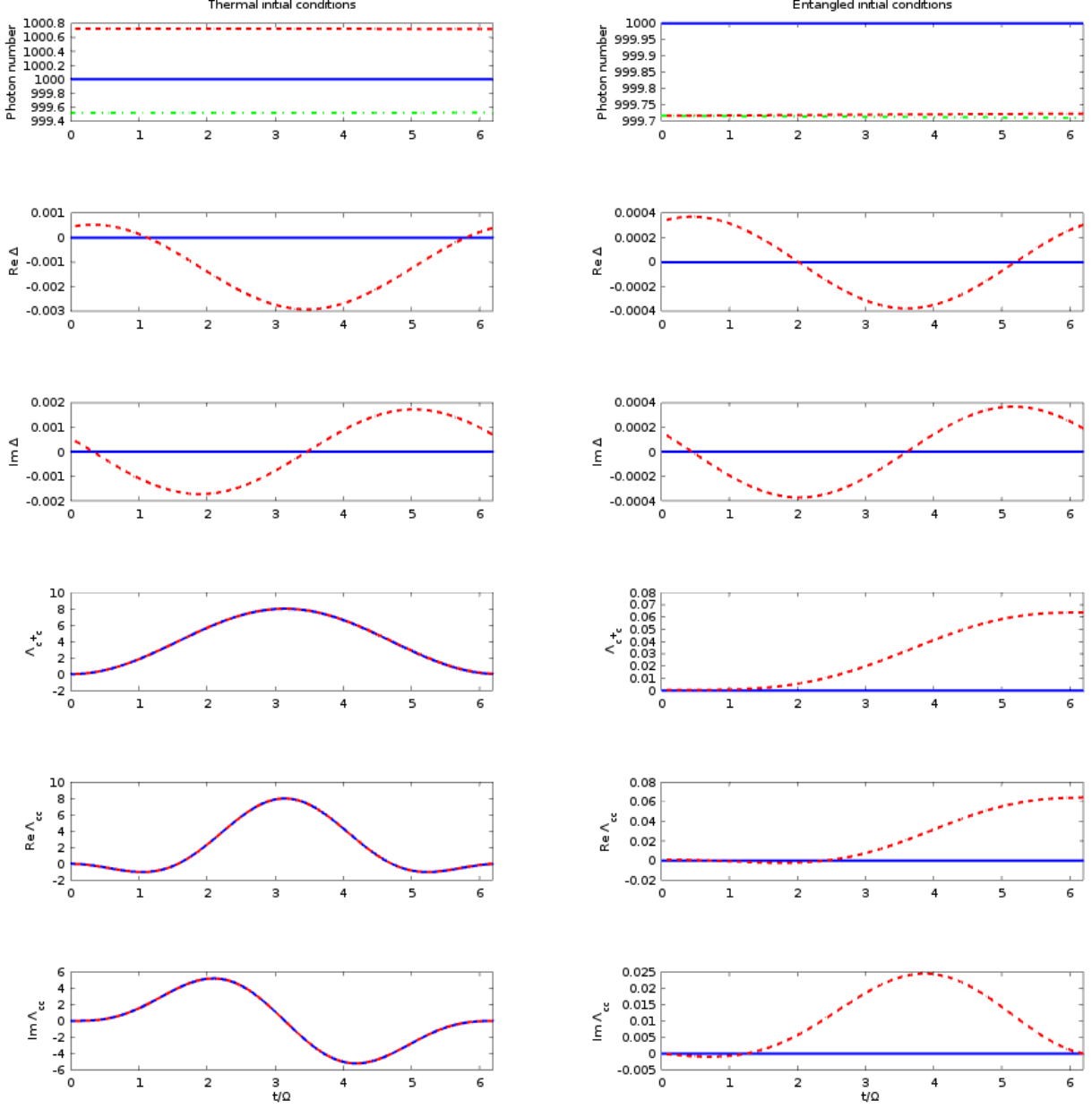

Figure 13:   Result of the simulations of Eqs. (122), corresponding to the membrane model within the truncated Wigner. We consider initial uncorrelated thermal optical states (right column) and an entangled state (left column). The parameters are $\bar{g} = 0.001$, $\bar{n} = 1000$, and $\lambda = 0.01$. We average over 10^6 stochastic paths, and show the simulations in dashed red and the analytical solutions of section 4.2 in blue.
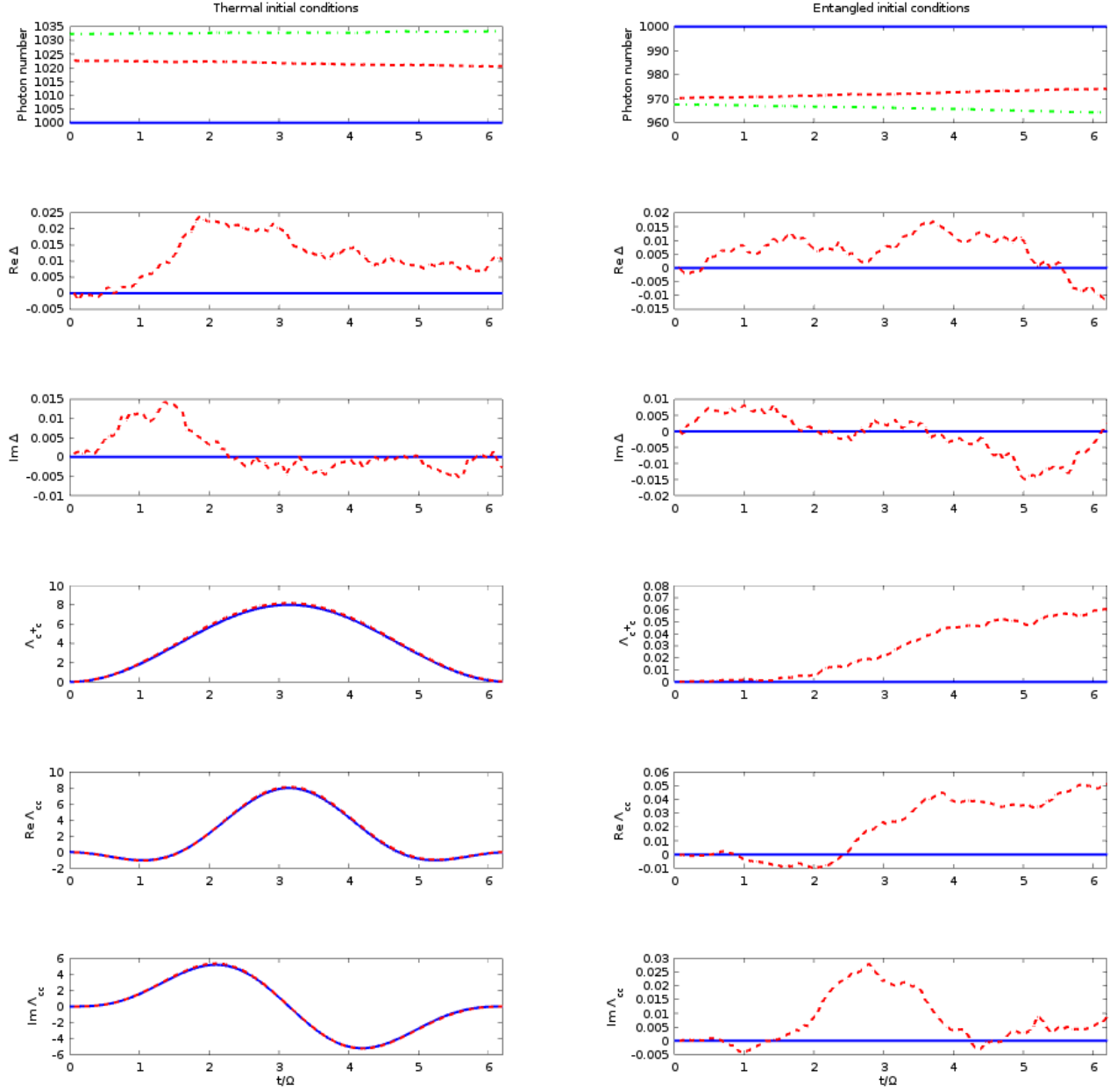
Figure 14: Result of the simulations of Eqs. (127), corresponding to the membrane model within the positive P representation. We consider initial uncorrelated thermal optical states (right column) and an entangled state (left column). The parameters are $\bar{g} = 0.001$, $\bar{n} = 1000$, and $\lambda = 0.01$. We average over 10^3 stochastic paths, and show the simulations in dashed red and the analytical solutions of section 4.2 in blue.
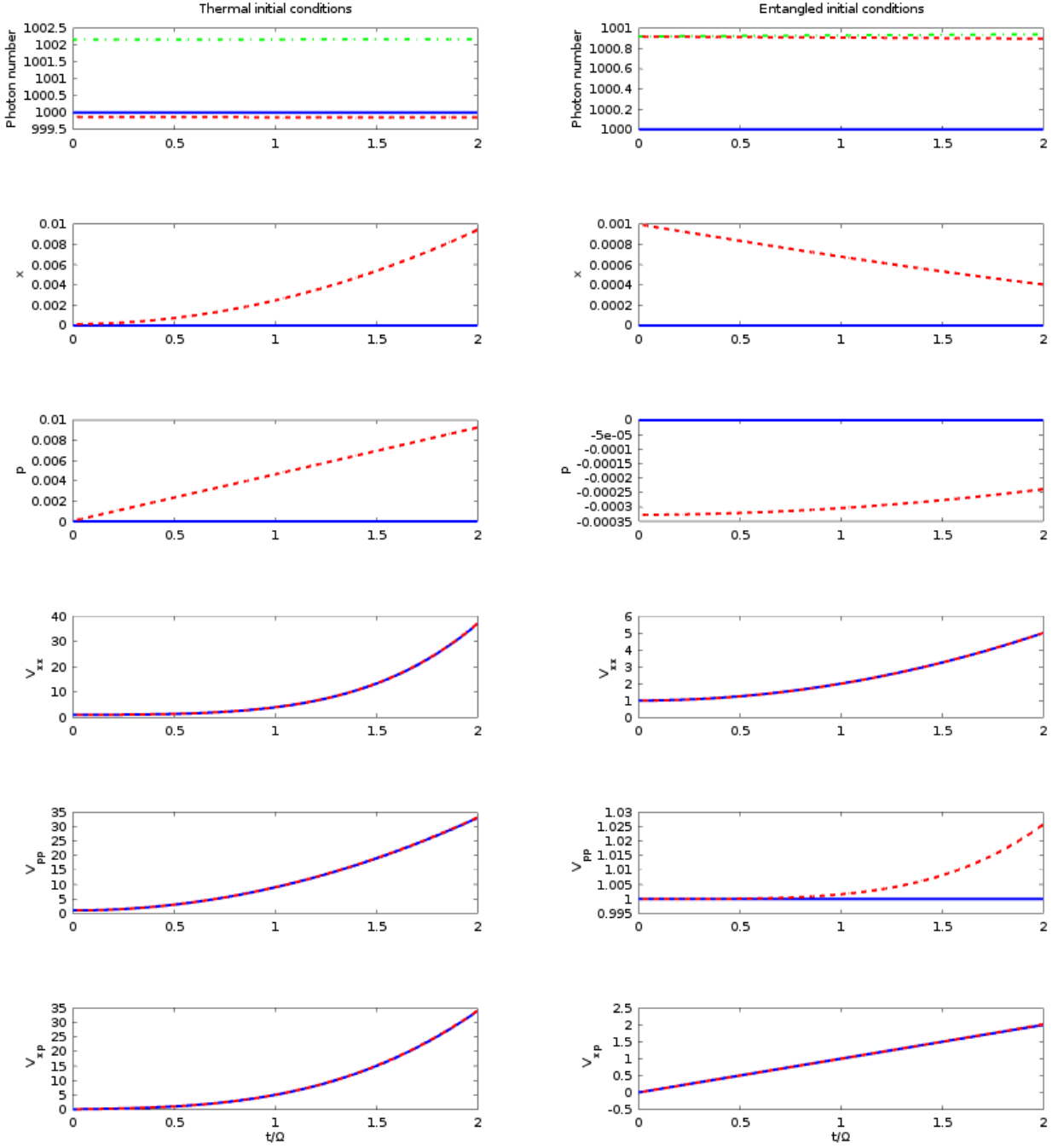
Figure 15: Result of the simulations of Eqs. (121), corresponding to the piston model within the truncated Wigner representation. We consider initial uncorrelated thermal optical states (right column) and an entangled state (left column). The parameters are $\bar{g} = 0.001$, $\bar{n} = 1000$, and $\lambda = 0.01$. We average over 10^6 stochastic paths, and show the simulations in dashed red and the analytical solutions of section 4.2 in blue.

Figure 16: Result of the simulations of Eqs. (126), corresponding to the piston model within the positive P representation. We consider initial uncorrelated thermal optical states (right column) and an entangled state (left column). The parameters are $\bar{g} = 0.001$, $\bar{n} = 1000$, and $\lambda = 0.01$. We average over 10^6 stochastic paths, and show the simulations in dashed red and the analytical solutions of section 4.2 in blue.
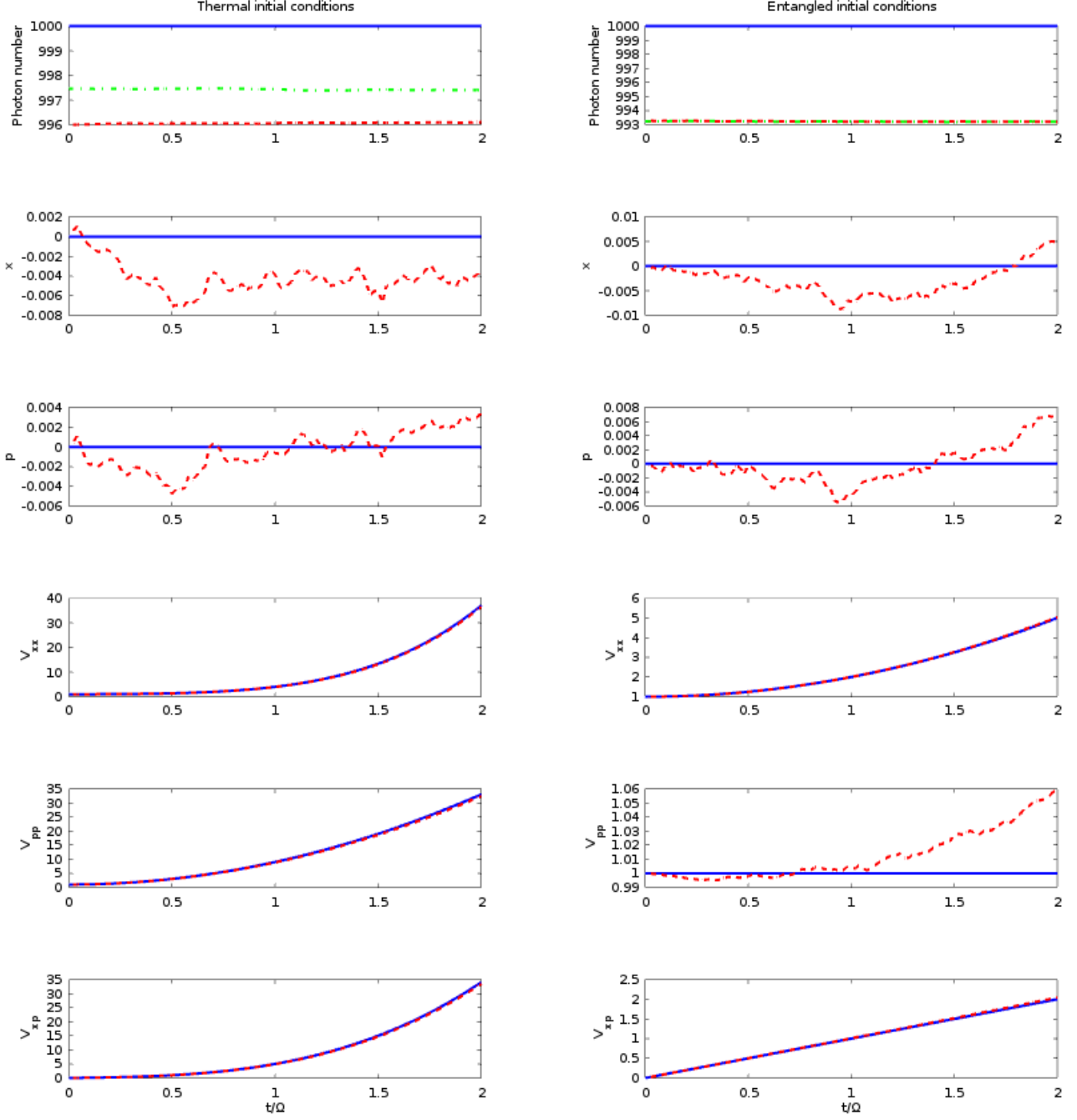
C Codes

This appendix gives the XML codes of the simulations as well as indications on the way to use them under Linux. It is divided into 3 sections. The first two sections are dedicated to the membrane and the piston, respectively. The third section shows how to compile the codes and extract the data for plots. All the codes have a similar structure. Thus, we start by showing a complete example and then we just show which parts have to be replaced in order to change the representation or the initial condition.

C.1 Membrane

A first code is displayed below. As written in the description, it simulates the case of the Wigner representation for thermal initial conditions. (Notice that the outputs can only be real).

```
1  <?xml version="1.0" encoding="UTF-8"?>
2  <simulation xmds-version="2">
3      <name>2MemWigTher</name>
4
5      <author>Grigoriou Emmanouil</author>
6      <description>
7      System of stoochastic differential equations for:
8      - Wigner distribution
9      - No environments
10     - Membrane + Beam-splitter
11     - 2 cavities
12     - Thermal state for cavities
13     - Gaussian state for piston
14     </description>
15
16     <features>
17         <globals>
18         <![CDATA[
19             real g = 0.001;
20             real lambda = 10;
21             real n = 1000;
22         ]]>
23         </globals>
24     </features>
25
26     <geometry>
27         <propagation_dimension> t </propagation_dimension>
28     </geometry>
29
30     <!-- This line defines the number of stochastic paths -->
31     <driver name="multi-path" paths="1000000" />
32
33     <!-- Next we define a noise vector for the sampling of the initial conditions
       -->
34     <noise_vector name="initialConditionsSampling" dimensions="" kind="gauss" type
       ="complex" method="solirte">
35     <components>n1 n2 n3 </components>
36     </noise_vector>
37
38     <!-- 'vector' describes the variables that we will be evolving. -->
39     <vector name="stochasticVariables" type="complex">
40         <components>
41             a b x
42         </components>
43         <initialisation>
```

```
44            <dependencies>initialConditionsSampling</dependencies>
45            <![CDATA[
46                a = sqrt(n+0.5)*n1;
47                b = sqrt(n+0.5)*n2;
48                x = n3*sqrt(0.5);
49            ]]>
50        </initialisation>
51    </vector>
52
53    <sequence>
54        <integrate algorithm="ARK89" interval="6.2" tolerance="1e-15">
55            <samples>100</samples>
56            <operators>
57            <integration_vectors>stochasticVariables</integration_vectors>
58            <![CDATA[
59                da_dt =  i*g*(x+conj(x))*a − i*lambda*b;
60                db_dt = −i*g*(x+conj(x))*b − i*lambda*a;
61                dx_dt = −i*x + i*g*(a*conj(a)−b*conj(b));
62            ]]>
63            </operators>
64        </integrate>
65    </sequence>
66
67    <!-- This part defines what data will be saved in the output file -->
68    <output format="hdf5" filename="2MemWigTher_g0001_l10_n1000FINAL.xsil">
69        <sampling_group initial_sample="yes">
70        <moments>anorm bnorm cR cI ccR ccI cnorm </moments>
71        <dependencies>stochasticVariables</dependencies>
72        <![CDATA[
73          anorm = a.Re()*a.Re() + a.Im()*a.Im();
74          bnorm = b.Re()*b.Re() + b.Im()*b.Im();
75          cR = x.Re();
76          cI = x.Im();
77          ccR = x.Re()*x.Re()−x.Im()*x.Im();
78          ccI = 2*x.Re()*x.Im();
79          cnorm = x.Re()*x.Re() + x.Im()*x.Im();
80        ]]>
81        </sampling_group>
82    </output>
83 </simulation>
84
```

To change the initial conditions of the simulation, one has to change the content of the tags
$< initialisation >< /initialisation >$. Entangled intitial conditions as sampled in section 4.3 are
obtained by replacing them with the following piece of code:

```
1         <initialisation>
2         <dependencies>initialConditionsSampling</dependencies>
3           <![CDATA[
4         a = 1/sqrt(8) * (exp(r)*xplus+exp(−r)*xminus +
5             i*exp(−r)*pplus+i*exp(r)*pminus);
6         b = 1/sqrt(8) * (exp(r)*xplus−exp(−r)*xminus+
7             i*exp(−r)*pplus−i*exp(r)*pminus);
8         x = (n1 +i*n2)*0.5;
9           ]]>
10        </initialisation>
11
```

where we defined r in

```
1            <globals>
2              <![CDATA[
3              real g = 0.001;
4              real lambda = 10;
5              real n = 1000;
6              real r = asinh(sqrt(n));
7              ]]>
8            </globals>
9
```

In the case of the P distribution, we have to define a longer vector for the variables of the extended phase space[10]. For example in the thermal case the code will be:

```
1          <vector name="stochasticVariables" type="complex">
2              <components>
3                a ap b bp x xp
4              </components>
5              <initialisation>
6              <dependencies>initialConditionsSampling</dependencies>
7                <![CDATA[
8                  a = sqrt(n)*n1;
9                  ap = conj(a);
10                 b = sqrt(n)*n2;
11                 bp = conj(b);
12                 x = 0;
13                 xp = 0;
14                ]]>
15             </initialisation>
16         </vector>
17
```

The system of equations (127) is:

```
1    <sequence>
2      <integrate algorithm="ARK89" interval="6.2" tolerance="1e-7">
3        <samples>100</samples>
4        <operators>
5          <integration_vectors>stochasticVariables</integration_vectors>
6      <dependencies>QuantumNoise</dependencies>
7          <![CDATA[
8          da_dt =  i*g*(x+xp)*a - i*lambda*b + sqrt(i*g*a)* ksi1;
9          dap_dt = -i*g*(x+xp)*ap + i*lambda*bp +sqrt(-i*g*ap)* ksi2;
10         db_dt = -i*g*(x+xp)*b - i*lambda*a + sqrt(-i*g*b)*ksi3;
11         dbp_dt = i*g*(x+xp)*bp + i*lambda*ap + sqrt(i*g*bp)*ksi4;
12         dx_dt = -i*x + i*g*(ap*a-bp*b) + sqrt(i*g*a)* conj(ksi1)
13                                        + sqrt(-i*g*b)*conj(ksi3);
14         dxp_dt = i*xp - i*g*(ap*a-bp*b) + sqrt(-i*g*ap)*conj(ksi2)
15                                         + sqrt(i*g*bp)*conj(ksi4);
16          ]]>
17        </operators>
18      </integrate>
19    </sequence>
```

---

[10]We use substrict p for the new variables, for example, ap $\equiv \alpha^+$.

Finally, we also have to change the outputs :

```
1        <!-- This part defines what data will be saved in the output file -->
2    <output format="hdf5" filename="2MemPdisTher_g0001_l10_n1000_1000FINAL.xsil">
3      <sampling_group initial_sample="yes">
4       <moments>photonNumberaR photonNumberaI photonNumberbR photonNumberbI cR cI
5      ccR ccI phononNumberR phononNumberI na2R na2I nb2R nb2I nanbR nanbI</moments>
6        <dependencies>stochasticVariables</dependencies>
7        <![CDATA[
8          photonNumberaR = ap.Re()*a.Re() - ap.Im()*a.Im();
9          photonNumberaI = ap.Im()*a.Re() + ap.Re()*a.Im();
10         photonNumberbR = bp.Re()*b.Re() - bp.Im()*b.Im();
11         photonNumberbI = bp.Im()*b.Re() + bp.Re()*b.Im();
12         cR = x.Re();
13         cI = x.Im();
14         ccR = x.Re()*x.Re()-x.Im()*x.Im();
15         ccI = 2*x.Re()*x.Im();
16         phononNumberR = xp.Re()*x.Re() - xp.Im()*x.Im();
17         phononNumberI = xp.Im()*x.Re() + xp.Re()*x.Im();
18         na2R = ( ap.Re() * ap.Re() - ap.Im()*ap.Im() )
19                 *( a.Re() * a.Re() - a.Im()*a.Im() )
20                 - 4*ap.Re()*ap.Im()*a.Re()*a.Im();
21         na2I = 2*ap.Re()*ap.Im() *( a.Re() * a.Re() - a.Im()*a.Im() )
22                 + a.Re()*a.Im()*( ap.Re() * ap.Re() - ap.Im()*ap.Im() );
23         nb2R = ( bp.Re() * bp.Re() - bp.Im()*bp.Im() )
24                 *( b.Re() * b.Re() - b.Im()*b.Im() )
25                 - 4*bp.Re()*bp.Im()*b.Re()*b.Im();
26         nb2I = 2*bp.Re()*bp.Im() *( b.Re() * b.Re() - b.Im()*b.Im() )
27                 + b.Re()*b.Im()*( bp.Re() * bp.Re() - bp.Im()*bp.Im() );
28         nanbR = (ap.Re()*a.Re()-ap.Im()*a.Im())*(bp.Re()*b.Re()-bp.Im()*b.Im())
29                 - (ap.Im()*a.Re() + ap.Re()*a.Im())*(bp.Im()*b.Re()
30                 + bp.Re()*b.Im());
31         nanbI = (ap.Im()*a.Re()+ap.Re()*a.Im())*(bp.Re()*b.Re()-bp.Im()*b.Im())
32                 + (ap.Re()*a.Re() - ap.Im()*a.Im())*(bp.Im()*b.Re()
33                 + bp.Re()*b.Im());
34       ]]>
35     </sampling_group>
36   </output>
37
```

C.2   Piston

The codes of the piston are similar to those of the membrane. But the variables and their initialization, the equations and the outputs are different. Thus, we start with a complete example. We give the one of the positive P representation for entangled initial conditions as it may be the more complicated and the most different from the previous one.

```
1  <?xml version="1.0" encoding="UTF-8"?>
2  <simulation xmds-version="2">
3    <name>2PistPdisEnt</name>
4
5    <author>Grigoriou Emmanouil</author>
6    <description>
7      System of stochastic differential equations for:
8    - positive P distribution
9    - No environments
10   - Piston + Beam-splitter
11   - Entangled state for cavities
12   </description>
13
```

```xml
14
15    <features>
16      <globals>
17          <![CDATA[
18          real g = 0.001;
19          real lambda = 10;
20          real n = 1000;
21          real r = asinh(sqrt(n));
22          real cr = cosh(r);
23          ]]>
24      </globals>
25    </features>
26
27    <geometry>
28      <propagation_dimension> t </propagation_dimension>
29    </geometry>
30
31    <driver name="multi-path" paths="10000" />
32
33
34    <noise_vector name="initialConditionsSampling" dimensions="" kind="gauss" type="
        real" method="solirte">
35      <components>n1 n2 n3 n4 n5 n6 n7 n8</components>
36    </noise_vector>
37
38    <vector name="stochasticVariables" type="complex">
39      <components>
40        a ap b bp x p
41      </components>
42      <initialisation>
43      <dependencies>initialConditionsSampling</dependencies>
44        <![CDATA[
45        a = sqrt(cr)*0.5 *( i*exp(r*0.5)*n1- exp(-r*0.5)*n2 - exp(r*0.5)*n5
46                        - i*exp(-r*0.5)*n6 ) + 0.5*(n3 - n7 + i*n4 - i*n8 );
47        ap = sqrt(cr)*0.5*( i*exp(r*0.5)*n1 - exp(-r*0.5)*n2 + exp(r*0.5)*n5
48                        + i*exp(-r*0.5)*n6 ) + 0.5*(n3 + n7 + i*n4 + i*n8 );
49        b = sqrt(cr)*0.5*( - i*exp(r*0.5)*n1 - exp(-r*0.5)*n2 - exp(r*0.5)*n5
50                        + i*exp(-r*0.5)*n6 ) + 0.5*(- n3 + n7 + i*n4 - i*n8 );
51        bp= sqrt(cr)*0.5 *( - i*exp(r*0.5)*n1 - exp(-r*0.5)*n2 + exp(r*0.5)*n5
52                        - i*exp(-r*0.5)*n6 ) + 0.5*(- n3 - n7 + i*n4 + i*n8 );
53        x = 0;
54        p = 0;
55        ]]>
56      </initialisation>
57    </vector>
58
59    <noise_vector name="QuantumNoise" dimensions="" kind="wiener" type="complex"
        method="solirte" >
60      <components>ksi1 ksi2 ksi3 ksi4 ksim</components>
61    </noise_vector>
62
63
64     <sequence>
65      <integrate algorithm="ARK89" interval="2" tolerance="1e-7">
66        <samples>100</samples>
67        <operators>
68          <integration_vectors>stochasticVariables</integration_vectors>
69      <dependencies>QuantumNoise</dependencies>
70          <![CDATA[
71          da_dt =  i*g*x*a - i*lambda*b + sqrt(i*g*a)* ksi1;
```

```
72        dap_dt = −i*g*x*ap + i*lambda*bp +sqrt(−i*g*ap)* ksi2;
73        db_dt = −i*g*x*b − i*lambda*a + sqrt(−i*g*b)*ksi3;
74        dbp_dt = i*g*x*bp + i*lambda*ap + sqrt(i*g*bp)*ksi4;
75        dx_dt = p + sqrt(i)*ksim +
76               sqrt(i*g)*(i*sqrt(ap)*conj(ksi2)+sqrt(a)*conj(ksi1)
77               + i*sqrt(−bp)*conj(ksi4)+sqrt(−b)*conj(ksi3));
78        dp_dt = 2*g*(ap*a−bp*b)−i*sqrt(i)*conj(ksim)+
79               sqrt(−i*g)*(i*sqrt(ap)*conj(ksi2)−sqrt(a)*conj(ksi1)
80               + i*sqrt(−bp)*conj(ksi4)−sqrt(−b)*conj(ksi3));
81       ]]>
82     </operators>
83    </integrate>
84  </sequence>
85
86  <!−− This part defines what data will be saved in the output file −−>
87  <output format="hdf5" filename="2PistPdisEnt_g0001_l10_n1000_10000FINAL.xsil">
88    <sampling_group initial_sample="yes">
89      <moments>photonNumberaR photonNumberaI photonNumberbR photonNumberbI xR xI
   x2R x2I pR pI p2R p2I xpR xpI na2R na2I nb2R nb2I nanbR nanbI </moments>
90      <dependencies>stochasticVariables</dependencies>
91      <![CDATA[
92        photonNumberaR = ap.Re()*a.Re() − ap.Im()*a.Im();
93        photonNumberaI = ap.Im()*a.Re() + ap.Re()*a.Im();
94        photonNumberbR = bp.Re()*b.Re() − bp.Im()*b.Im();
95        photonNumberbI = bp.Im()*b.Re() + bp.Re()*b.Im();
96        xR = x.Re();
97        xI = x.Im();
98        x2R = x.Re()*x.Re()−x.Im()*x.Im();
99        x2I = 2*x.Re()*x.Im();
100       pR = p.Re();
101       pI = p.Im();
102       p2R = p.Re()*p.Re()−p.Im()*p.Im();
103       p2I = 2*p.Re()*p.Im();
104       xpR = x.Re()*p.Re()−x.Im()*p.Im();
105       xpI = x.Re()*p.Im()+x.Im()*p.Re();
106       na2R = ( ap.Re() * ap.Re() − ap.Im()*ap.Im() )
107              *( a.Re() * a.Re() − a.Im()*a.Im() )
108              − 4*ap.Re()*ap.Im()*a.Re()*a.Im();
109       na2I = 2*ap.Re()*ap.Im() *( a.Re() * a.Re() − a.Im()*a.Im() )
110              + a.Re()*a.Im()*( ap.Re() * ap.Re() − ap.Im()*ap.Im() );
111       nb2R = ( bp.Re() * bp.Re() − bp.Im()*bp.Im() )
112              *( b.Re() * b.Re() − b.Im()*b.Im() )
113              − 4*bp.Re()*bp.Im()*b.Re()*b.Im();
114       nb2I = 2*bp.Re()*bp.Im() *( b.Re() * b.Re() − b.Im()*b.Im() )
115              + b.Re()*b.Im()*( bp.Re() * bp.Re() − bp.Im()*bp.Im() );
116       nanbR = (ap.Re()*a.Re()−ap.Im()*a.Im())*(bp.Re()*b.Re()−bp.Im()*b.Im())
117              −(ap.Im()*a.Re()+ap.Re()*a.Im())*(bp.Im()*b.Re()+bp.Re()*b.Im());
118       nanbI = (ap.Im()*a.Re()+ap.Re()*a.Im())*(bp.Re()*b.Re()−bp.Im()*b.Im())
119              + (ap.Re()*a.Re()−ap.Im()*a.Im())*(bp.Im()*b.Re()+bp.Re()*b.Im());
120      ]]>
121    </sampling_group>
122  </output>
123 </simulation>
124
```

For completeness we also give the equations and the outputs of the Wigner distribution

```
1      <sequence>
2        <integrate algorithm="ARK89" interval="2" tolerance="1e−15">
3          <samples>100</samples>
4           <operators>
5            <integration_vectors>stochasticVariables</integration_vectors>
```

```
6              <![CDATA[
7                  da_dt =  i*g*x*a − i*lambda*b;
8                  db_dt = −i*g*x*b − i*lambda*a;
9                  dx_dt = p;
10                 dp_dt = 2*g*(a*conj(a)−b*conj(b));
11             ]]>
12             </operators>
13         </integrate>
14     </sequence>
15
16
```

```
1     <output format="hdf5" filename="2PistWigTher_g0001_l10_n1000FINAL.xsil">
2           <sampling_group initial_sample="yes">
3         <moments>anorm bnorm xR x2R pR p2R xpR </moments>
4         <dependencies>stochasticVariables</dependencies>
5         <![CDATA[
6             anorm = a.Re()*a.Re() + a.Im()*a.Im();
7             bnorm = b.Re()*b.Re() + b.Im()*b.Im();
8             xR = x.Re();
9             x2R = x.Re()*x.Re()−x.Im()*x.Im();
10            pR = p.Re();
11            p2R = p.Re()*p.Re()−p.Im()*p.Im();
12            xpR = x.Re()*p.Re()−x.Im()*p.Im();
13        ]]>
14        </sampling_group>
15    </output>
16
```

C.3   Compiling and plotting under Linux

In order to compile an xmds program, you must first save your code in a xmds file. Then you can open a terminal in the adequate repertory and enter the command[11]

xmds2 fileName.xmds

And that's it, the simulation is compiled. To launch it you can then use

./fileName

This will execute the simulations and output an .xsil file and an .h5 file containing the data. In order to plot the data of the simulation, you can convert the .xsil file to a Matlab file using

xsil2graphics2 -m fileName.xsil

This generates a Matlab file that loads the h5 file and transform it into readable Matlab arrays. For example, the generated code for the case of the piston within the Wigner representation with thermal initial conditions is

```
1 if (exist('OCTAVE_VERSION', 'builtin')) % Octave
2   load 2PistWigTher_g0001_l0_n1000FINAL.h5
3   t_1 = eval('_1.t');
4   mean_anorm_1 = eval('_1.mean_anorm');
5   mean_anorm_1 = permute(mean_anorm_1, ndims(mean_anorm_1):−1:1);
6   mean_bnorm_1 = eval('_1.mean_bnorm');
```

---

[11]For more detailled information you can consult the site of XMDS2: http://www.xmds.org/

```matlab
     mean_bnorm_1 = permute(mean_bnorm_1, ndims(mean_bnorm_1):-1:1);
     mean_xR_1 = eval('_1.mean_xR');
     mean_xR_1 = permute(mean_xR_1, ndims(mean_xR_1):-1:1);
     mean_x2R_1 = eval('_1.mean_x2R');
     mean_x2R_1 = permute(mean_x2R_1, ndims(mean_x2R_1):-1:1);
     mean_pR_1 = eval('_1.mean_pR');
     mean_pR_1 = permute(mean_pR_1, ndims(mean_pR_1):-1:1);
     mean_p2R_1 = eval('_1.mean_p2R');
     mean_p2R_1 = permute(mean_p2R_1, ndims(mean_p2R_1):-1:1);
     mean_xpR_1 = eval('_1.mean_xpR');
     mean_xpR_1 = permute(mean_xpR_1, ndims(mean_xpR_1):-1:1);
     stderr_anorm_1 = eval('_1.stderr_anorm');
     stderr_anorm_1 = permute(stderr_anorm_1, ndims(stderr_anorm_1):-1:1);
     stderr_bnorm_1 = eval('_1.stderr_bnorm');
     stderr_bnorm_1 = permute(stderr_bnorm_1, ndims(stderr_bnorm_1):-1:1);
     stderr_xR_1 = eval('_1.stderr_xR');
     stderr_xR_1 = permute(stderr_xR_1, ndims(stderr_xR_1):-1:1);
     stderr_x2R_1 = eval('_1.stderr_x2R');
     stderr_x2R_1 = permute(stderr_x2R_1, ndims(stderr_x2R_1):-1:1);
     stderr_pR_1 = eval('_1.stderr_pR');
     stderr_pR_1 = permute(stderr_pR_1, ndims(stderr_pR_1):-1:1);
     stderr_p2R_1 = eval('_1.stderr_p2R');
     stderr_p2R_1 = permute(stderr_p2R_1, ndims(stderr_p2R_1):-1:1);
     stderr_xpR_1 = eval('_1.stderr_xpR');
     stderr_xpR_1 = permute(stderr_xpR_1, ndims(stderr_xpR_1):-1:1);
     clear _1;
else % MATLAB
     t_1 = hdf5read('2PistWigTher_g0001_l0_n1000FINAL.h5', '/1/t');
     mean_anorm_1 = hdf5read('2PistWigTher_g0001_l0_n1000FINAL.h5', '/1/mean_anorm');
     mean_anorm_1 = permute(mean_anorm_1, ndims(mean_anorm_1):-1:1);
     mean_bnorm_1 = hdf5read('2PistWigTher_g0001_l0_n1000FINAL.h5', '/1/mean_bnorm');
     mean_bnorm_1 = permute(mean_bnorm_1, ndims(mean_bnorm_1):-1:1);
     mean_xR_1 = hdf5read('2PistWigTher_g0001_l0_n1000FINAL.h5', '/1/mean_xR');
     mean_xR_1 = permute(mean_xR_1, ndims(mean_xR_1):-1:1);
     mean_x2R_1 = hdf5read('2PistWigTher_g0001_l0_n1000FINAL.h5', '/1/mean_x2R');
     mean_x2R_1 = permute(mean_x2R_1, ndims(mean_x2R_1):-1:1);
     mean_pR_1 = hdf5read('2PistWigTher_g0001_l0_n1000FINAL.h5', '/1/mean_pR');
     mean_pR_1 = permute(mean_pR_1, ndims(mean_pR_1):-1:1);
     mean_p2R_1 = hdf5read('2PistWigTher_g0001_l0_n1000FINAL.h5', '/1/mean_p2R');
     mean_p2R_1 = permute(mean_p2R_1, ndims(mean_p2R_1):-1:1);
     mean_xpR_1 = hdf5read('2PistWigTher_g0001_l0_n1000FINAL.h5', '/1/mean_xpR');
     mean_xpR_1 = permute(mean_xpR_1, ndims(mean_xpR_1):-1:1);
     stderr_anorm_1 = hdf5read('2PistWigTher_g0001_l0_n1000FINAL.h5', '/1/
       stderr_anorm');
     stderr_anorm_1 = permute(stderr_anorm_1, ndims(stderr_anorm_1):-1:1);
     stderr_bnorm_1 = hdf5read('2PistWigTher_g0001_l0_n1000FINAL.h5', '/1/
       stderr_bnorm');
     stderr_bnorm_1 = permute(stderr_bnorm_1, ndims(stderr_bnorm_1):-1:1);
     stderr_xR_1 = hdf5read('2PistWigTher_g0001_l0_n1000FINAL.h5', '/1/stderr_xR');
     stderr_xR_1 = permute(stderr_xR_1, ndims(stderr_xR_1):-1:1);
     stderr_x2R_1 = hdf5read('2PistWigTher_g0001_l0_n1000FINAL.h5', '/1/stderr_x2R');
     stderr_x2R_1 = permute(stderr_x2R_1, ndims(stderr_x2R_1):-1:1);
     stderr_pR_1 = hdf5read('2PistWigTher_g0001_l0_n1000FINAL.h5', '/1/stderr_pR');
     stderr_pR_1 = permute(stderr_pR_1, ndims(stderr_pR_1):-1:1);
     stderr_p2R_1 = hdf5read('2PistWigTher_g0001_l0_n1000FINAL.h5', '/1/stderr_p2R');
     stderr_p2R_1 = permute(stderr_p2R_1, ndims(stderr_p2R_1):-1:1);
     stderr_xpR_1 = hdf5read('2PistWigTher_g0001_l0_n1000FINAL.h5', '/1/stderr_xpR');
     stderr_xpR_1 = permute(stderr_xpR_1, ndims(stderr_xpR_1):-1:1);
end
```